2.4 The MM5 modelling system

Investigations have been carried out to determine whether a meteorological model could realistically predict rainfall patterns over the Mawddach catchment for the example storm events described in section 2.1. The system chosen is the MM5 Mesoscale Model, developed over a number of years by Richard Anthes at Pennsylvania State University (Anthes and Warner, 1978) and subsequently by the National Center for Atmospheric Research in Boulder, Colorado (Grell, Dudhia and Stauffer, 1995). The system is now a robust and reliable code for solving a wide range of meteorological problems.

Weather simulations require initial and boundary conditions to be supplied, in the form of land and sea surface characteristics for the study region, and gridded meteorological data at the start and subsequent time intervals during the run. Suitable global meteorological data sets are provided by the US National Center for Environmental Protection (NCEP). This gridded data specifies sea level pressure at surface grid points, and

- wind speed and direction
- temperature
- relative humidity
- geopotential height (approximately the altitude)

at the surface and at atmospheric levels where the pressure is 1 000, 850, 700, 500, 400, 300, 250, 200, 150 and 100mb.
This data is generated from observations by land stations, ships, aircraft and balloon ascents worldwide. Data sets are issued in electronic format at 6-hourly intervals, both as records of actual readings, and as advance forecasts of probable atmospheric conditions.

The task of MM5 is to take the gridded sets of land surface and air parameters, and simulate a likely sequence of weather phenomena occurring in the study region over the next time period of 6 or 12 hours. Modelling will include the patterns of winds, and vertical air movements leading to condensation. Distribution and intensity of rainfall and snowfall can be mapped. Specialist applications of MM5 are to predict

the likely occurrence and tracks of electrical storms and tornados, or to predict the dispersal patterns of airborne pollutants from events such as forest fires.
MM5 is a modular system, made up from a series of software packages written mainly in the language FORTRAN 90 (fig.2.71). The programs can be run under a Unix operating system on a mainframe computer, or under Linux on a microcomputer. Modern high speed microcomputers are capable of carrying out a 1 day weather simulation on a 1km resolution grid within 3 hours of processing time. A 12-processor minicomputer using parallel processing is able to achieve a 1 day simulation in less than 1 hour.

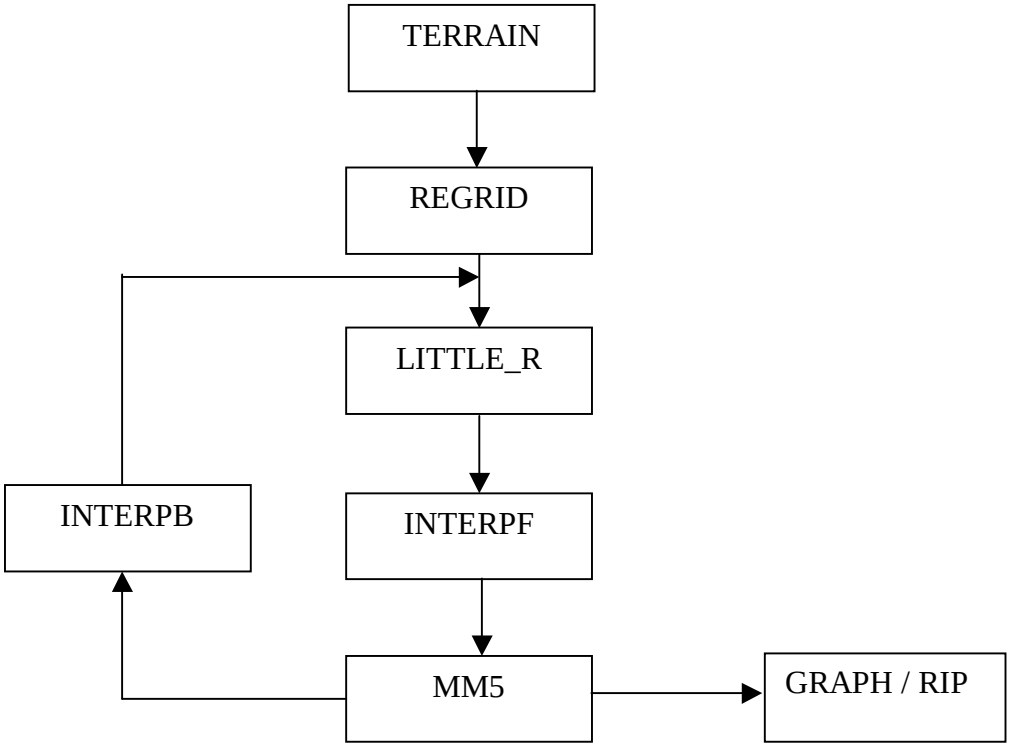

Figure 2.71: The principal modules of the MM5 modelling system

TERRAIN module

The setting up of a meteorological model begins with the TERRAIN module. It is usual to establish a series of nested domains, which will capture large synoptic weather patterns and apply these as local boundary conditions for a mesoscale area of interest. The MM5 model for the Mawddach catchment uses five domains, illustrated in fig.2.72:

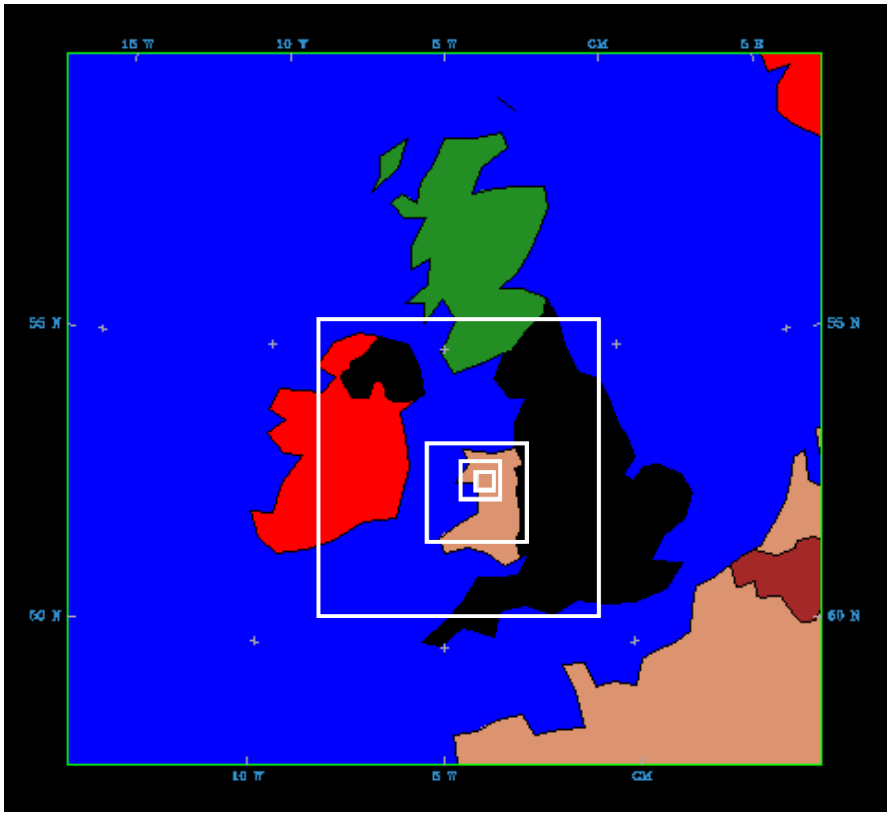

Domain	Region	Grid resolution (km)	Grid columns	Grid rows
1	British Isles	27	52	49
2	Irish Sea	9	58	61
3	Wales	3	61	61
4	Gwynedd	1	70	70
5	Mawddach	0.33	91	91

Figure 2.72: Nested domains for the Mawddach meteorological model

The TERRAIN module creates land surface boundary condition files for each of the domains, to allow the modelling of processes within the planetary boundary layer (PBL). The PBL makes up approximately the lowest 1 000m of the troposphere, and is the zone in which large scale weather patterns may be modified by properties of the land or sea surfaces over which the airflows move.

A series of data sets with global coverage have been provided by the National Center for Atmospheric Research in conjunction with the US Geological Survey, for use in initialising MM5 domains. These are listed in Table 2.1, and are illustrated for the Mawddach catchment in figures 2.73-2.77.

Data set	Provided by	Resolution	Illustrated by:
Terrain height	USGS	30sec (~1km)	fig.2.69
Land use and vegetation	USGS Simple Biosphere model	30sec (~1km)	fig.2.70
Monthly vegetation fraction	NOAA Advanced Very High Resolution Radiometer	10min (~20km)	fig.2.71
Soil data	U N Food and Agriculture Organisation	30sec (~1km)	fig.2.72
Deep soil temperature	European Center for Medium range Weather Forecasting	10min (~20km)	fig.2.73

Table 2.1: Data sets used to initialise the Mawddach PBL model

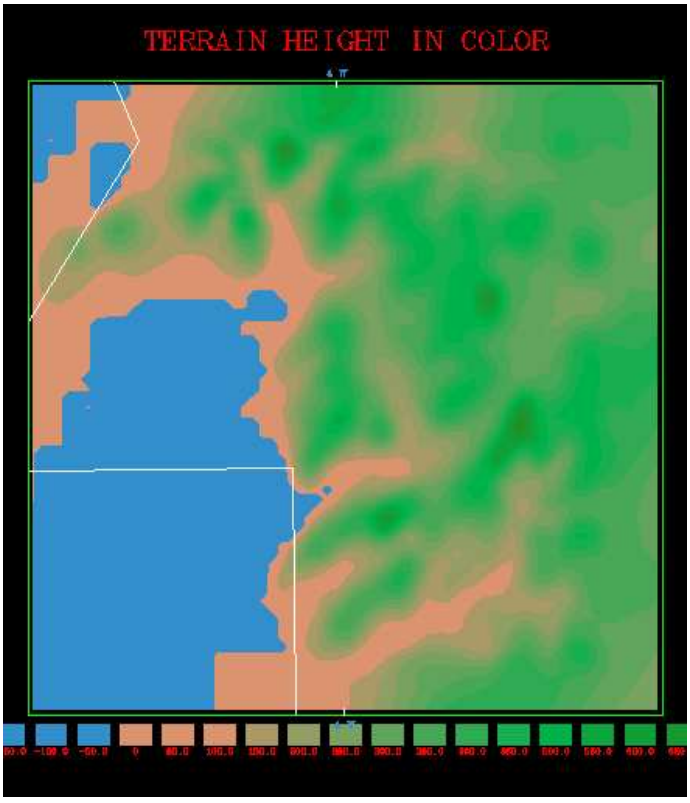

Figure 2.73: Terrain height data for the Mawddach model

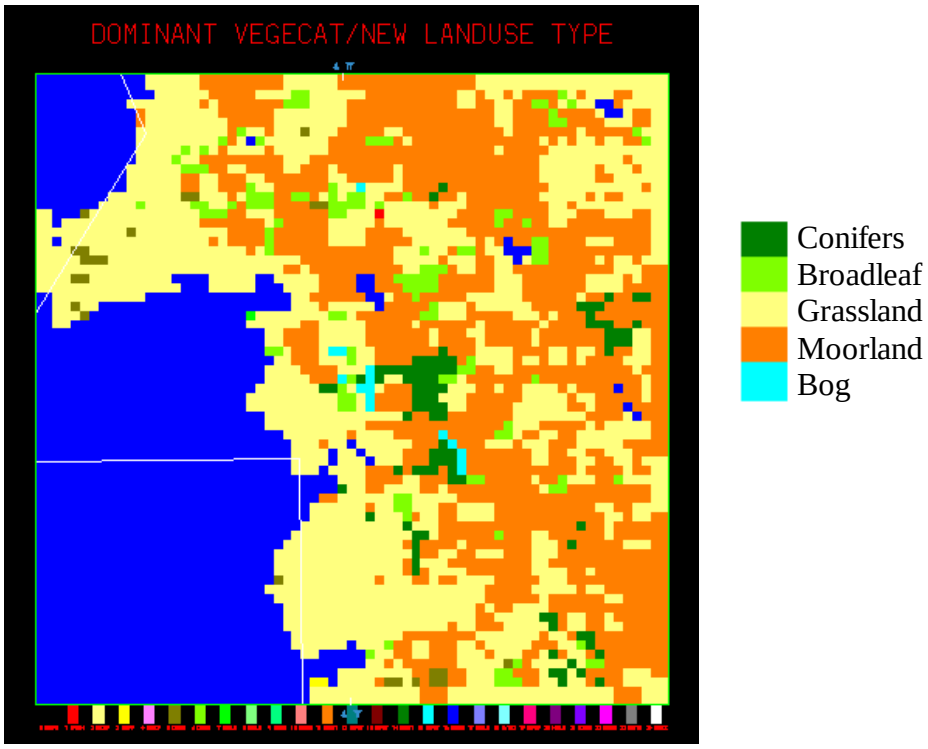

Figure 2.74: Land use classification for the Mawddach model

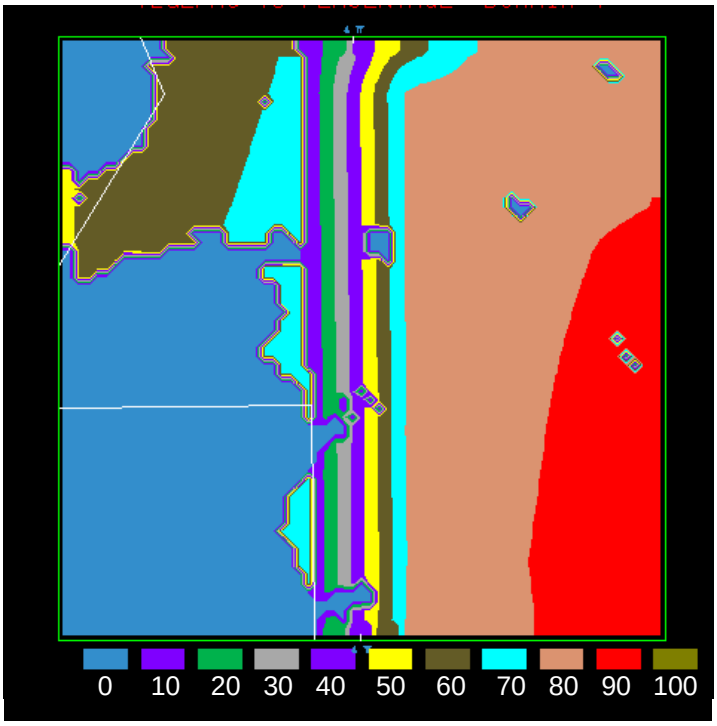

Figure 2.75: Monthly vegetation fraction for the Mawddach model – October, representing an estimate of the percentage of ground covered by vegetation.

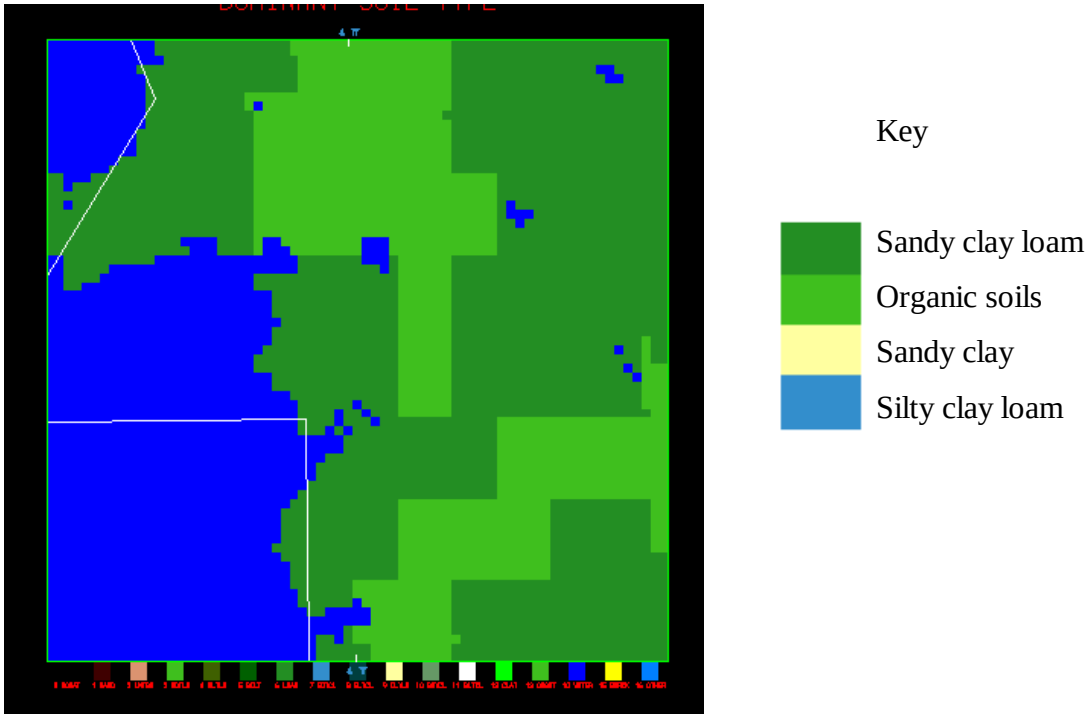

Figure 2.76: Dominant soil type for the Mawddach model

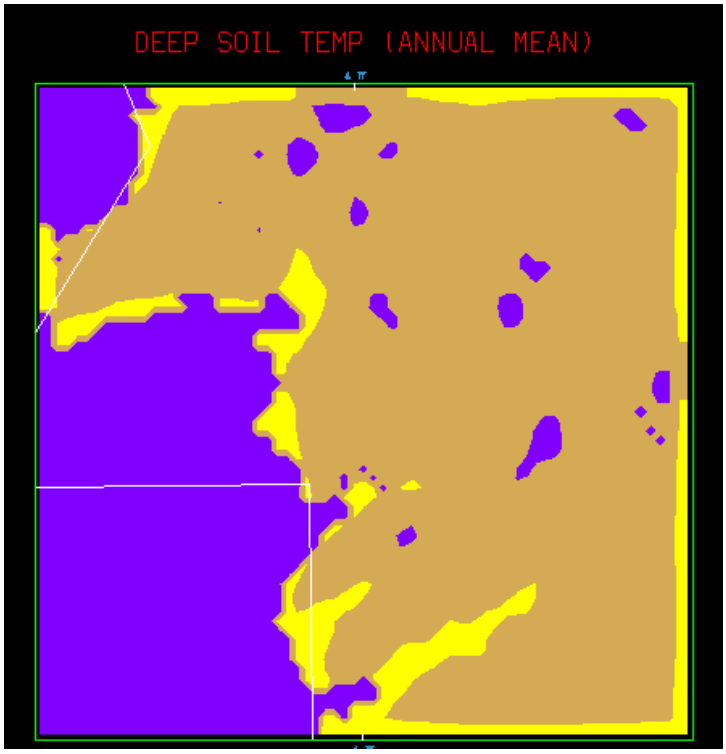

Figure 2.77: Mean annual deep soil temperature for the Mawddach model

REGRID module

The second module of the MM5 system is REGRID. Meteorological models usually involve significant sections of the globe for the outer model domains. Land surface and meteorological data are provided for latitude and longitude points, and this data has to be projected onto a horizontal grid for use in the model.

The length of east-west arc representing 1 degree of longitude will vary according to distance from the equator. This variation must be taken into consideration so that the mass of air moving through the model is conserved.

For modelling middle latitudes, the gridded latitude-longitude data is first plotted in Lambert Projection. The advantage of this projection is in preserving the shapes of small areas exactly. The map scale may, however, vary slightly from point to point and it is necessary to apply a correction factor **m** in the model to allow for this (Calvert, 2005).

Geometrically, the Lambert Projection represents the transfer of the earth's surface onto a cone which just touches the globe at some latitude φ (fig.2.78). When the cone is unwrapped, it forms a sector of a circle which does not quite meet at the edges (fig.2.79).

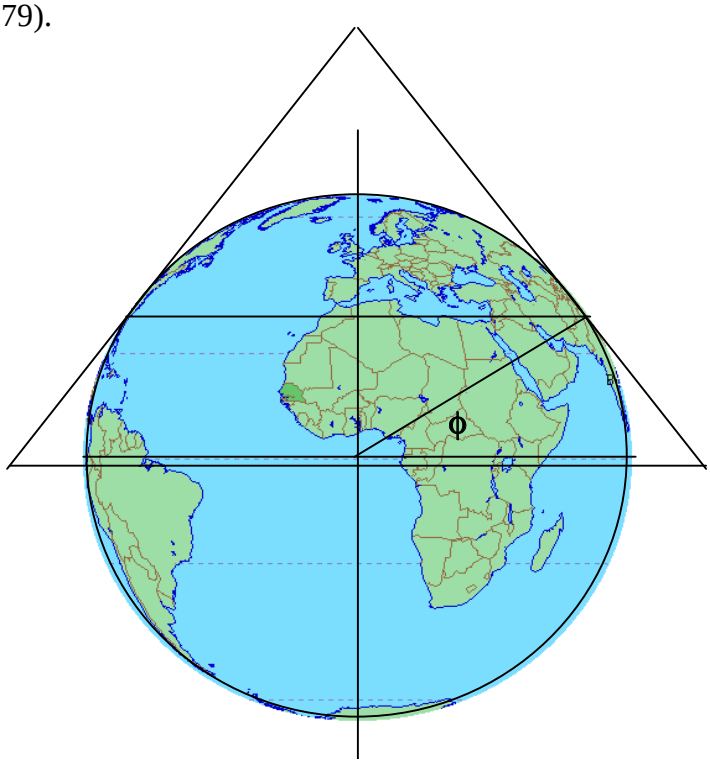

Figure 2.78: Method of generating the Lambert Projection

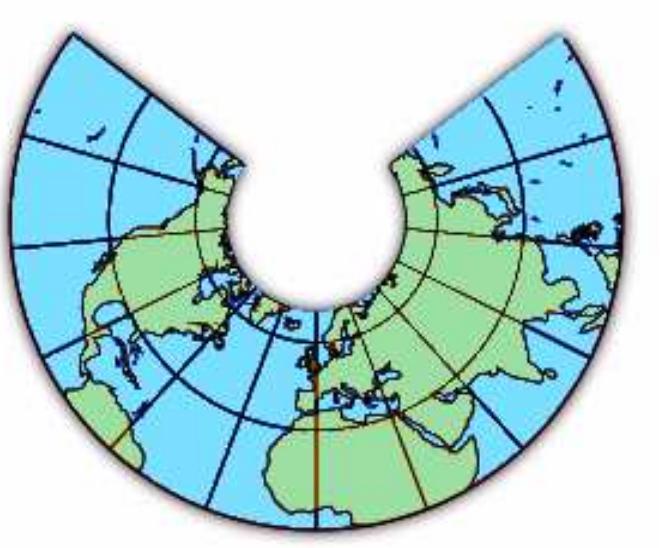

Figure 2.79: Lambert Projection onto a plane surface

In a Lambert map, the parallels of latitude are represented by concentric circles. The map has two standard parallels where the scale is unity. The Lambert conformal grid is true at latitudes 30^0 and 60^0 N, so the map scale factor is given by **m** =1 at these latitudes.

$$\mathbf{m} = \frac{\text{distance on grid}}{\text{actual distance on earth}}$$

For any other latitude ϕ, the map scale factor can be calculated from:

$$m = \frac{\sin\psi_1}{\sin\phi}\left[\frac{\tan\phi/2}{\tan\psi_1/2}\right]^{0.716}$$

where: $\psi_1 = 30^0$

Latitude-longitude data can then be transferred to corresponding positions on a rectangular grid for use in the MM5 model (fig.2.80):

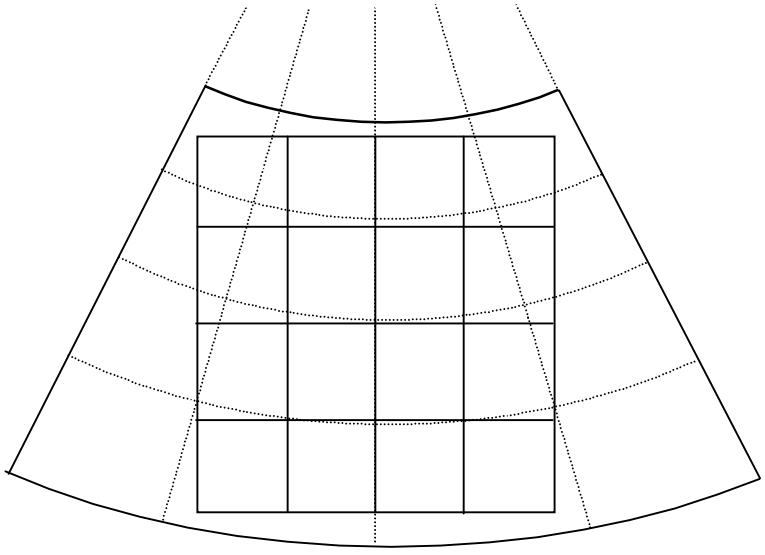

Figure 2.80: Mapping of data from a Lambert Projection to a rectangular grid

LITTLE_R module

The LITTLE_R module allows the incorporation of additional meteorological data to improve the accuracy or resolution of the original gridded input set. This new data may have come from surface observations or radiosonde balloon ascents carried out in a research area, or the interpretation of remote sensing data from satellites or radar. LITTLE_R adjusts surrounding readings according to the confidence level which the user wishes to place on the new data.

INTERPF module

The purpose of INTERPF is to convert the gridded data from pressure levels into a form which is simpler for the model to process. S*igma levels* are defined to represent intervals between the ground surface and the horizontal top surface of the model (fig.2.81). Sigma pressure levels are defined according to the equation:

$$\sigma = \frac{(p - p_t)}{(p_s - p_t)}$$

where p is the pressure at level σ, p_s is the surface pressure and p_t is the pressure at the top of the model at the same horizontal grid location. The sigma levels have values range from 0 at the model top to 1 at the earth's surface. Appropriate vertical intervals are chosen, with closer spacing near the ground where accurate calculation of meteorological variables will be most critical for the model. The Mawddach model uses 23 levels.

Sigma levels are numbered downwards, starting with K=1 at the model top surface. During runs of the MM5 model, some variables are calculated for the sigma surfaces, whilst others are calculated at the half-level positions between sigma levels (fig.2.77):

Sigma surfaces

Vertical air velocity, Pressure gradient

Half-levels

Horizontal air velocity, Temperature, Pressure, Relative humidity

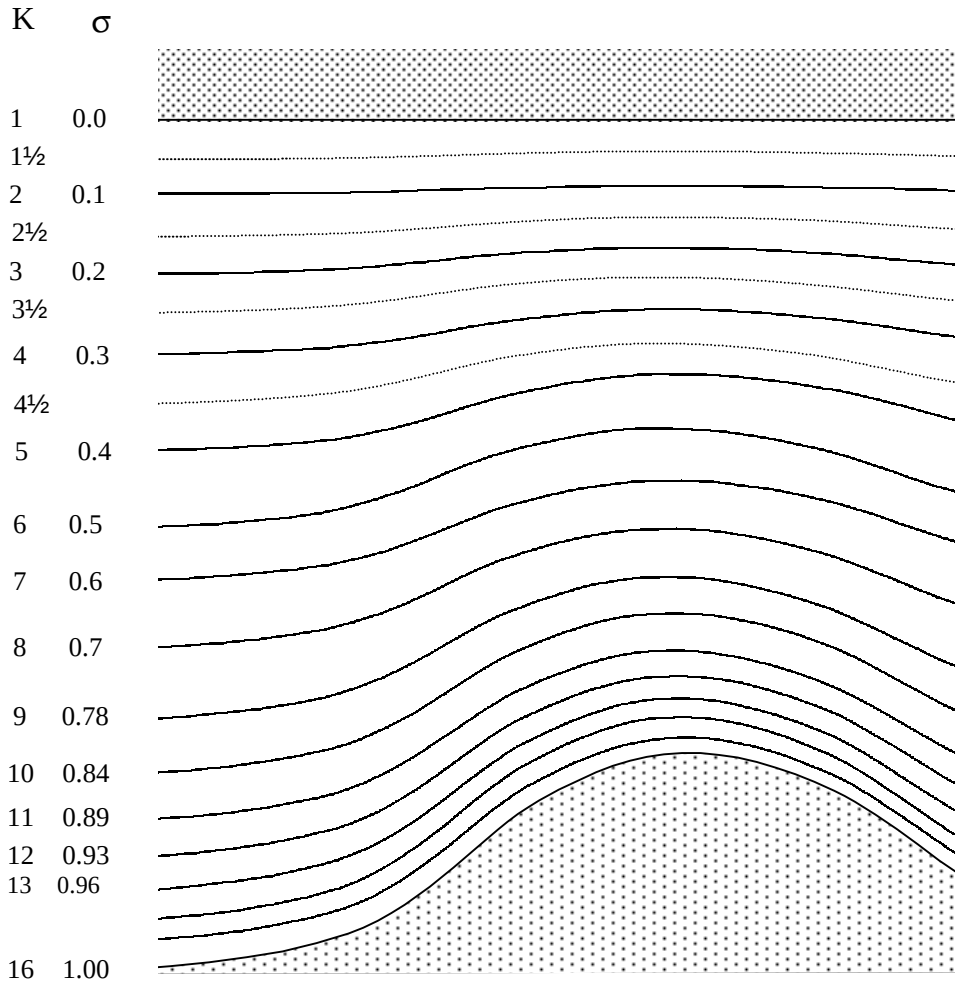

Figure 2.81: An example of sigma levels defined in a meteorological model

The meteorological model is run by the MM5 module, using the data set for initial and boundary conditions prepared by the previous modules.

Much of the mathematical formulation of meteorological models is based on the advection equation. This is demonstrated in fig.2.82 for the case of a smoke plume, but the principle is applicable to the transport of other physical properties such as temperature and pressure. The equation:

$$\frac{dN}{dt} = \frac{\partial N}{\partial t} + (v \cdot \nabla)N$$

or its three-dimensional expanded form:

$$\frac{dN}{dt} = \frac{\partial N}{\partial t} + u\frac{\partial N}{\partial x} + v\frac{\partial N}{\partial y} + w\frac{\partial N}{\partial x}$$

states that the rate of change of a property N depends on two factors:

- the rate at which the property is varying in the source region, which provides a base value
- the rate at which the base value varies as the point of measurement moves away from the source.

There is an assumption that the rates of change remain steady whilst the calculation is being made. In practice, this means that variations to the state of the system occur on a relatively long time scale compared to the time steps of the model. Typically an MM5 model recalculates for each 60sec. time step during the simulation.

The **continuity equation for air**, the **thermodynamic energy equation,** the **equation of state,** and the **momentum equations** make up the set of equations of atmospheric dynamics which form the core of the MM5 model. The significance of these functions is outlined on the following pages.

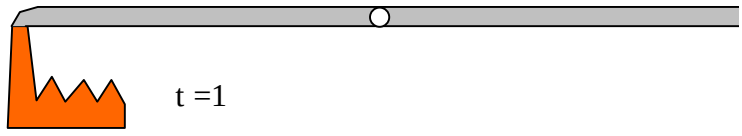

Concentration is constant with distance from the source at any time instant, but gradually changes with time.

The concentrations recorded at the moving sample point depend only on changes with time.

$$\frac{dN}{dt} = \frac{\partial N}{\partial t}$$

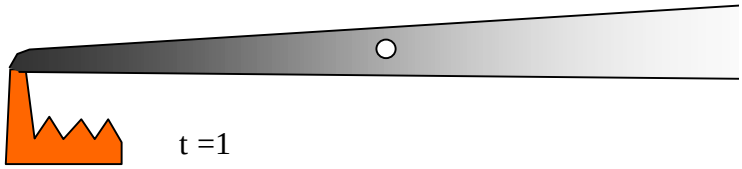

Concentration varies with distance from the source at any time instant, but the distribution remains constant with time.

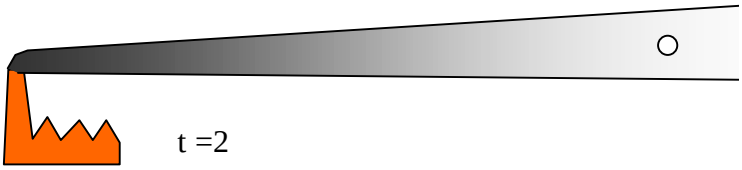

The concentrations recorded at the moving sample point depend only on the rate at which the concentration varies with position, and the velocity of the moving point.

$$\frac{dN}{dt} = u\frac{\partial N}{\partial x}$$

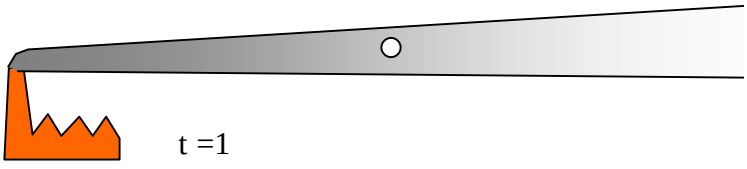

Concentration varies with distance from the source at any time instant, but the distribution also varies with time.

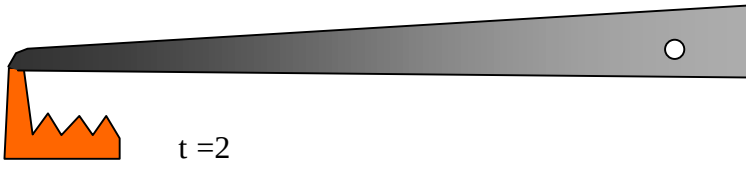

The concentrations recorded at the moving sample point depend on both the changes with time at a fixed point, and the rate at which the concentration varies with position at a fixed time.

$$\frac{dN}{dt} = \frac{\partial N}{\partial t} + u\frac{\partial N}{\partial x}$$

or for three coordinates:

$$\frac{dN}{dt} = \frac{\partial N}{\partial t} + (\mathbf{v}\cdot\nabla)N$$

Figure 2.82: The advection equation.

Equation of state

It is important to predict changes in temperature which accompany changes in pressure and volume, for example when an air mass expands as it rises to an altitude where atmospheric pressure is lower. The relationship between amount of gas, its pressure, volume and temperature is given by the Ideal gas law:

$$p = \frac{nRT}{V}$$

where p is pressure, n is the mass of gas, T is temperature, V is volume, and R is the Universal gas constant.

Thermodynamic energy equation

The First law of thermodynamics relates change in temperature of a gas to the energy transfer between the gas and its environment and the work done on or by the gas:

$$dQ = dU + dW$$

where dQ is the energy transferred, dU is the change in internal energy of the gas, and dW is work done. When the gas expands, work is done by the gas:

$$dW = \frac{p\ dV}{M} = p\ d\alpha$$

where M is the mass, V the volume and p the pressure.

$$\alpha = \frac{V}{M} = \frac{1}{\rho}$$

where α is the volume of a unit mass of air, known as the *specific volume*, which is the reciprocal of the density.

The change in internal energy of an air body is the change in temperature multiplied by the energy required to change its temperature by one degree:

$$dU = \left(\frac{\partial Q}{\partial T}\right) dT = c_v dT$$

where c_v is the specific heat of moist air at constant volume. This varies with the amount of water vapour in the air.

These results can be combined to give the First law of thermodynamics for the atmosphere:

$$dQ = c_v dT + p\ d\alpha$$

In an ***adiabatic*** process, no energy is transferred between the air parcel and its surroundings, so dQ = 0. The temperature of the parcel changes because of pressure variation as it ascends or descends. A rising parcel of air expands and cools, or a descending parcel of air compresses and warms according to the relation:

$$c_v dT = -p d\alpha$$

Continuity equation

An essential property of a meteorological model is that mass is conserved as air parcels move through the modelled region; mass is neither created nor destroyed. Continuity equations are a formulation of the requirements for conservation of mass.

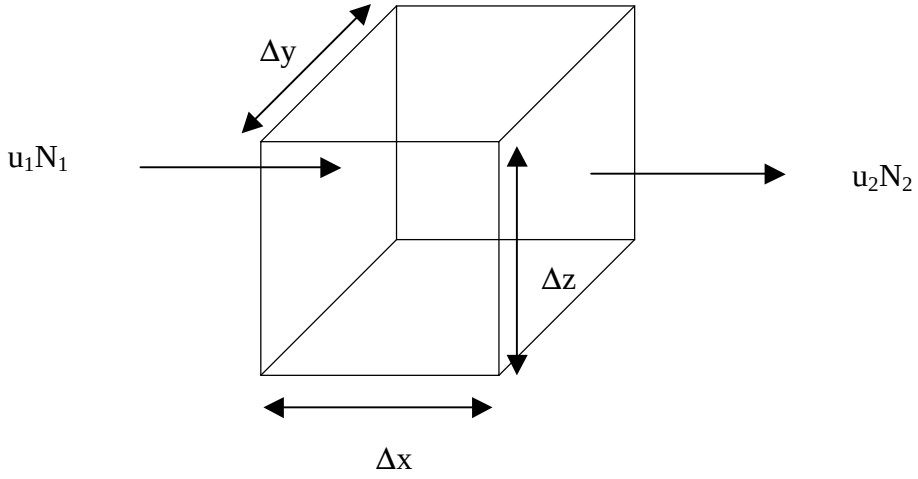

Fig 2.83: Gas flow through a cell

Fig.2.83 illustrates a cell through which a gas is passing in the x-direction. N represents gas concentration and u represents velocity. The rate of change of concentration of the gas within the cell must equal the difference between the inflow and outflow quantities of gas, as measured by the product of concentration N and flow rate u at the cell boundaries. It can be shown that:

$$\frac{\partial N}{\partial t} = -\frac{\partial (uN)}{\partial x}$$

Expanding to three dimensions:

$$\frac{\partial N}{\partial t} = -\frac{\partial (uN)}{\partial x} - \frac{\partial (uN)}{\partial y} - \frac{\partial (uN)}{\partial z} = -\nabla \cdot (\mathbf{v}N)$$

Momentum equations

In addition to mass, a model must ensure that momentum is conserved during air motions. The Momentum equation is used to predict wind velocity, and must balance the various forces which might act on an air body to affect its movement. These forces include: the *local acceleration*, the earth's *centrifugal force*, the apparent *Coriolis force*, *gravitational force*, *pressure-gradient force*, *viscous force* and *turbulent-flux divergence*.

When considering forces related to the motion of the earth, it is convenient to use spherical polar coordinates in preference to the normal cartesian coordinate system. The nomenclature for spherical polar coordinates is given in fig.2.84.

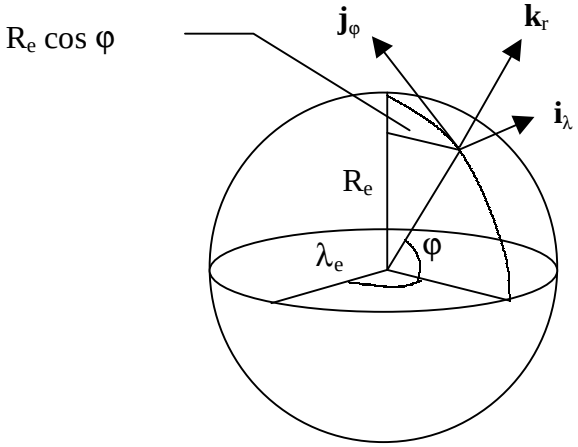

Figure 2.84: Spherical polar coordinates

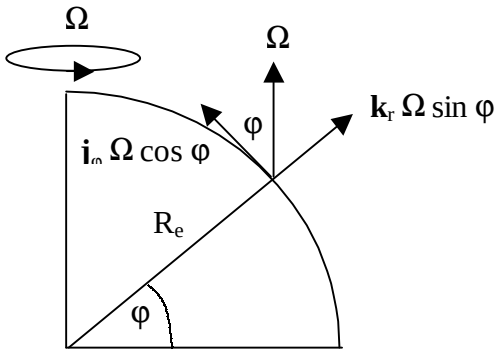

Figure 2.85: Components of the earth's angular velocity

The angular velocity $\boldsymbol{\Omega}$ of the earth is 7.292 x 10^{-5} radians s^{-1}. The components of the earth's angular velocity parellel and perpendicular to the surface are shown in fig.2.85, where φ is the latitude.

The ***Coriolis force*** deflects moving bodies towards the right in the northern hemisphere. It can be shown that the Coriolis acceleration is given by

$$\mathbf{a}_c = 2\boldsymbol{\Omega} \times \mathbf{v}$$

as twice the vector cross product of the earth's angular velocity with the local velocity of the body. There is no Coriolis force on a body which is stationary with respect to the earth's surface.

The ***centrifugal force*** is given by

$$\mathbf{a}_r = \boldsymbol{\Omega} \times (\boldsymbol{\Omega} \times \mathbf{R}_e)$$

where R_e is the radius vector of the earth. The effect of the double vector cross product is to determine the force direction as outwards from the earth's surface in a direction perpendicular to the axis of rotation.

From a reference frame fixed on the earth's surface, a momentum equation can be derived which relates local acceleration $\mathbf{a}_l$ to other accelerations and forces acting on an air mass:

$$\mathbf{a}_l + \mathbf{a}_c + \mathbf{a}_r = \frac{1}{M_a}\left(\mathbf{F}_g + \mathbf{F}_p + \mathbf{F}_v\right)$$

where $\mathbf{a}_c$ is the Coriolis acceleration, $\mathbf{a}_r$ is the centrifugal acceleration, $\mathbf{F}_g$ is the gravitational force, $\mathbf{F}_p$ is the pressure force, and $\mathbf{F}_v$ is the viscous force.

The ***local acceleration*** is given by the advection equation (fig.2.82) as:

$$\mathbf{a}_l = \frac{d\mathbf{v}}{dt} = \frac{\partial \mathbf{v}}{\partial t} + (\mathbf{v} \cdot \nabla)\mathbf{v}$$

The local acceleration of an air parcel equals the acceleration at a fixed source point plus a variation in local acceleration due to a velocity flux gradient along the line of motion.

The ***Gravitational force*** is given by:

$$\frac{F_g}{M_a} = \frac{GM_e}{R_e^2}$$

where M_e and M_a are the masses of the earth and the air mass respectively, R_e is the radius of the earth, and G is the gravitational constant.

The ***Pressure-gradient force*** is:

$$\frac{F_p}{M_a} = -\frac{1}{\rho_a}\nabla p_a = -\frac{1}{\rho_a}\left(\mathbf{i}\frac{\partial p_a}{\partial x} + \mathbf{j}\frac{\partial p_a}{\partial y} + \mathbf{k}\frac{\partial p_a}{\partial z}\right)$$

where ρ_a is air density. This expression specifies the rate of change of pressure in terms of components along the three cartesian axes.

The ***Viscous force*** is a measure of the resistance to motion of an air mass over the ground surface. The change of wind velocity with height ($\partial u/\partial z$) is known as the *wind shear*. This can produce a shear stress τ given by:

$$\tau = \eta \frac{\partial u}{\partial z}$$

where η is the dynamic viscosity of air.

Turbulent flux divergence occurs in first 300m above the ground where wind speeds may increase logarithmically with height and wind shear is strongly developed. Turbulence consists of many eddies of different sizes operating together. Eddies are created downwind of obstacles as turbulent wakes. Surface heating can also create thermal turbulence. Flux turbulence can be formulated as:

$$\frac{F_t}{M_a} = -\frac{1}{\rho_a}(\nabla \cdot \rho_a \mathbf{K}_m \nabla)\mathbf{v}$$

where **K** is the eddy diffusion coefficient tensor. The turbulence force opposing air motion is thus a function of the air flow velocity.

Combining the expressions for accelerations and forces gives the three **Momentum equations** in the cartesian directions. Ignoring the viscous force which is small in comparison to other terms:

$$\frac{du}{dt} = \frac{\partial u}{\partial t} + u\frac{\partial u}{\partial x} + v\frac{\partial u}{\partial y} + w\frac{\partial u}{\partial z} = fv - \frac{1}{\rho_a}\frac{\partial p_a}{\partial x} + \frac{1}{\rho_a} \times \left[\frac{\partial}{\partial x}\left(\rho_a K_{m,xx}\frac{\partial u}{\partial x}\right) + \frac{\partial}{\partial y}\left(\rho_a K_{m,yx}\frac{\partial u}{\partial y}\right) + \frac{\partial}{\partial z}\left(\rho_a K_{m,zx}\frac{\partial u}{\partial z}\right)\right]$$

$$\frac{dv}{dt} = \frac{\partial v}{\partial t} + u\frac{\partial v}{\partial x} + v\frac{\partial v}{\partial y} + w\frac{\partial v}{\partial z} = -fu - \frac{1}{\rho_a}\frac{\partial p_a}{\partial y} + \frac{1}{\rho_a} \times \left[\frac{\partial}{\partial x}\left(\rho_a K_{m,xy}\frac{\partial v}{\partial x}\right) + \frac{\partial}{\partial y}\left(\rho_a K_{m,yy}\frac{\partial v}{\partial y}\right) + \frac{\partial}{\partial z}\left(\rho_a K_{m,zy}\frac{\partial v}{\partial z}\right)\right]$$

$$\frac{dw}{dt} = \frac{\partial w}{\partial t} + u\frac{\partial w}{\partial x} + v\frac{\partial w}{\partial y} + w\frac{\partial w}{\partial z} = -g - \frac{1}{\rho_a}\frac{\partial p_a}{\partial z} + \frac{1}{\rho_a} \times \left[\frac{\partial}{\partial x}\left(\rho_a K_{m,xz}\frac{\partial w}{\partial x}\right) + \frac{\partial}{\partial y}\left(\rho_a K_{m,yz}\frac{\partial w}{\partial y}\right) + \frac{\partial}{\partial z}\left(\rho_a K_{m,zz}\frac{\partial w}{\partial z}\right)\right]$$

This completes the description of the **continuity equation for air**, the **thermodynamic energy equation,** the **equation of state,** and the **momentum equations,** which form the basis for the MM5 model core.

A central function of the MM5 model in its hydrological application is the determination of rainfall rates on a high resolution grid scale. Moisture and precipitation are handled by the determination of three mixing ratios:

Water vapour mixing ratio

$$\frac{\partial p^* q_v}{\partial t} = -m^2\left[\frac{\partial p^* u q_v / m}{\partial x} + \frac{\partial p^* u q_v / m}{\partial y}\right] - \frac{\partial p^* q_v \dot{\sigma}}{\partial \sigma} + \delta_{nh} q_v DIV + p^*\left(-P_{RE} - P_{CON} - P_{II} - P_{ID}\right) + D_{qv}$$

Cloud water mixing ratio

$$\frac{\partial p^* q_c}{\partial t} = -m^2\left[\frac{\partial p^* u q_c / m}{\partial x} + \frac{\partial p^* u q_c / m}{\partial y}\right] - \frac{\partial p^* q_c \dot{\sigma}}{\partial \sigma} + \delta_{nh} q_c DIV + p^*\left(P_{ID} + P_{II} - P_{RC} - P_{RA} + P_{CON}\right) + D_{qc}$$

Rain water mixing ratio

$$\frac{\partial p^* q_r}{\partial t} = -m^2\left[\frac{\partial p^* u q_r / m}{\partial x} + \frac{\partial p^* u q_r / m}{\partial y}\right] - \frac{\partial p^* q_r \dot{\sigma}}{\partial \sigma} + \delta_{nh} q_r DIV - \frac{\partial V_f \rho g q_r}{\partial \sigma} + p^*(P_{RE} + P_{RC} + P_{RA}) + D_{qr}$$

These equations include a range of physical processes involving water phase conversion:

P_{RE} is evaporation of rain drops,

P_{CON} is condensation of water vapour,

P_{II} is initiation of ice crystals,

P_{ID} is deposition of vapour onto ice crystals,

P_{RC} is conversion of cloud drops to rain drops,

P_{RA} is accretion of cloud drops by rain drops.

The basic model provides for condensation whenever relative humidity reaches 100%, with subsequent production of raindrops and fallout under gravity. The model successfully handles seeder-feeder mechanisms, where raindrops produced in high cloud layers fall through lower saturated air and increase their volume. Advection of raindrops during descent to the ground surface is also handled correctly.

Rain accretion rate is calculated from

$$P_{RA} = \frac{1}{4}\pi\rho a q_c E N_0 \frac{\Gamma(3+b)}{\lambda^{3+b}}$$

where parameter **a** has a value of 842.99 for rain or 11.72 for snow, parameter **b** has a value of 0.8 for rain or 0.41 for snow, and Γ is the gamma- function. The parameter $N_0 = 8 \times 10^6$ for rain, 2×10^7 for snow. q_c is the cloud water mixing ratio.

The fall speed of rain is calculated from

$$V_f = a\frac{\Gamma(4+b)}{6}\lambda^{-b}$$

where

$$\lambda = \left(\frac{\pi N_0 \rho_w}{\rho q_r}\right)^{1/4}$$

Modelling of thunderstorm events where vertical motions are dominant presents a greater modelling challenge. MM5 offers a series of cumulus parameterisation schemes to model rainfall generation. The principle of cumulus parameterisation is that convective motion can take place on a scale smaller than a model grid cell. Whilst the mean relative humidity within a cell may not reach 100%, there may be zones within the cell where water vapour is concentrated and condensation may occur (figure 2.86). Condensation will produce rainfall, but also releases latent heat which can drive upward convection.

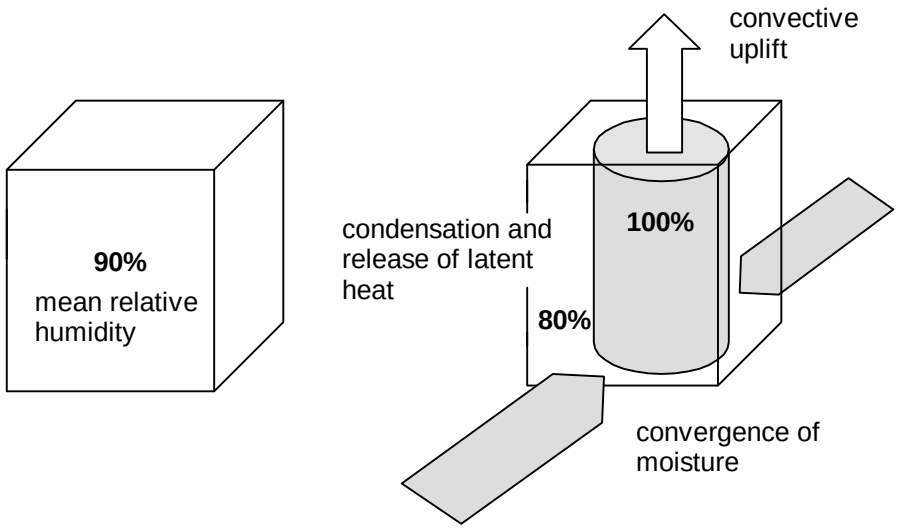

Figure 2.86: Principles of the Anthes-Kuo cumulus parameterisation scheme

The simplest cumulus parameterisation is the Anthes-Kuo scheme (Anthes, 1976; Kuo and Raymond, 1980). The is based on an analysis of water vapour flux in the zone of convection (fig.2.87). An algorithm estimates the rate of convergence of moisture M_t at the boundaries of a grid call using:

$$M_t = -\frac{1}{g}\int_{.0}^{p_s} \nabla \cdot \overline{\mathbf{V}}\overline{q}\,dp$$

where p_s is surface pressure, $\overline{\mathbf{V}}$ is mean horizontal air velocity, $\bar{q}$ is mean specific humidity and g is gravity force. If moisture convergence is above a threshold value of 3×10^{-5} kg m^{-2} s^{-1} then the temperatures for grid cells in the overlying vertical air column are checked to determine if convection is possible.

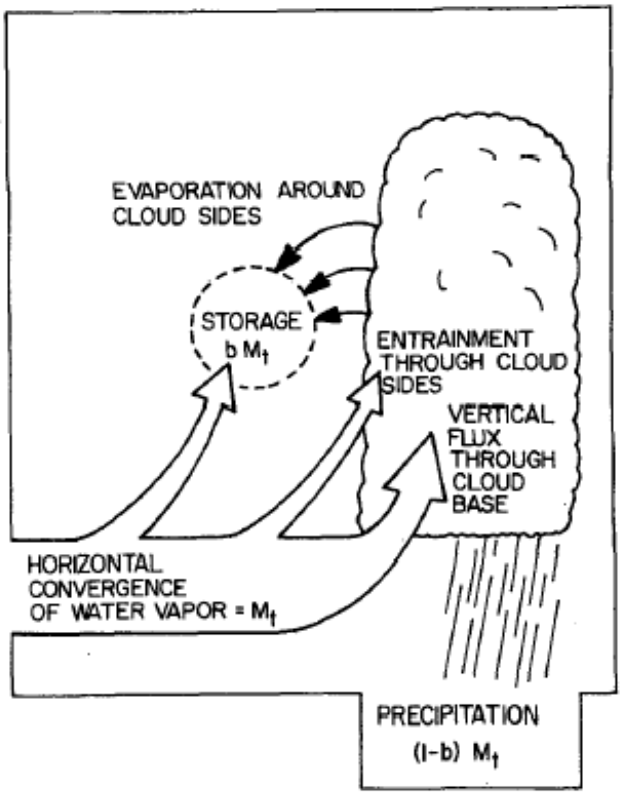

Figure 2.87: Schematic diagram showing moisture cycle in a column which contains convection. Figure and caption from: Anthes, 1977

The base and top level of cloud is then determined. Convection is assumed if the cloud depth is greater than a critical value $\Delta\sigma \geq 0.3$.

Vertical air motion is computed from:

$$\frac{dw^2/2}{dz} = \frac{gB}{(1+\alpha)} - gQ_{lw} - \mu w^2$$

where: w is vertical air velocity, B is buoyancy, $\alpha = 0.5$ is a compensating factor to allow for non-hydrostatic pressure perturbations, Q_{lw} is total liquid water as the ratio of mass of water to mass of air, and μ is the rate of entrainment of air from the environment around the convection cell. This equation shows that vertical ascent velocity in a convecting cloud is related to buoyancy of the air parcel, but counteracted by the weight of liquid water being carried upwards and by the amount

of entrained air which reduces the contrast in physical properties between the cloud and its surrounding air mass. The buoyancy term is given by:

$$B = \frac{T_v - T_{ve}}{T_{ve}}$$

where T_v is the virtual temperature of the convective updraft at a particular pressure level within the cloud, and T_{ve} is the virtual temperature of the surrounding airmass at the same pressure level.

A theoretical temperature function within the convecting column is used to calculate condensation and rainfall production. It is found from atmospheric soundings that convective heating often has a parabolic shape with a maximum in the upper half of the cloud (fig.2.88).

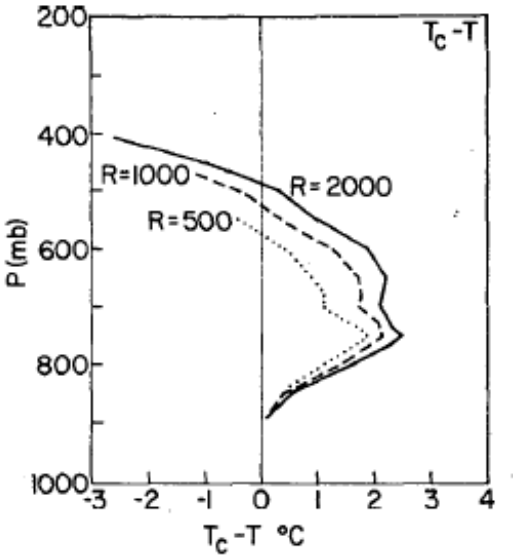

Figure 2.88: Vertical profile of (T_c–T) in three clouds of radii 500, 1000 and 2000m. The environment sounding was that for Pittsburgh, Pa., 1200 GMT 25 May 1976.
Figure and caption from:
Anthes, 1977

Tc: cloud virtual temperature
T: environment virtual temperature

The water vapour mixing ratio within cells is reduced to compensate for rainfall production, and the temperature is increased to allow for latent heat released during condensation.

An alternative convective scheme within the MM5 system is Grell cumulus parameterisation. This is a more sophisticated scheme in which individual clouds are modelled, along with the mechanisms of rainfall generation within them (figure 2.89).

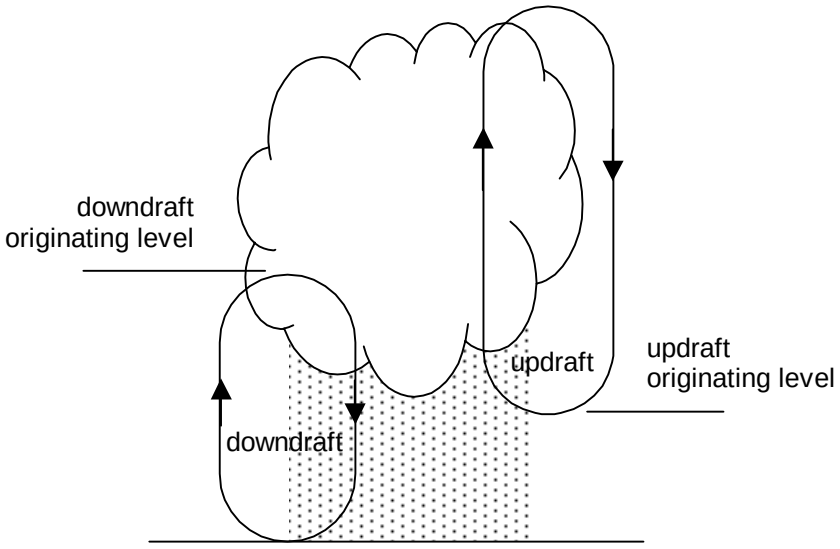

Figure 2.89: Air movements within a cloud, modelled by the Grell cumulus scheme. After: Grell, Dudhia and Stauffer (1995)

In the Grell scheme, clouds are modelled as two steady-state circulations, caused by an updraft and a downdraft. There is no entrainment of environmental air into the cloud except at the top and bottom of the circulations.

Warming occurs through condensation from ascending saturated air as it cools, but evaporation and re-absorption of water vapour can take place in descending air as it warms adiabatically. An energy budget balances these effects, with rainfall being generated from cloud water which escapes reabsorption.

Configuring and running the MM5 model

Running the MM5 module involves several stages:

- The input files from the TERRAIN and INTERPF modules are placed in a directory where they can be accessed by the MM5 program.
- An MM5 program is built specially for the current run. When creating this program, it is necessary to specify the number of nested domains which will be modelled, and the type of computer system in use.
- A file of options is created, which will be accessed by the program while it is running. This file specifies a range of parameters including: details of the domain grid sizes, choices of cumulus schemes and planetary boundary layer schemes, and options for the complexity with which phase changes between water vapour, liquid water and ice crystals will be handled when modelling cloud microphysics.
- The MM5 program is run. This generates a series of output files for chosen time intervals, representing conditions within each of the nested domains. A finite difference scheme is used within MM5 to model the progression of pressure, momentum and temperature across the modelling domain. At intervals, new observational values for these parameters will be supplied to the outer boundary. Cells within the outer rows of the model will then be progressively nudged towards the boundary values, to avoid the model diverging from observations over an extended simulation period.

GRAPH, RIP and VIS5D modules

Once a run is completed, several modules are available for producing graphical output from the domain data files:

- GRAPH is a simple plotting program for line drawings, which generates maps, cross sections and skew-T plots.
- RIP is a more flexible package which produces colour shaded images (Stoelinga, 2003). This has been used for most MM5 example data displayed in this chapter.
- VIS5D produces three-dimensional solid images, and may be used to display patterns of cloud and rainfall using isosurfaces.

Methods for creating graphical output with these packages are outlined in Appendix 4.

INTERPB module

The INTERPB module can convert MM5 output files from sigma coordinates back to pressure level (mb) data. This provides a facility for repeating the modelling cycle after addition of further meteorological observations through the LITTLE_R module.

Frontal rainfall events

Testing of the MM5 system has been carried out using a simulation of 6 hour forecasting mode. Global gridded data is updated at 6 hour intervals by US National Centre for Environmental Protection (NCEP) and distributed to forecasters via the Internet FTP service.

The MM5 model was run for the example storms presented in Chapter 2.2:

- 8 November 2002
- 29 December 2002
- 22 May 2003
- 2-4 February 2004

using data files which would have been available 6 hours in advance. Results from the model could then be evaluated against the raingauge data recorded in the catchment during the actual storm event. The objectives of the test were:

- to determine whether the high resolution 1km grid MM5 model was able to distinguish the Types A and B rainfall patterns observed over the Mawddach catchment,
- to determine whether the rainfall intensities predicted were consistent with gauge readings.

In examining the rainfall distribution maps which follow, it should be appreciated that the raingauge distribution across the Mawddach catchment is still relatively sparse for a mountain area liable to microclimate effects. The field maps were prepared from raingauge data before modelling was carried out. They represent only one interpretation of the rainfall distribution, and in some cases substantial changes to the positions of isohyets could be made to improve correspondence with the MM5 results whilst still remaining consistent with observations. Absolutely accurate field data on a 1km grid scale is not currently available for full evaluation of the rainfall forecast model.

In the following sections, predicted rainfall totals for 3-hour periods are compared with rain gauge data collected for the same periods during the storm events:

8 November 2002

A sequence of MM5 3-hour rainfall simulations for 8 November 2002 are shown in fig.2.90, with raingauge data covering the same periods for comparison.

The 03h – 06h simulation correctly identifies a type B rainfall pattern along the axis of the Rhinog mountain range, but also predicts high rainfall (9.69mm) over the Arennig mountains. There is some uncertainty about the actual rainfall pattern in the Arennig area as no gauges were present on the upper mountain slopes.

The 06h – 09h simulation shows rainfall becoming widespread across the Mawddach catchment, with maximums of approximately 10mm along the Rhinog range. A rainfall high of 11.5mm recorded for Cader Idris is beyond the geographical limit of the raingauge array, so there is uncertainty about true rainfall totals in this area.

The 09h – 12h simulation shows the rainfall axis moving eastwards to Coed y Brenin, although maximums of around 14mm are lower than the gauge readings of 21-23mm in this area. A maximum is again predicted over the ungauged summit of Cader Idris where verification is not available.

The 12h – 15h simulation correctly demonstrates a shift to a type A rainfall distribution extending inland across the catchment. Insufficient gauge data is available to verify the maximum of 17.92mm near the southern end of the Rhinog range. A predicted maximum of around 12mm in the vicinity of Rhobell Fawr and Pared yr Ychain is, however, considerably lower than the observed totals of 20-28mm.

The MM5 rainfall simulation for the 8 November 2002 storm event has reproduced approximately correct patterns of precipitation over the Mawddach catchment, although rainfall predictions are significantly lower than observed rainfall totals for some time periods at inland locations.

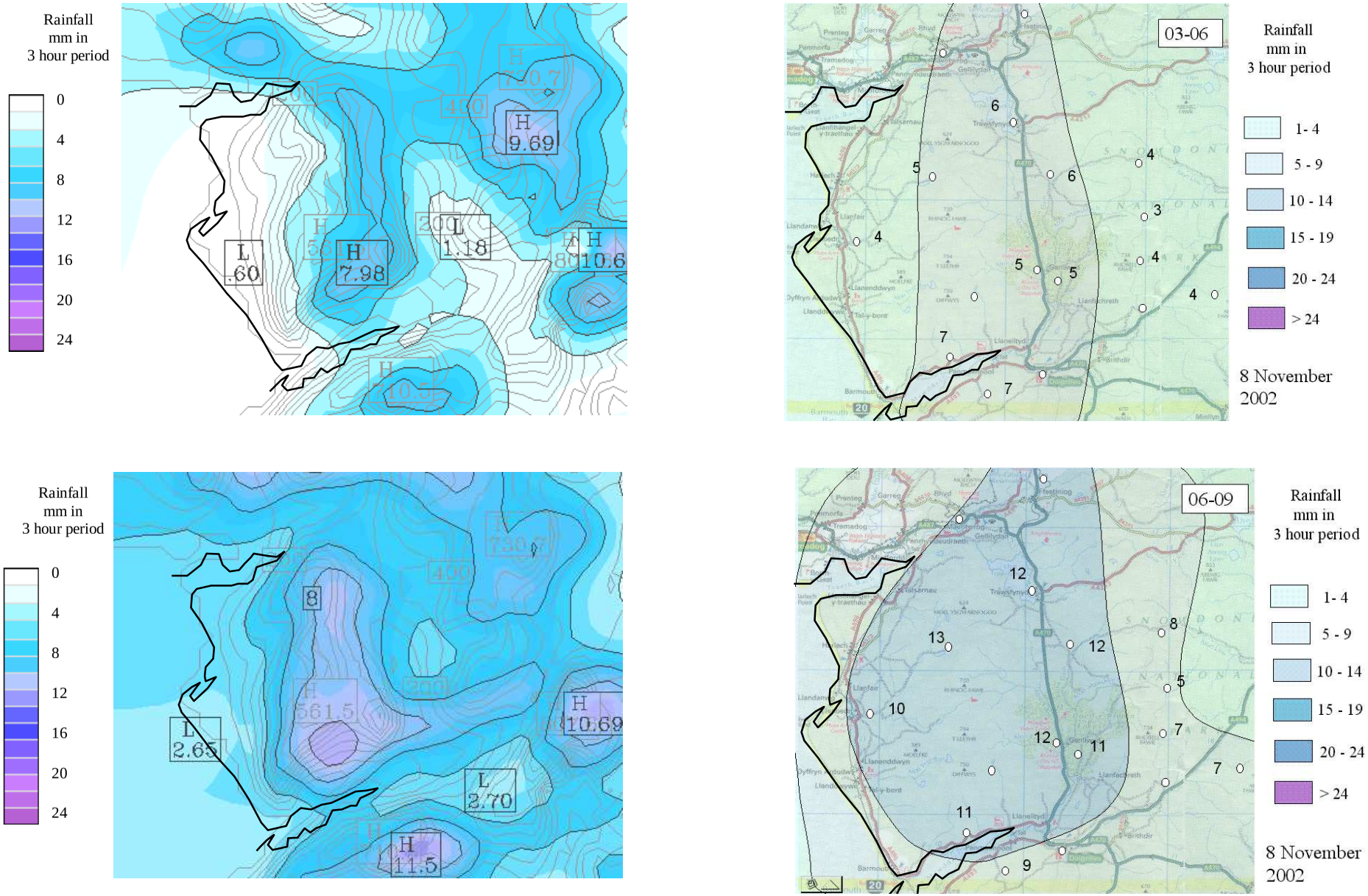

Figure 2.90: MM5 3-hour rainfall simulations (left) and 3-hour raingauge totals (right): Above: 03:00h – 06:00h, 8 November 2002 Below: 06:00h – 09:00h, 8 November 2002

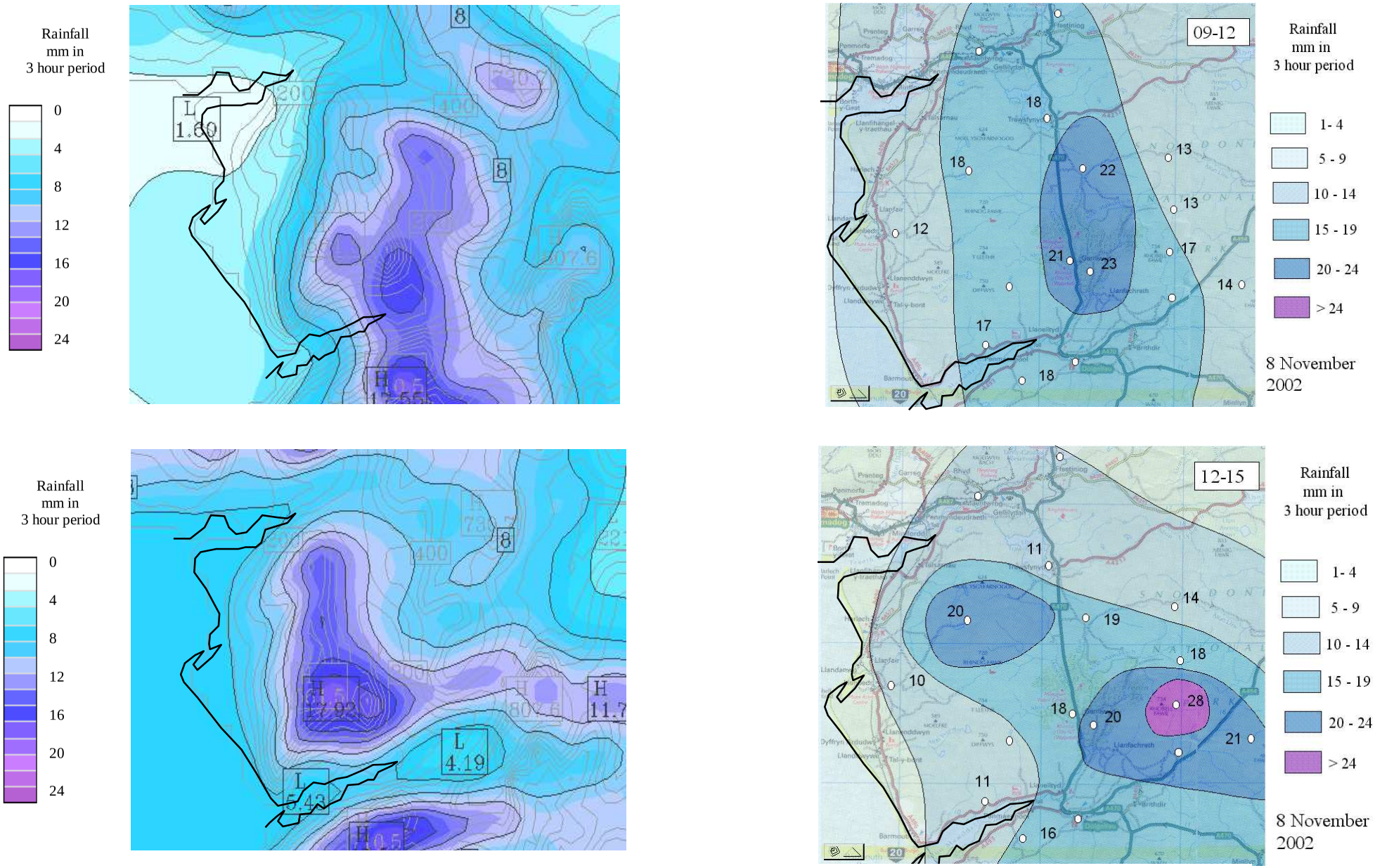

Figure 2.90(cont.) MM5 3-hour rainfall simulations (left) and 3-hour raingauge totals (right): Above: 09:00h – 12:00h, 8 November 2002 Below: 12:00h – 15:00h, 8 November 2002

29 December 2002

MM5 3-hour rainfall simulations and 3-hour raingauge totals for 29 December 2002 are shown in fig.2.91.

The 06h – 09h simulation correctly identifies a broad band of rainfall across the catchment. A maximum of 11.56mm at the southern end of the Rhinog range is consistent with the limited raingauge data available. A zone of high rainfall is predicted for the Aran ridge along the southern margins of the Mawddach catchment, which agrees with the 11mm gauge reading at Pared yr Ychain. Insufficient data is available to verify the south western continuation of this high rainfall zone.

The 09h – 12h simulation predicts an intensification of rainfall across the whole catchment, with a maximum on the inland slopes of the Rhinog mountains. This is broadly in agreement with the rain gauge data. The exact rainfall total at the southern end of the Rhinog range is uncertain due to lack of recordings.

The 15h – 18h simulation shows an inland rainfall maximum of 18.14mm at Pared yr Ychain which is close to the observed total of 20mm. A rainfall maximum is aligned north-south along the Rhinog range, but a lack of raingauge data prevents verification of the prediction. The observed total of 18mm at Trawsfynydd is roughly consistent with the simulated value of 15mm at this point.

The 18h – 21h simulation is roughly in agreement with the observed data. A type A pattern is generated, with maxima in the areas of Trawsfynydd and Pared yr Ychain. A low rainfall zone between these maxima appears in the simulation, but was not observed in the field data where a more consistent band of high rainfall crosses the catchment.

As in the previous case of 8 November 2002, the 29 December 2002 simulation produces rainfall patterns which are largely consistent with field observations. Some local variance occurs, particularly in the central area of the catchment for some time intervals. Predicted rainfall totals are, however, closer to observed values than in the November case and no significant underestimation of inland rainfall occurs.

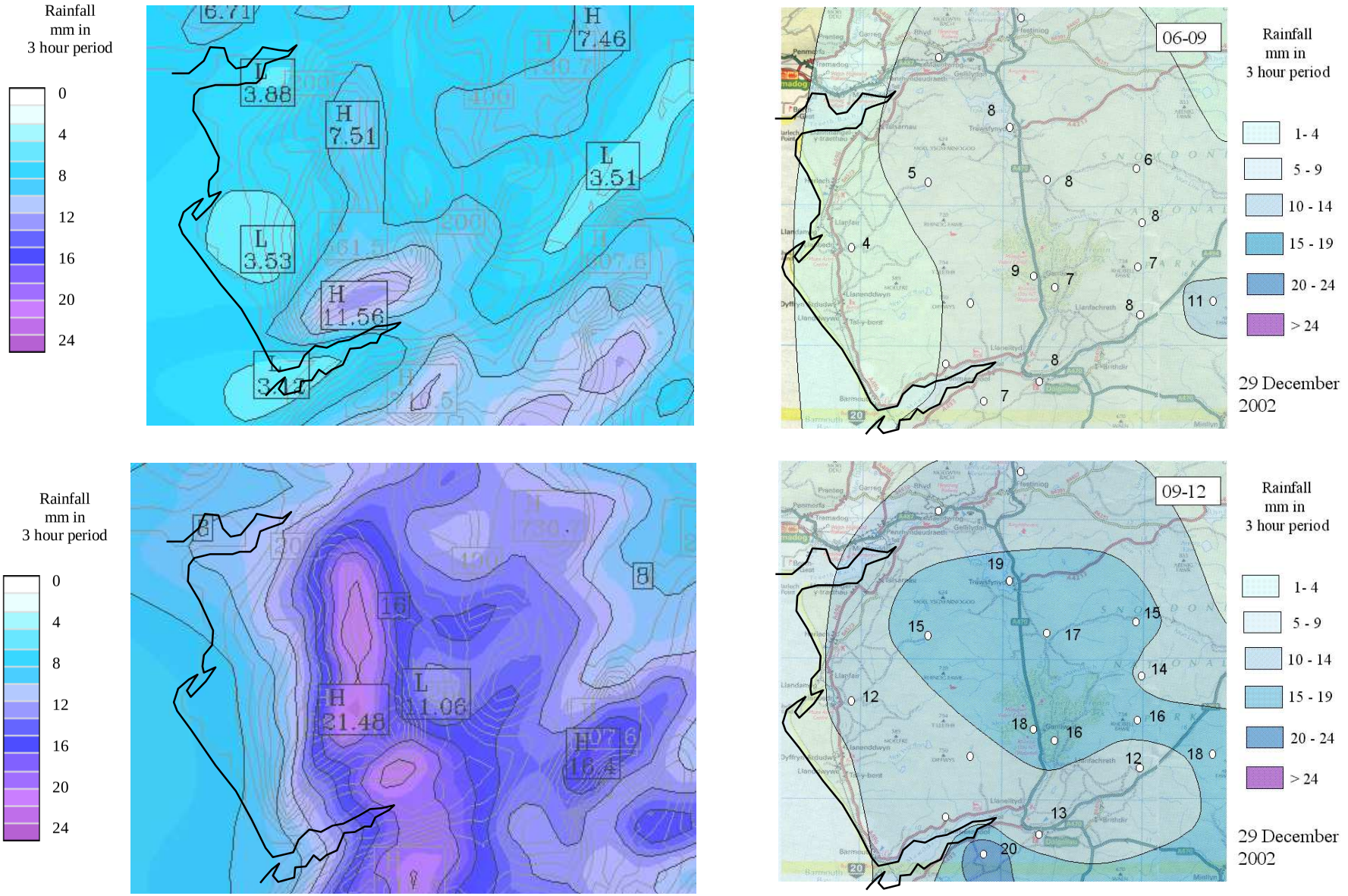

Figure 2.91: MM5 3-hour rainfall simulations (left) and 3-hour raingauge totals (right): Above: 06:00h – 09:00h, 29 December 2002 Below: 09:00h – 12:00h, 29 December 2002

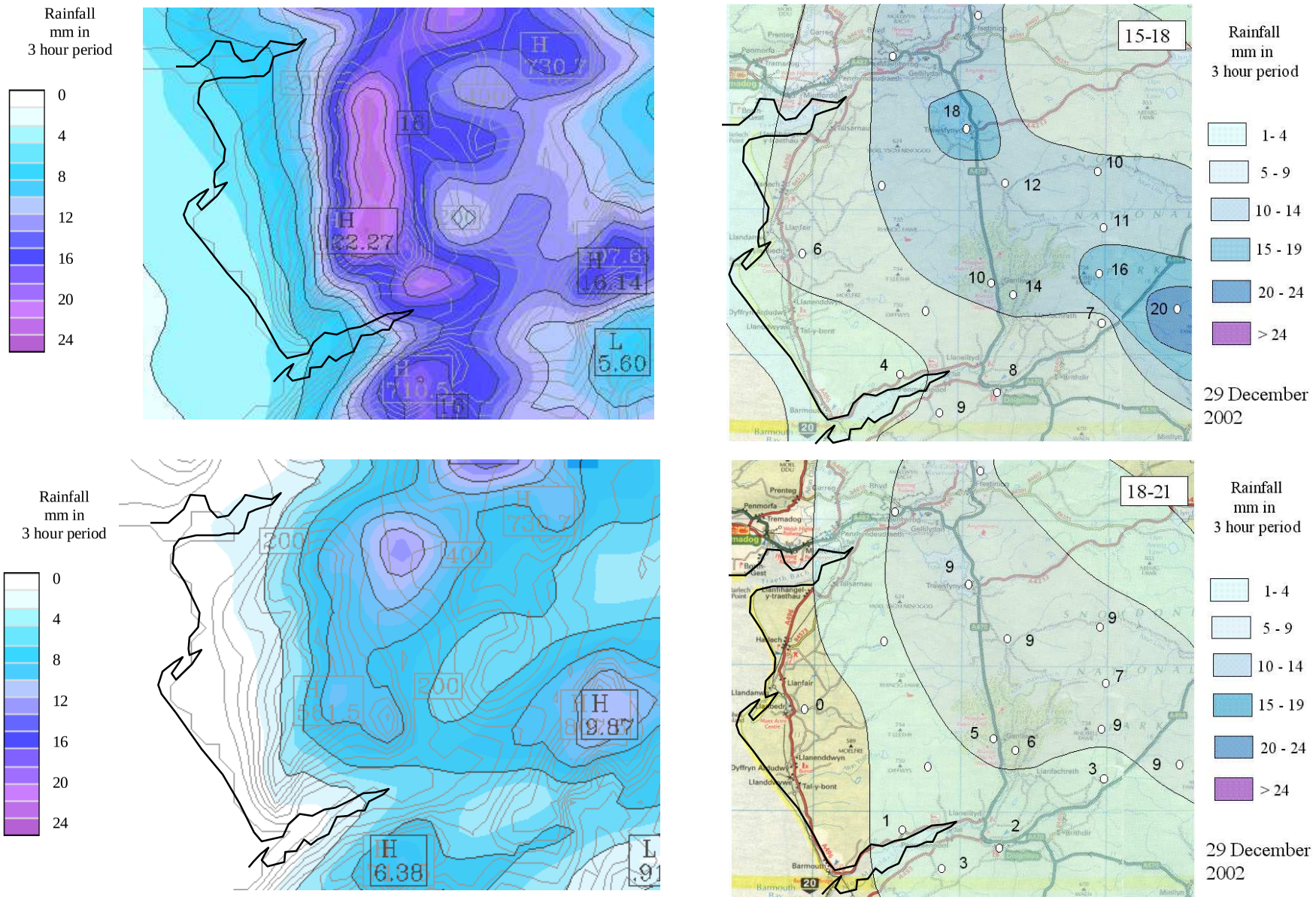

Figure 2.91 (cont.) MM5 3-hour rainfall simulations (left) and 3-hour raingauge totals (right):
Above: 15:00h – 18:00h, 29 December 2002 Below: 18:00h – 21:00h, 29 December 2002

22 May 2003

MM5 3-hour rainfall simulations and 3-hour raingauge totals for 22 May 2003 are shown in fig.2.92.

The 03h-06h simulation identifies the commencement of widespread rainfall. Values of approximately 5mm across much of the Mawddach catchment are a little higher than recorded values of 2-4mm. A zone of higher rainfall intensity over the southern Rhinog mountains is consistent with gauge readings, though a second rainfall high of 7.94mm in the Pared yr Ychain area was not recorded in the field. A rainfall total of 8mm is, however, recorded for Pared yr Ychain during the following 3-hour period which is not reflected in the simulated rainfall pattern. This seems to be an instance of the model rainfall timing being a little earlier than actually occurred.

The 06h-09h simulation correctly positions a type B pattern of high rainfall over the Rhinog mountain range, with a 3-hour maximum of 23.37mm close to the highest gauge reading of 26mm. A southwards extension of the high rainfall zone over Cader Idris cannot be verified due to lack of gauge data.

The 12h-15h simulation shows transition to a type A rainfall pattern, with the zone of high rainfall intensity extending inland across the catchment to the Pared yr Ychain area. 3-hour rainfall values are approximately in agreement with gauge readings: a modelled maximum of 26.38mm in the southern Rhinog range is close to the observed maximum of 30mm, and both the model and field data give maximums around 17mm at Pared yr Ychain. Some minor differences in detail occur around Coed y Brenin in the central area of the catchment.

The 15h-18h simulation indicates a decline in rainfall towards the end of the storm event, though not as rapid a reduction as observed from gauge readings. There again appears to be some discrepancy in timing, in the order of one hour, between the model and actual rainfall.

The MM5 simulation for the 22 May 2003 storm event has been quite successful in identifying the main patterns and intensities of rainfall across the Mawddach catchment.

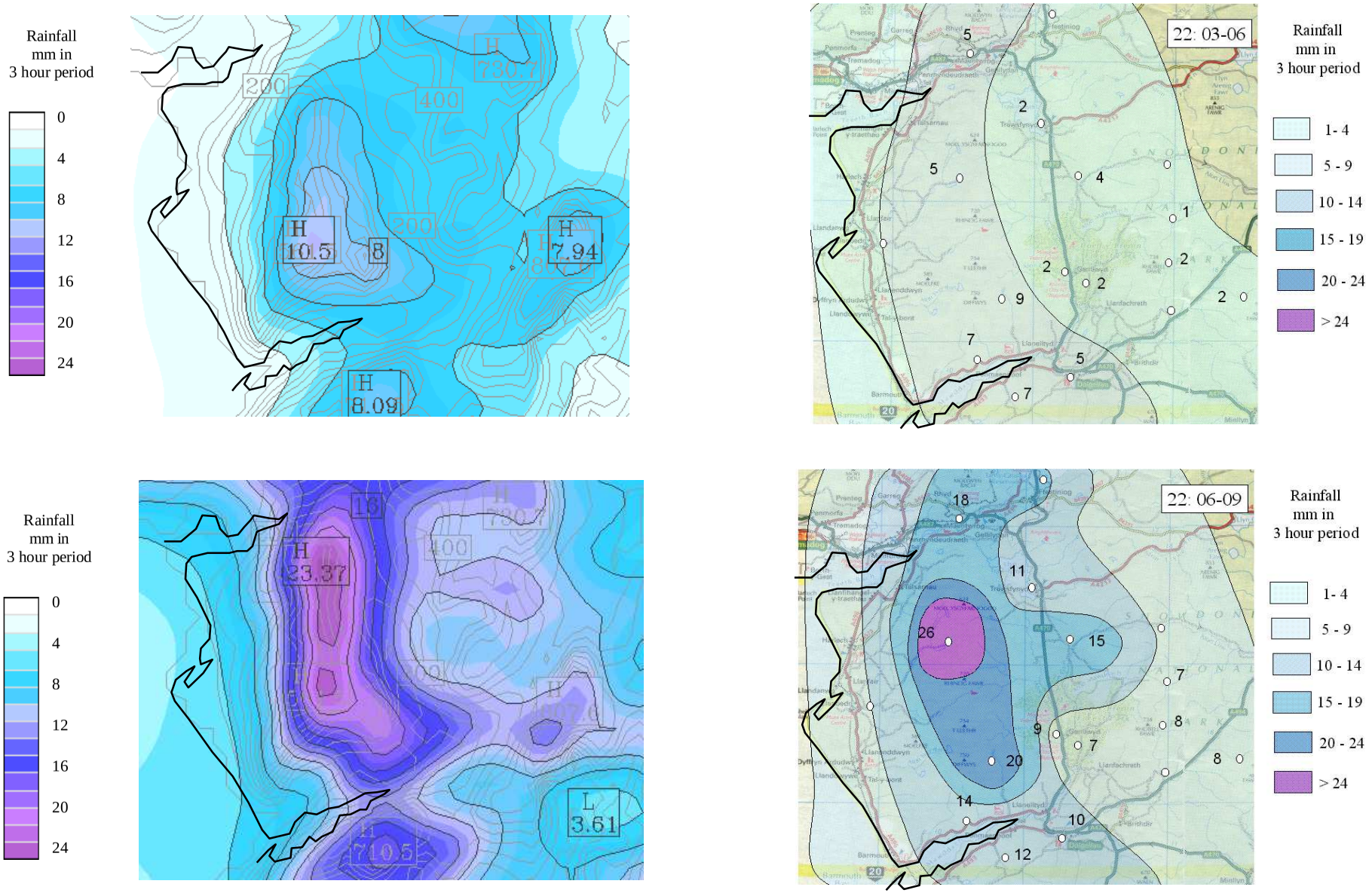

Figure 2.92: MM5 3-hour rainfall simulations (left) and 3-hour raingauge totals (right): Above: 03:00h – 06:00h, 22 May 2003 Below: 06:00h – 09:00h, 22 May 2003

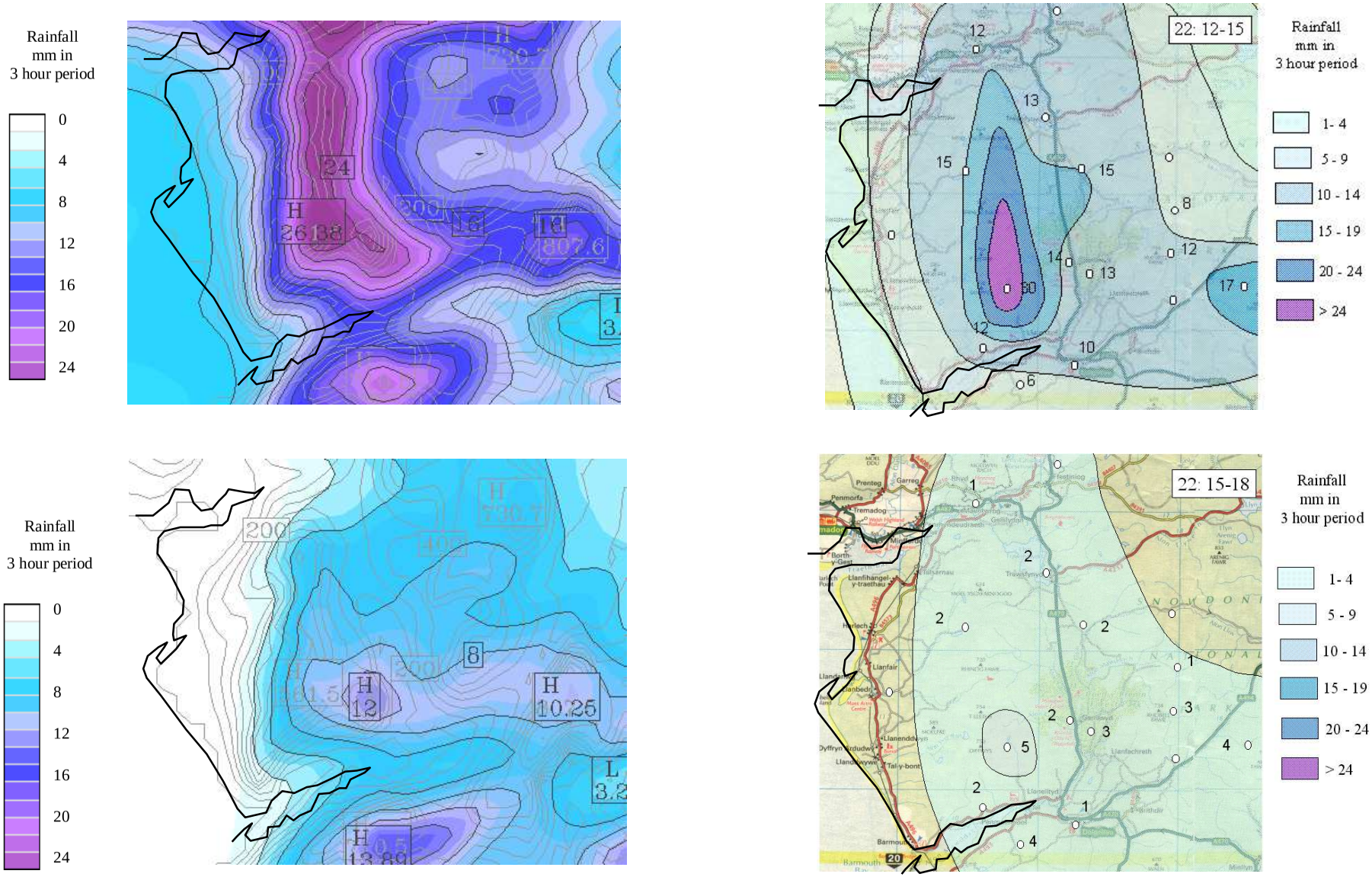

Figure 2.92(cont.) MM5 3-hour rainfall simulations (left) and 3-hour raingauge totals (right): Above: 12:00h – 15:00h, 22 May 2003 Below: 15:00h – 18:00h, 22 May 2003

2-4 February 2004

The Mawddach catchment was subjected to major flooding during the period 2-4 February 2004. An MM5 rainfall simulation of this event will be used as input for evaluation of the integrated hydrological model in Chapter 4.

The February 2-4 rainfall simulation is illustrated in fig.2.94. For much of the period, conveyors of ascending warm moist air were generating rainfall over the Mawddach catchment. Output from the MM5 model has been examined by plotting three-dimensional images with the post-processor program Vis5D (Hibbard and Kellum, 2005). An example is shown in fig.2.93 which illustrates zones of high cloud mixing ratio (yellow) and high rainfall mixing ratio (blue). This shows well the development of stratiform cloud inland from Cardigan Bay, with downwards enhancement of rainfall over the Mawddach catchment through the seeder-feeder mechanism.

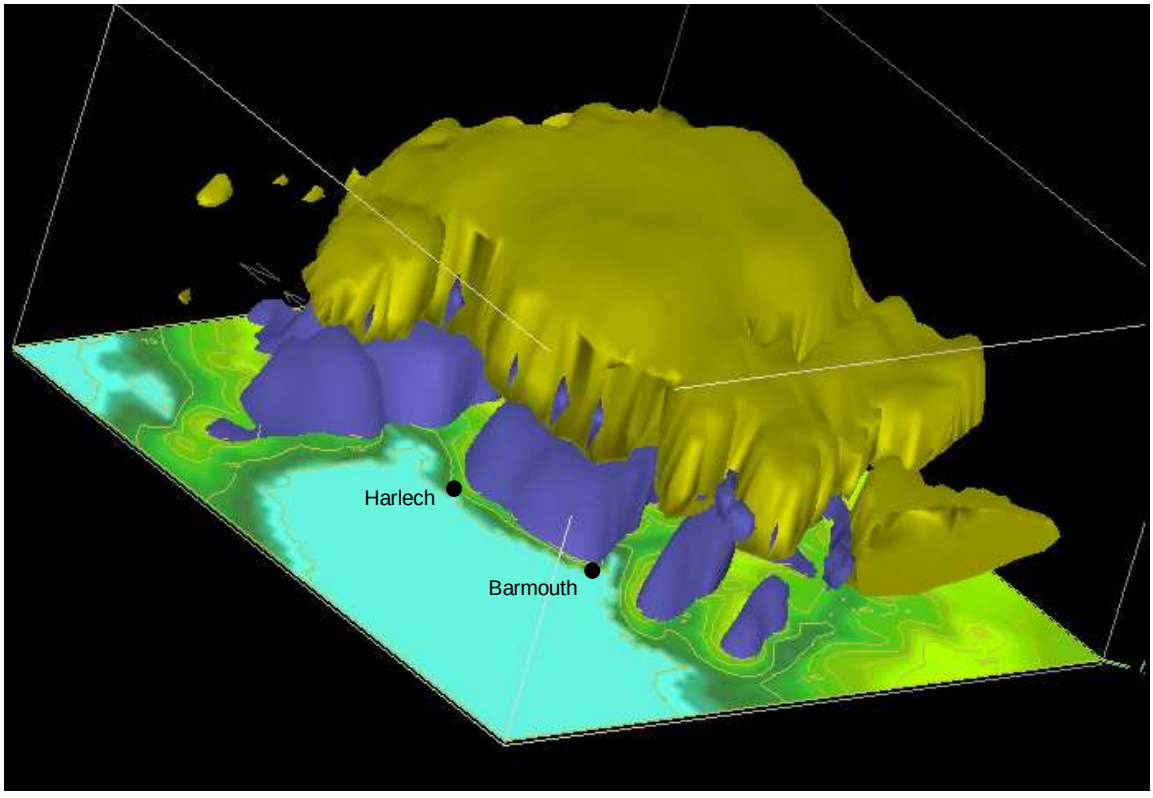

Figure 2.93: Zones of mixing ratios >0.4 for cloud (yellow) and rainfall (blue), 06:00h, 3 February 2004.

The MM5 simulation period 03h-06h on 2 February shows correctly a type A rainfall pattern extending across the catchment. A maximum 3-hour rainfall prediction of 16.81mm is close to the 18mm gauge reading in the southern Rhinog mountains.

Continuation of rainfall in the period 00h-03h on 3 February shows a simulated total of 20.65mm in the Arennig mountains and 19.51mm at Pared yr Ychain. These totals are higher than observations, although the distribution of rainfall across the catchment is similar to the actual rainfall pattern.

Rainfall simulations for the three periods covering 03h to 12h on 3 February are in reasonable agreement with raingauge records. A zone of low rainfall is predicted along the Wnion valley, and can be seen as a thinning of the stratiform cloud in the Vis5D plot of fig.2.93. This low rainfall zone is consistent with the limited raingauge data available for the Wnion valley.

Rainfall continued on 4 February, to reach a maximum intensity during the period 12h-15h which was concentrated inland of the Rhinog mountains as a type A distribution across the Mawddach catchment. This distribution is reasonably represented by the simulation. An axis of low rainfall along the Mawddach estuary and Wnion valley is again predicted, and would be consistent with the limited raingauge readings available.

For the 2-4 February 2006 storm period, the MM5 simulation is in reasonable agreement with raingauge data. The patterns of rainfall across the Mawddach catchment have been plausibly predicted, although some simulated rainfall totals are greater than actual recordings from raingauges.

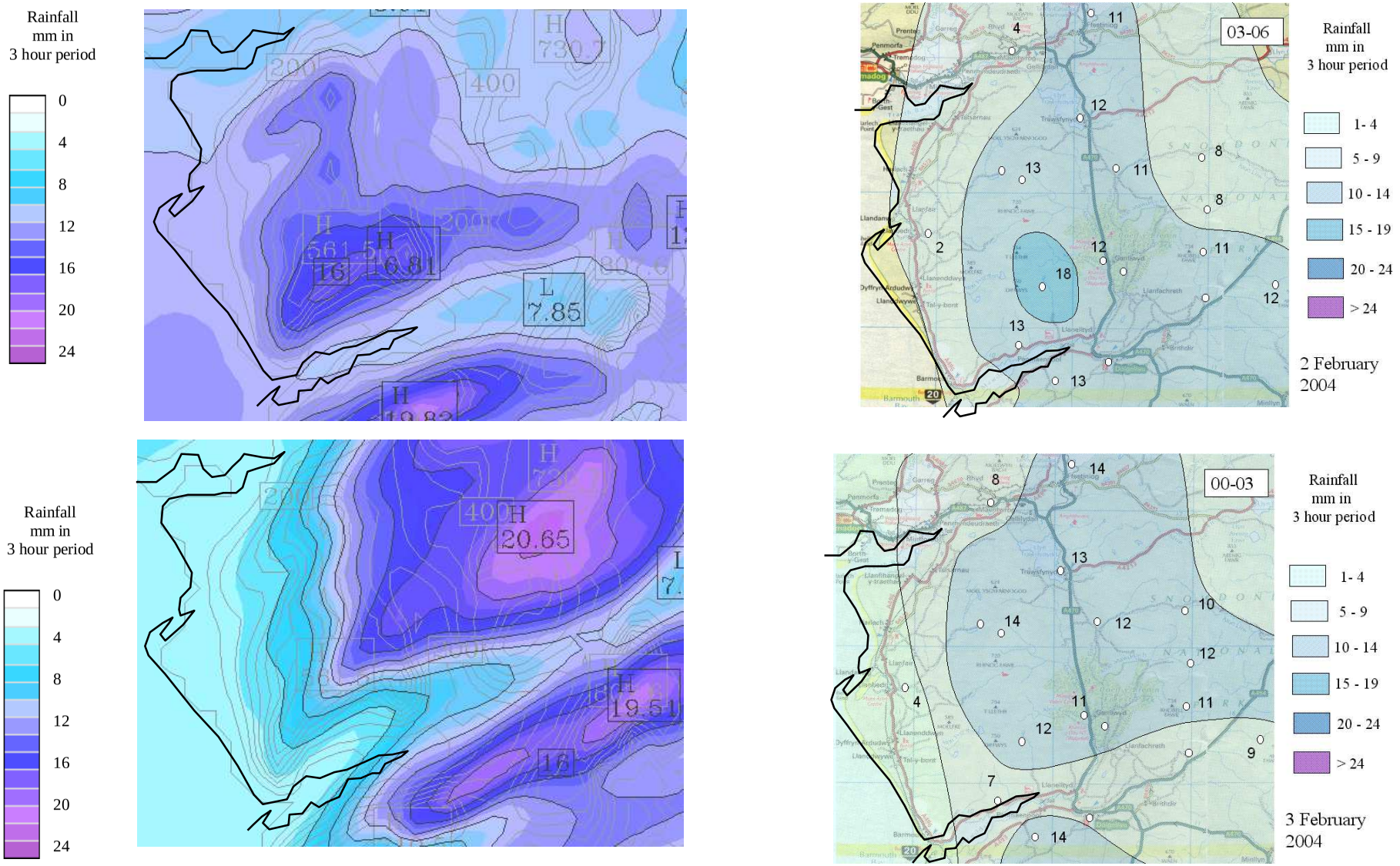

Figure 2.94: MM5 3-hour rainfall simulations (left) and 3-hour raingauge totals (right): Above: 03:00h – 06:00h, 2 February 2004 Below: 00:00h – 03:00h, 3 February 2004

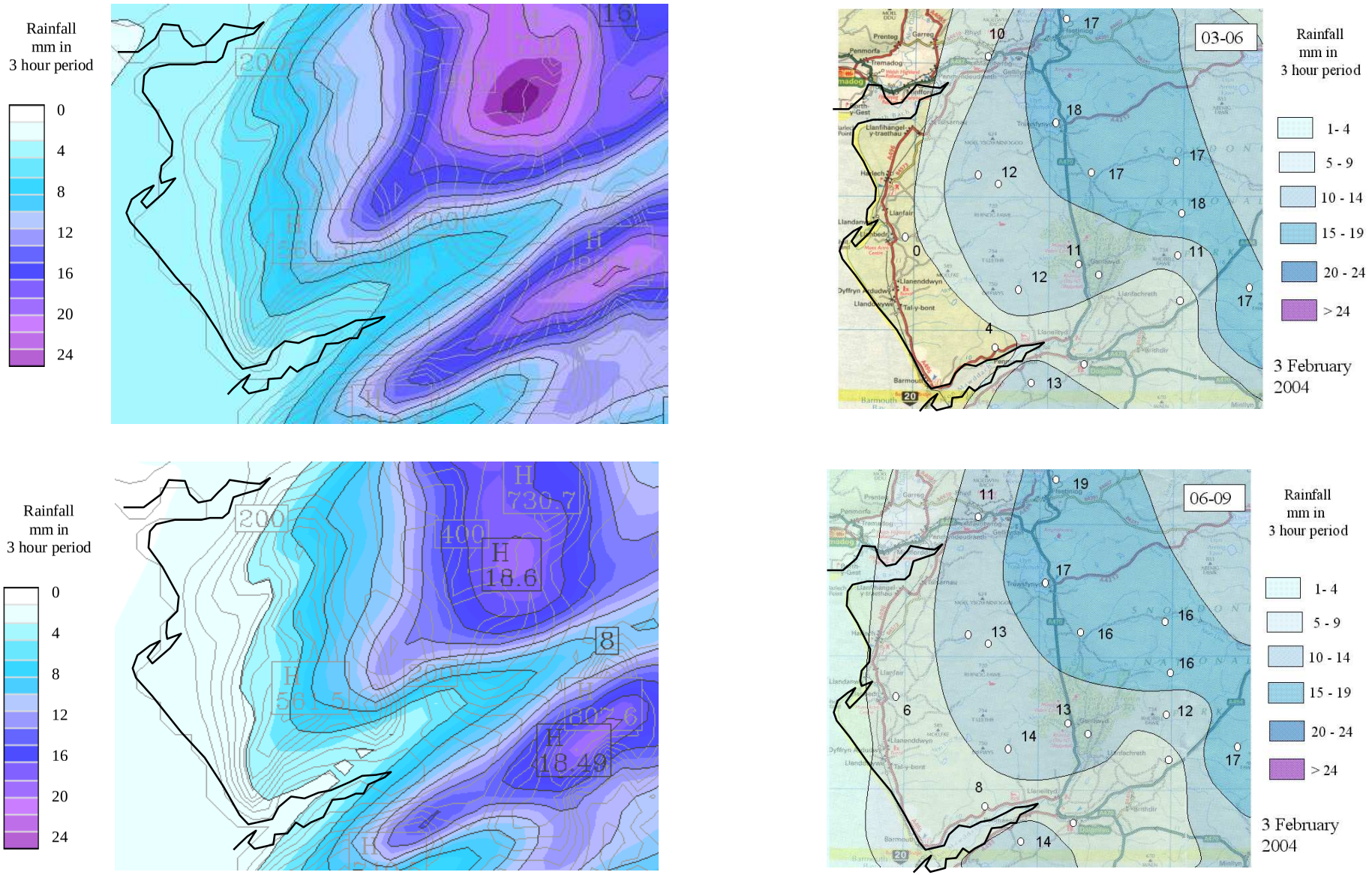

Figure 2.94 (cont.) MM5 3-hour rainfall simulations (left) and 3-hour raingauge totals (right): Above: 03:00h – 06:00h, 3 February 2004 Below: 06:00h – 09:00h, 3 February 2004

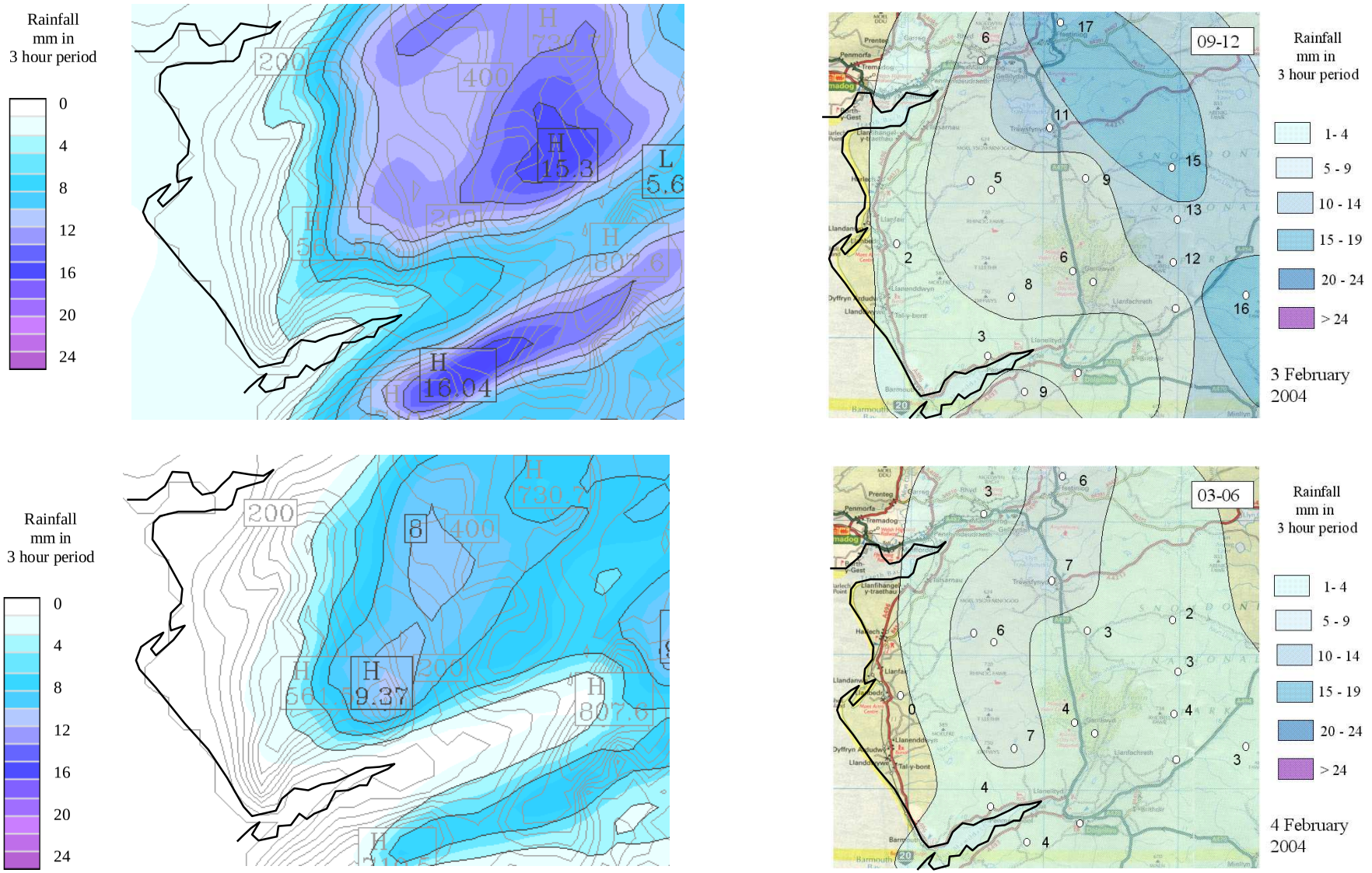

Figure 2.94 (cont.) MM5 3-hour rainfall simulations (left) and 3-hour raingauge totals (right): Above: 09:00h – 12:00h, 3 February 2004 Below: 03:00h – 06:00h, 4 February 2004

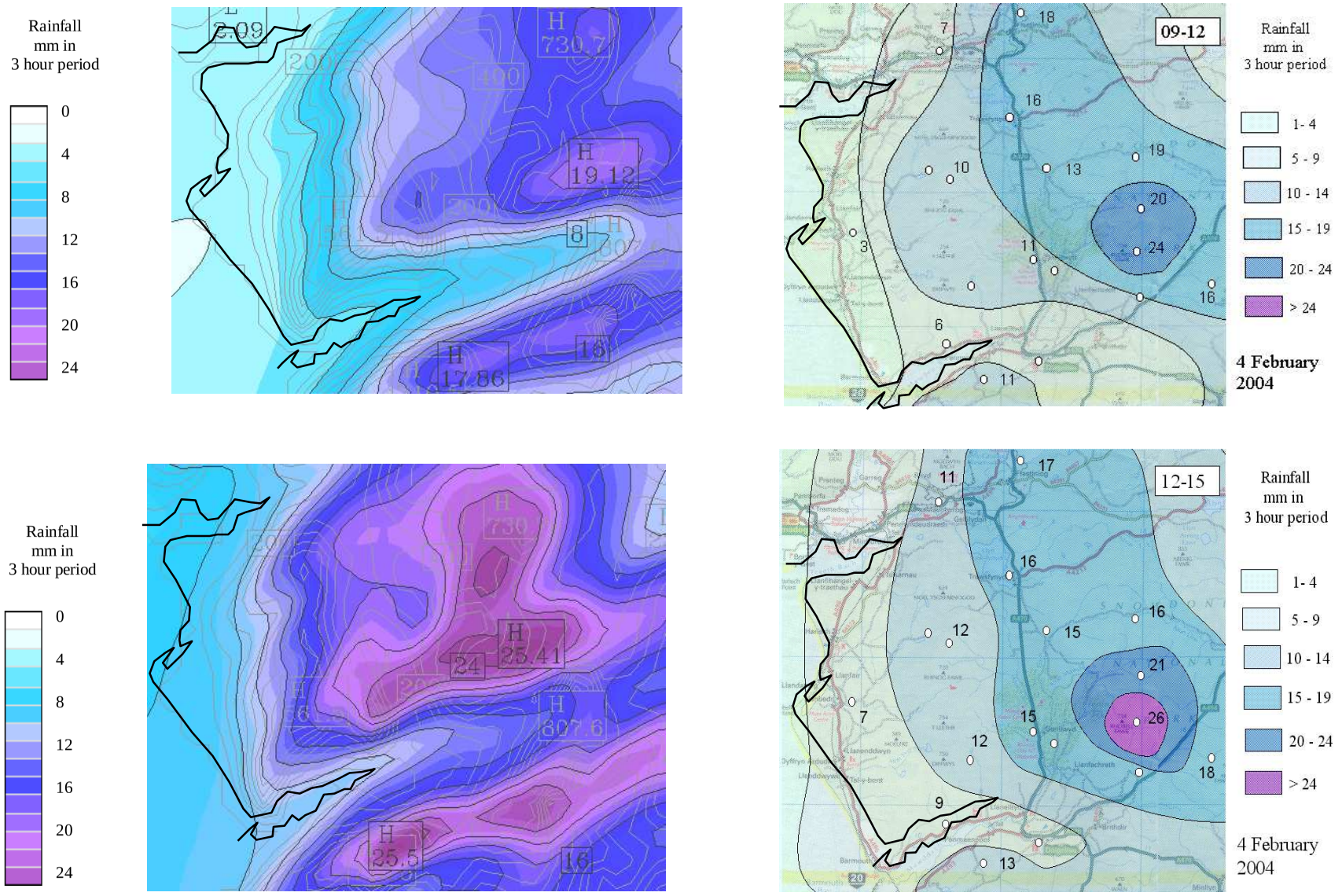

Figure 2.94 (cont.) MM5 3-hour rainfall simulations (left) and 3-hour raingauge totals (right): Above: 09:00h – 12:00h, 4 February 2004 Below: 12:00h – 15:00h, 4 February 2004

Statistical analysis

To obtain a quantitative comparison of simulation results for different storm events, a spreadsheet analysis has been carried out (fig.2.95). For each raingauge site and time period, the actual rainfall total is shown in the left column and the MM5 prediction to the right. Where the raingauge site lies on the boundary of two or more 1km MM5 grid squares, the MM5 value closest to the gauge reading is taken.

A ***mean absolute difference*** between raingauge readings and MM5 predictions averaged over all sites is calculated. This is an error value determined as a simple unsigned difference between pairs of values with no consideration as to which is larger.

A ***mean signed difference*** is also calculated as an average for all sites. This records differences between individual pairs of values as either positive or negative, allowing an overestimate at one site to offset an underestimate at another site.

These two measures allow a ***% absolute deviation*** and a ***% signed deviation*** to be calculated:

For a highly heterogeneous catchment where the pattern of rainfall is critical to hydrological response, the prediction error in stormwater flow may be close to the % absolute deviation.

For a homogeneous catchment where only total rainfall and not distribution pattern is critical, the prediction error in stormwater flow may be close to the % signed deviation.

In practice, the error in predicting stormwater volume is likely to lie between the % absolute deviation and the % signed deviation. The predicted storm volumes using the MM5 system are likely to be within 15% of actual flows for the storm events of 29 December 2002 and 2-4 February 2004, and within 25% for the event of 22 May 2003. Lower accuracy of 35% calculated for the event of 8 November 2002 may be due to a more restricted raingauge array operating at that time, which failed to record key aspects of the rainfall pattern for comparison with the simulation results.

		Llanbedr		Cwm Bychan		Caerdeon		Erw Wen		Cwm Mynach		Garllwyd		Tir Penrhos		Trawsfynydd		Bronaber		Aran Hall		Rhobell Fawr		Allt Lwyd		Blaen Liw		Pared yr Ychain		Dolgellau		Absolute total difference	Signed total difference	Stations	Mean absolute difference	Mean signed difference	Total recorded rainfall	Mean absolute difference (mm/h)	% absolute deviation	% signed deviation	Rainfall pattern
08-Nov-02	03-06	4	1	5	4	7	5	7	4			5	5	5	3	6	6	6	5			4	4	3	3	4	6	4	6			16	8	12	1.3	0.7	60				
	06-09	10	4	13	9	11	9	9	6			12	9	11	9	12	8	12	5			7	7	5	5	8	7	7	8			33	31	12	2.8	2.6	117				
	09-12	12	4	18	8	17	9	18	13			21	14	23	13	18	11	22	17			17	9	13	9	13	10	14	7			82	82	12	6.8	6.8	206				
	12-15	10	9	20	14	11	11	16	12			18	12	20	11	11	9	19	9			28	12	18	9	14	7	21	12			79	79	12	6.6	6.6	206				
																																						1.5	35.7	34.0	A1
29-Dec-02	06-09	4	4	5	6			7	6			9	7	7	7	8	5	8	6	8	5	7	4	8	5	6	6	11	7	8	8	22	20	13	1.7	1.5	96				
	09-12	12	8	15	16			20	16			18	14	16	14	19	14	17	14	12	13	16	13	14	13	15	13	18	16	13	18	37	23	13	2.8	1.8	205				
	15-18	6	4			4	7	9	10			10	12	14	12	18	16	12	14	7	12	16	14	11	11	10	10	20	14	8	14	33	-5	13	2.5	0.4	145				
	18-21	0	0			1	2	3	3			5	4	6	4	9	10	9	7	3	6	9	6	7	6	9	6	9	10	2	3	19	5	13	1.5	0.4	72				
																																						0.7	21.4	8.3	A2
22-May-03	03-06			5	5	7	4	7	4	9	10	2	6	2	6	2	5	4	5			2	4	1	4			2	7	5	5	29	-17	12	2.4	-1.4	48				
	06-09			26	22	14	10	12	14	20	19	9	13	7	13	11	13	15	10			8	12	7	10			8	10	10	10	37	-9	12	3.1	-0.8	147				
	12-15			15	20	12	12	6	16	30	26	14	18	13	18	13	17	15	13			12	14	8	14			17	16	10	12	45	-31	12	3.8	-2.6	165				
	15-18			2	2	2	2	4	4	5	6	2	7	3	7	2	3	2	5			3	6	1	5			4	6	1	4	26	-26	12	2.2	-2.2	31				
																																						1.0	35.0	21.2	B
02-Feb-04	03-06	2	7	13	12	13	11	13	11	18	17	12	13			12	11	11	10			11	12	8	10	8	9	12	10			20	0	12	1.7	0.0	133				
03-Feb-04	00-03	4	3	14	8	7	3	14	12	12	10	11	12			13	15	12	17			11	9	12	14	10	19	9	16			43	-9	12	3.6	-0.8	129				
	03-06	0	3	12	6	4	3	13	8	12	8	11	8			18	11	17	18			11	8	18	16	17	21	17	19			41	21	12	3.4	1.8	150				
	06-09	6	1	13	4	8	4	14	8	14	6	13	8			17	10	16	14			12	14	16	14	16	16	17	16			51	47	12	4.3	3.9	162				
	09-12	2	1	5	3	3	2	9	6	8	7	6	10			11	12	9	11			12	9	13	14	15	14	16	12			24	8	12	2.0	0.7	109				
04-Feb-04	03-06	0	0	6	2	4	1	4	1	7	8	4	7			7	6	3	8			4	4	3	5	2	6	3	5			28	-6	12	2.3	-0.5	47				
	09-12	3	3	10	5	6	3	11	6	10	11	11	13			16	12	13	12			24	18	20	18	19	15	16	12			37	31	12	3.1	2.6	159				
	12-15	7	9	12	15	9	10	13	14	12	16	15	20			16	19	15	18			26	22	21	22	16	18	18	16			31	-19	12	2.6	-1.6	180				A1/
																																					1.0	25.7	6.8	A2

Figure 2.95: Analysis of errors in rainfall prediction using the MM5 model.

Comparison of MM5 model predictions with observed storm rainfall was carried out by the Spearman rank test using the method of Chalmers and Parker (1986). This test compares the distributions of readings in the two data sets when sorted into order of size. A high correlation coefficient value close to 1 would indicate that MM5 had very closely predicted the spatial pattern of the rainfall distribution, although the test does not indicate whether the actual rainfall intensity was correctly predicted. A coefficient value of 0 would indicate that MM5 had predicted a distribution pattern with no apparent similarity to the true distribution. A negative correlation coefficient would suggest that MM5 had predicted high rainfall in areas where the rainfall was actually low, and *vice-versa*.

Scatter graphs and Spearman correlation coefficient values for the four example storms are given in figs 2.96-2.100.

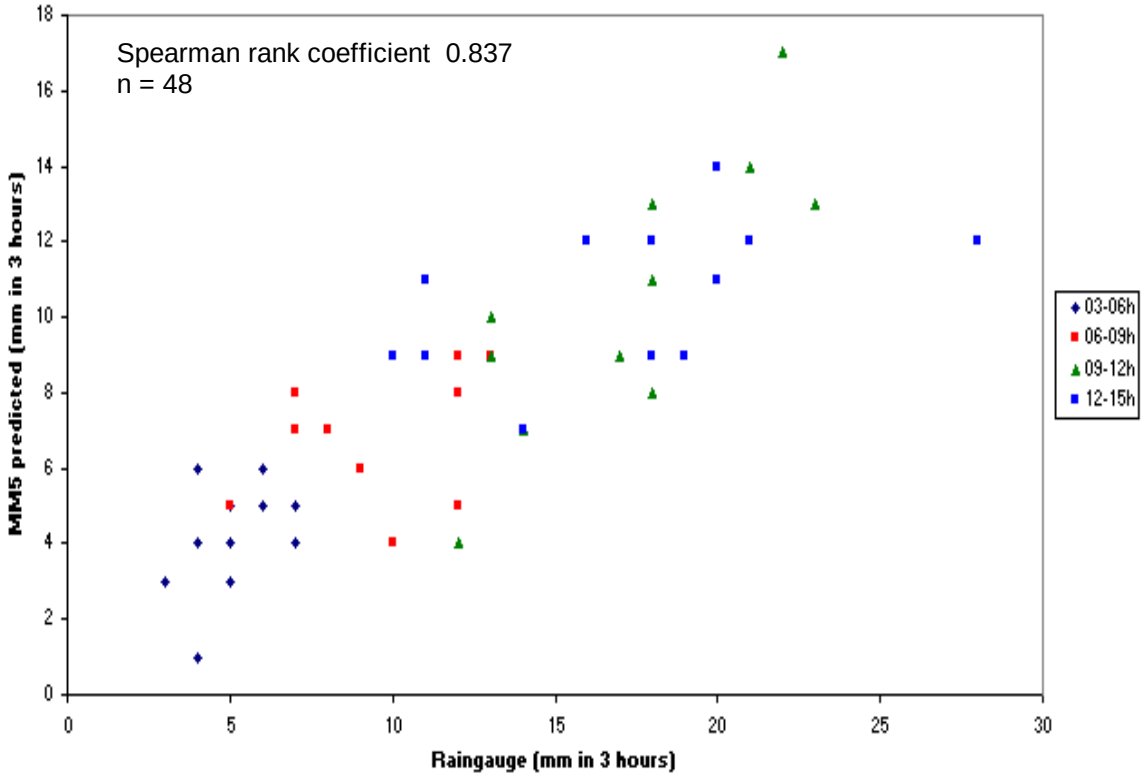

Figure 2.96: Storm event of 8 November 2002. Determination of Spearman rank correlation coefficient for MM5 rainfall forecast and observed rainfall

The highest correlation of 0.99 is obtained for the Type B storm event of 22 May 2003. High correlations above 0.8 are obtained for the Type A storms of 8 November and 29 December 2002.

The storm sequence of 3-4 February 2004 has been analysed as two rainfall events. A low correlation of 0.65 was obtained for rainfall on 3 February, with a higher correlation of 0.87 for 4 February. During the storm sequence the rainfall across the catchment changed from an initial Type A pattern, towards a more dominantly Type B pattern.

The results of the Spearman rank test need to be considered alongside the analysis of percentage deviation of rainfall totals (fig.2.95). Some tentative conclusions can be drawn.

The different degree of correlation for Type A and Type B rainfall events is a further indicator that these patterns are produced by physically different mechanisms of rainfall generation, modelled with different degrees of success by MM5.

MM5 is best able to predict Type B rainfall patterns, generated by a simple orographic mechanism. Type A patterns involve a more complex interaction between rising valley air flows and middle level saturated air.

Despite the very accurate prediction of spatial pattern for the 22 May Type B rainfall event, reference to fig.2.95 indicates that the total rainfall was underestimated by some 25%. Pattern correlation was poorer for the Type A rainfall events of 29 December 2002 and 3-4 February 2004, but total rainfall was estimated more accurately to around 15% in these cases.

The overall conclusions from analysis of the example storm events is that MM5 can adequately predict rainfall for frontal storm events over the Mawddach catchment. Where inaccuracies exist, they may be in spatial pattern or in total rainfall. The inaccuracies seem to be linked to limitations in the modelling of rainfall processes, particularly the production of orographic rainfall and rainfall enhancement by the seeder-feeder mechanism above deep valleys. These would be useful topics for further research and improvement of the MM5 program code.

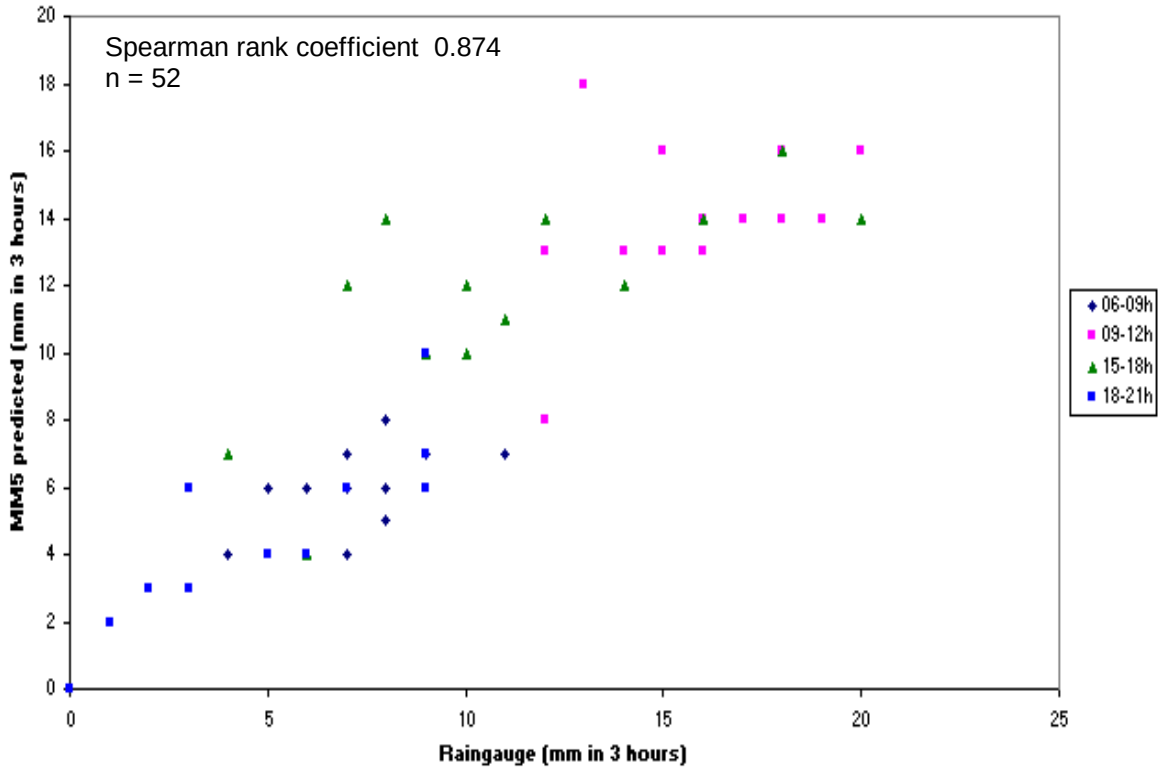

Figure 2.97: Storm event of 29 December 2002. Determination of Spearman rank correlation coefficient for MM5 rainfall forecast and observed rainfall

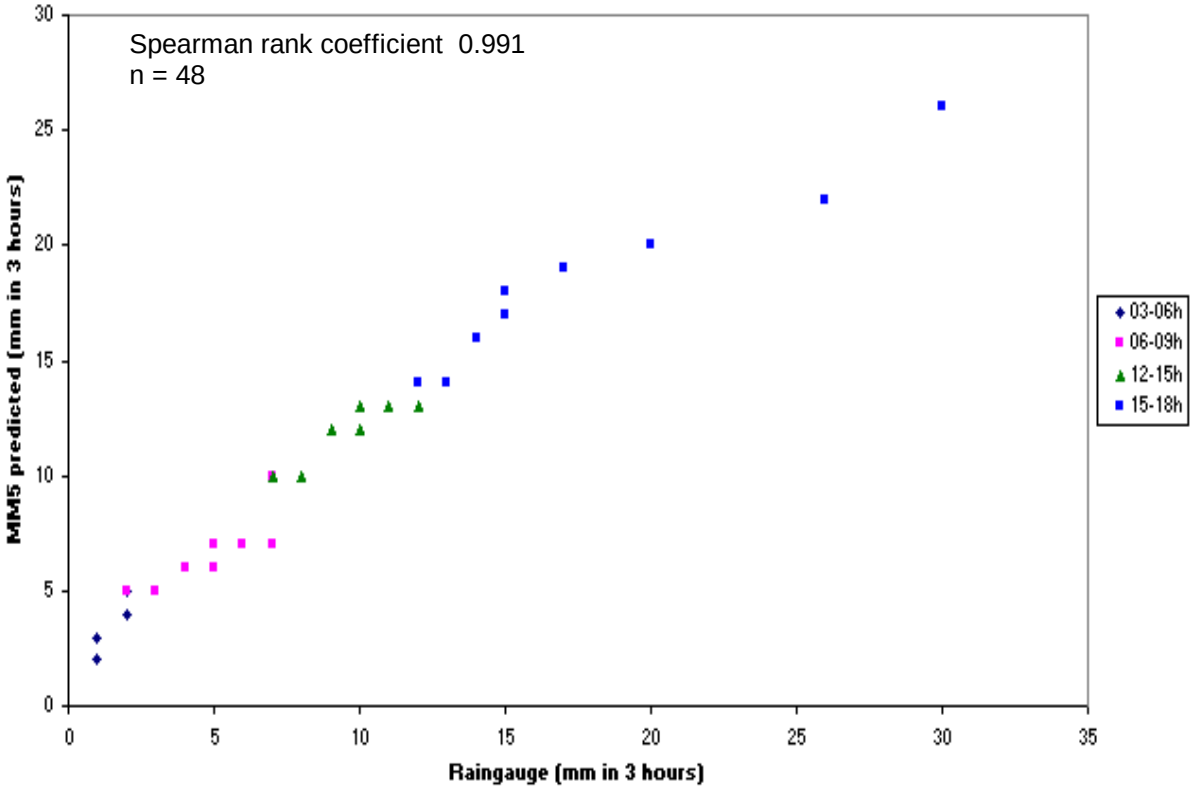

Figure 2.98: Storm event of 22 May 2003. Determination of Spearman rank correlation coefficient for MM5 rainfall forecast and observed rainfall

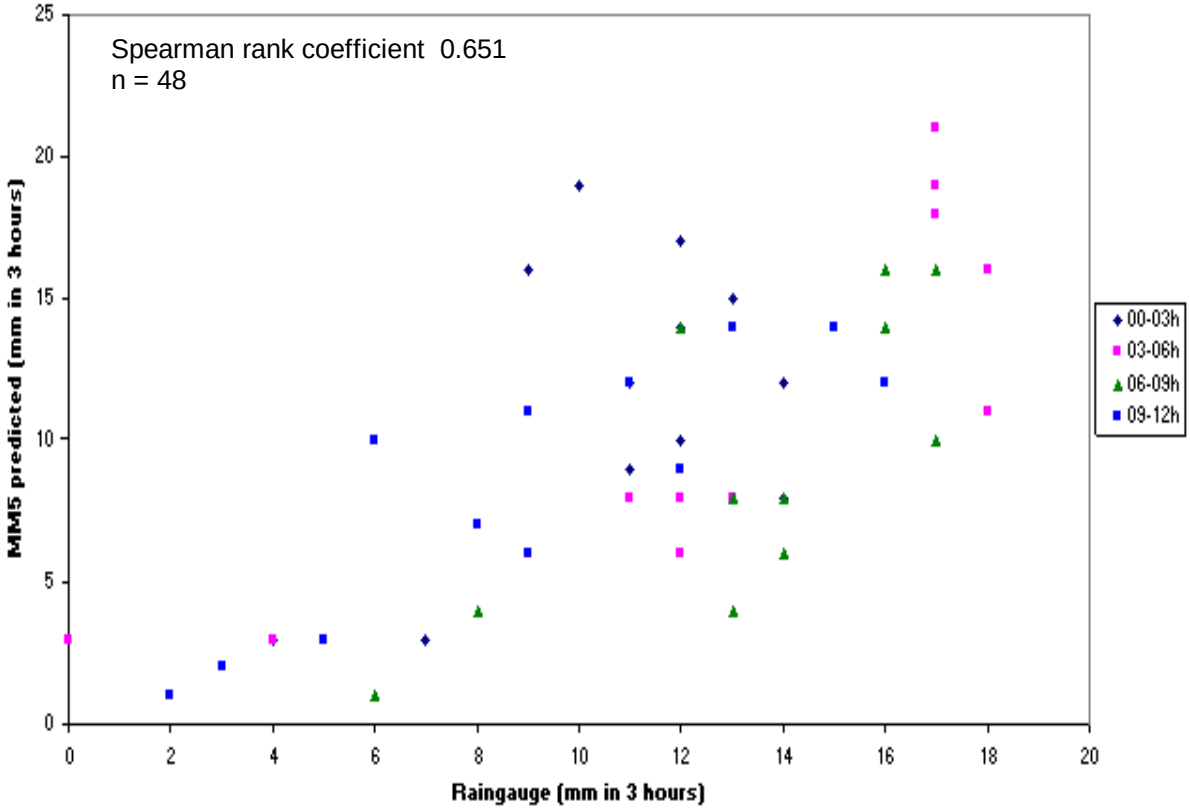

Figure 2.99: Storm event of 3 February 2004. Determination of Spearman rank correlation coefficient for MM5 rainfall forecast and observed rainfall

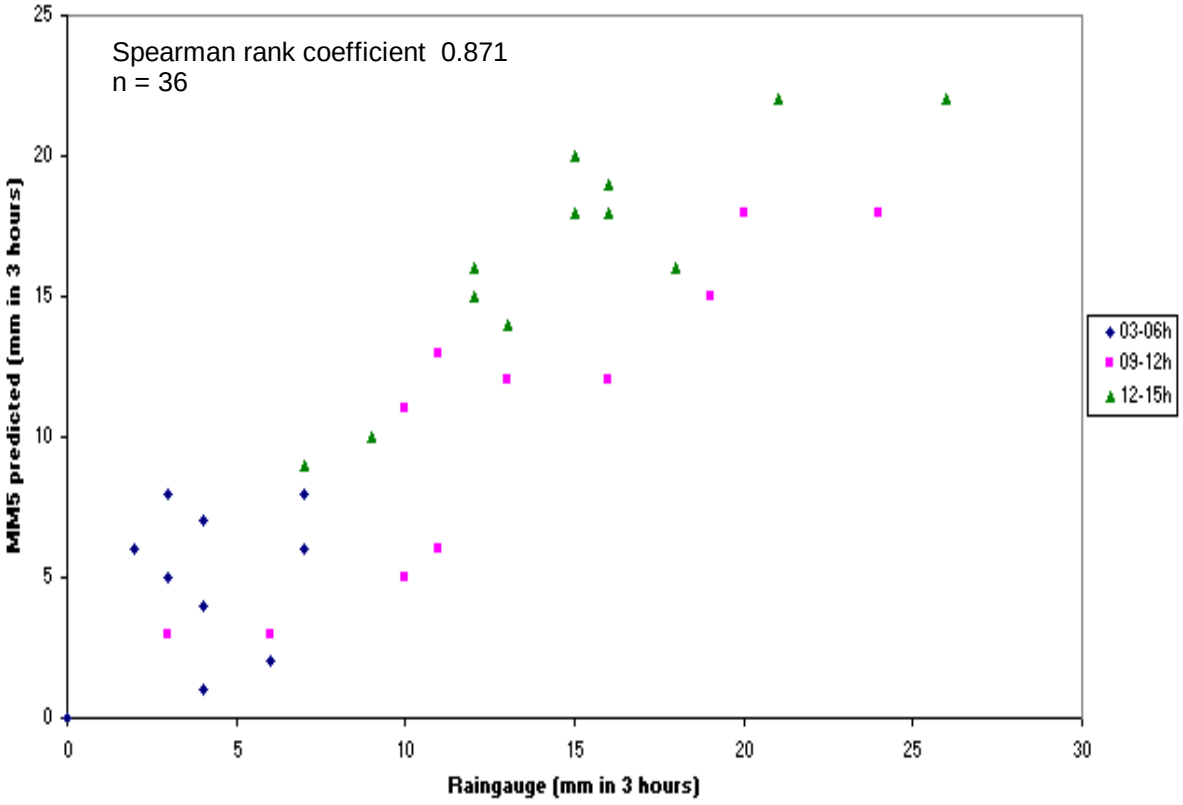

Figure 2.100: Storm event of 4 February 2004. Determination of Spearman rank correlation coefficient for MM5 rainfall forecast and observed rainfall

Rainfall radar

This chapter has examined the feasibility of computer modelling to provide rainfall input to a hydrological model. An alternative approach uses radar for rainfall estimation. The relative merits of the two methods should now be considered.

The tracking of storms by rainfall radar for is well developed in the USA, particularly in the mid-west and south-west where tornadoes and supercell thunderstorms are common (National Weather Service, 2005), and offshore in the Gulf of Mexico when hurricanes approach the coast. Cranston (2003) has examined the use of weather radar for flood forecasting in Scotland. Three weather radar installations cover the land area of Scotland and are producing promising results, but data suitable for use in operational flood warning systems is not yet being generated.

An essential difference exists between numerical weather modelling and rainfall radar observations. Modelling can provide a prediction of rainfall at a *future* point in time whilst radar patterns provide an estimate of rainfall rates at the *present* time. It is possible to make a forward extrapolation of rainfall radar patterns to predict rainfall at a future time, but this is dependant on knowledge of the manner in which weather systems move spatially and evolve chronologically within the forecasting region. As an example for discussion, a sequence of radar images at six-hourly intervals for 3 February 2004 are shown in fig.2.101, along with 3-hour MM5 rainfall predictions for corresponding times.

It is difficult to exactly compare the MM5 and rainfall radar images. MM5 integrates rainfall over a set time interval, in this case 3 hours, whilst the radar gives an estimate of rainfall rate at a particular instant. Some general observations can, however, be made.

Rainfall radar has a coarser resolution than the MM5 model. Radar uses an output grid of 5km or 10km squares, within which an average rainfall value is given. MM5 modelling may have an operational forecasting resolution down to 1km grid squares.

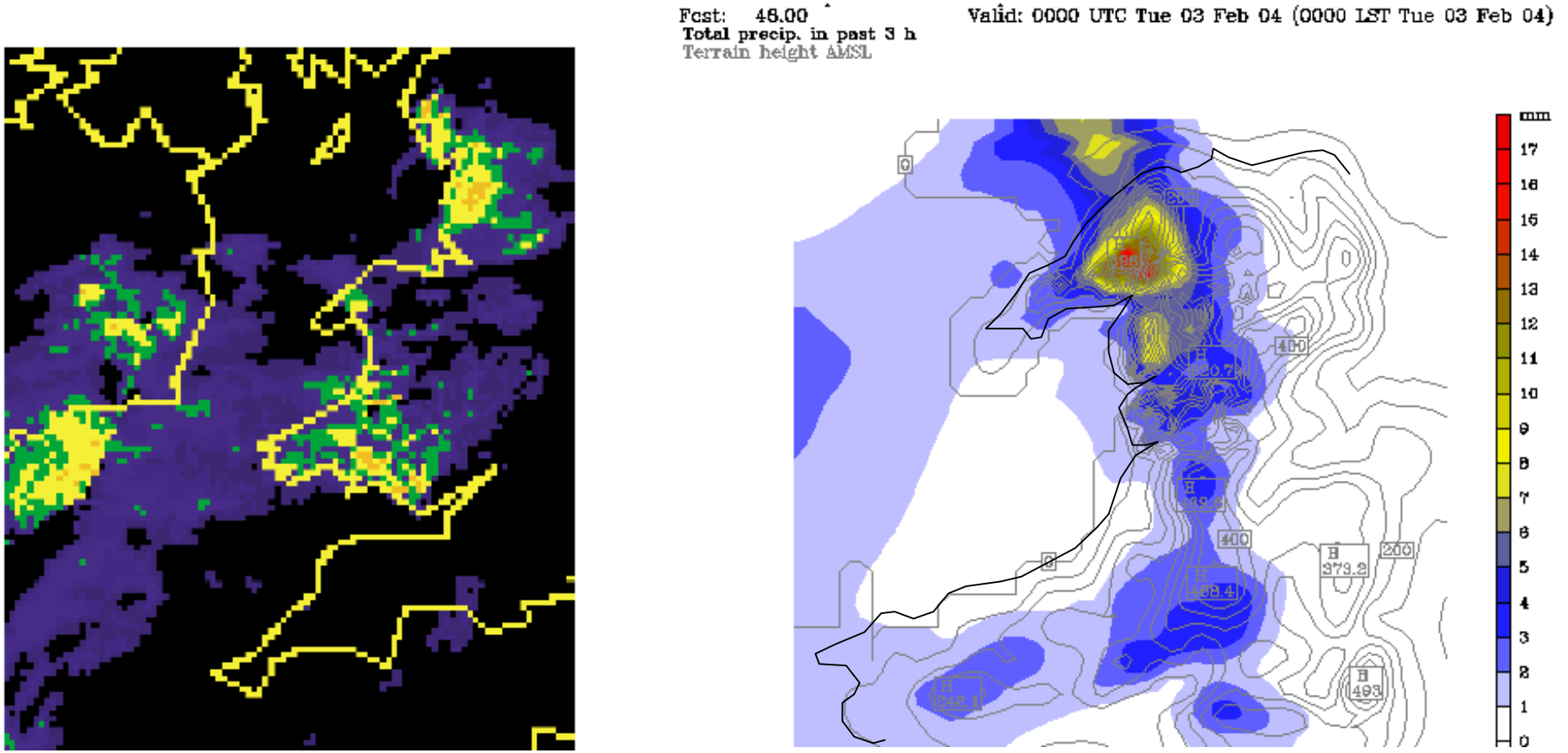

Figure 2-101: (left) Rainfall radar image for 00:00h 3 February 2004. Colour key (mm h^{-1}): blue<1 , green 1-2, yellow 2-4, orange 4-8, red >8.
(right) MM5 simulation for the 3-hour period 21:00h, 2 February to 00:00h, 3 February 2004.

Rainfall radar images must be calibrated for rainfall rate using raingauge data from rainfall events of known intensity. If calibration is based on lowland sites, inaccuracies may occur for mountain regions where rainfall generation mechanisms are more complex. Sibley (2005) discusses the accuracy of rainfall radar data for North Wales and comments that underestimation is common. He considers this to be due to the radar beam being angled upwards to clear the mountains, thereby missing lower layers of feeder cloud where much of the rainfall generation occurs. Underestimation may commonly exceed 50% for North Wales.

Flood forecasting based on current rainfall rates is limited to providing warnings of flood events a couple of hours in advance. For longer warning periods, advance predictions of storm rainfall will be needed. It is apparent that there would be difficulty in predicting the rainfall pattern of 6:00h on 3 February 2004 (fig.2.101), given only the information in the rainfall radar image of 0:00h on that day. Simple spatial translation of the rainfall pattern along a movement vector is insufficient.

Rainfall radar can play a valuable role in determining rainfall patterns as an alternative to telemetered rain gauge arrays, and will become more accurate with the development of the technology and improvement in coverage. There is a clear problem, however, in advance forecasting by means of rainfall radar images. This is particularly significant for mountain areas where weather systems can evolve rapidly and rainfall generation processes are complex.

Numerical weather forecasting is invaluable where advance warning of flooding is required on a timescale which exceeds the fast flow routing time of rain which has already fallen within the catchment . In the current state of the art, numerical weather forecasting is considered the most accurate method of generating rainfall input for the Mawddach hydrological model.

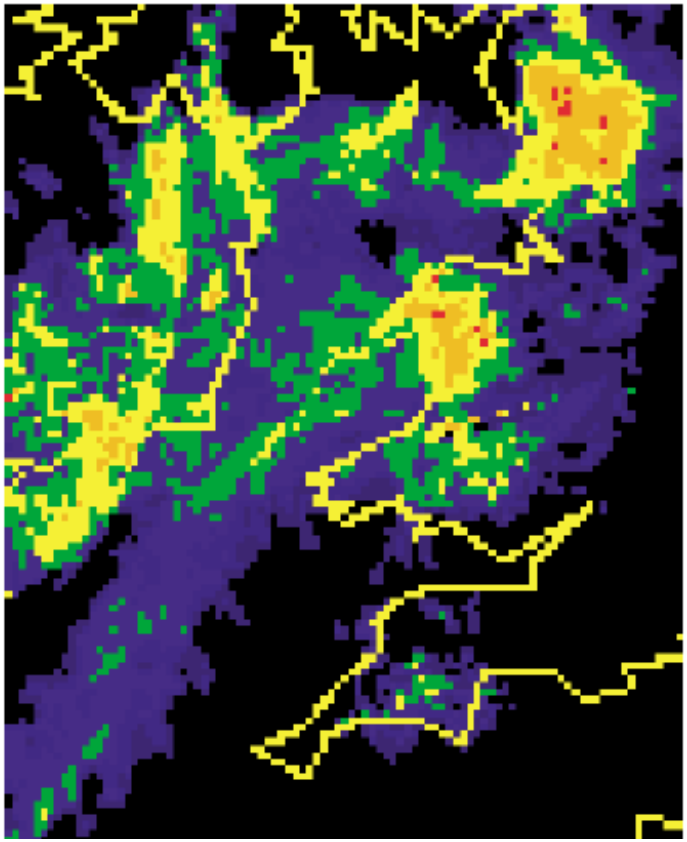

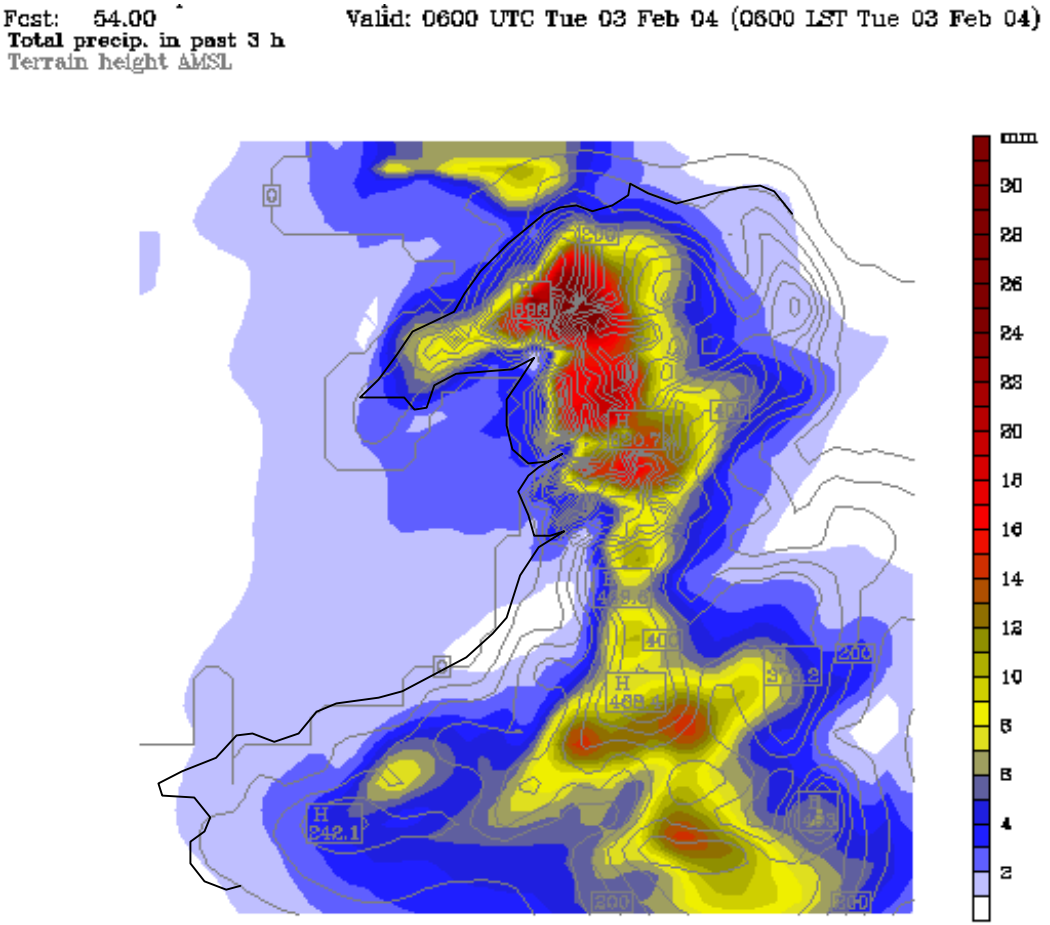

Figure 2.101 (cont.) (left) Rainfall radar image for 06:00h 3 February 2004. Colour key (mm h^{-1}): blue<1 , green 1-2, yellow 2-4, orange 4-8, red >8.
(right) MM5 simulation for the 3-hour period 03:00h - 06:00h, 3 February 2004.

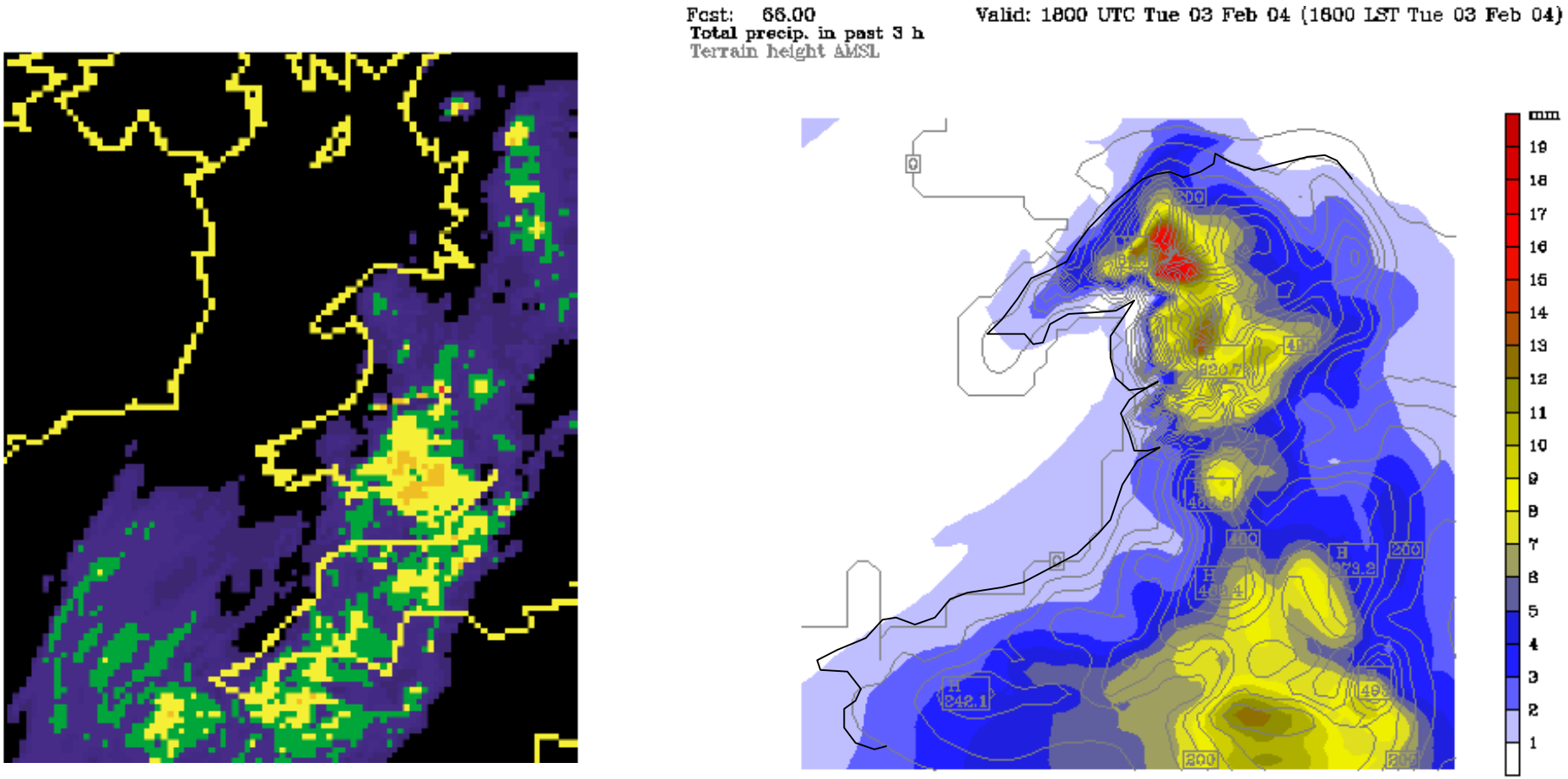

Figure 2.101 (cont.) (left) Rainfall radar image for 18:00h 3 February 2004. Colour key (mm h^{-1}): blue<1 , green 1-2, yellow 2-4, orange 4-8, red >8.
(right) MM5 simulation for the 3-hour period 15:00h - 18:00h, 3 February 2004.

Optimisation of MM5 models using a Neural Network

It was shown that inaccuracies may exist in rainfall predictions by the MM5 model, both in terms of the location and intensity of rainfall:

$$r_{ij} = R_{ij} + e_{ij}$$

where r is true rainfall, R is rainfall predicted by the model, and e is the error in prediction, for location i, j within the catchment. It is possible that e_{ij} is not randomly distributed, but is some systematic function of position and/or rainfall intensity resulting from imperfect modelling of meteorological processes:

$$e_{ij} = f(i, j, R)$$

If an error function f could be determined by comparison of predicted and actual rainfall, it would then be possible to apply this function to subsequent predictions in order to improve their accuracy.

Experiments have been carried out to determine whether MM5 rainfall predictions can be improved by application of an error function during post-processing with a neural network. For this work, the Neural Network Toolbox within the MATLAB mathematical software package has been used (Demuth and Beale, 2000).

The principle of a neural network is to apply mathematical transformations to input data in order to produce output which is, by some measure, a more accurate result. A variety of mathematical transformations are possible. After experimentation, it was found that best results for the MM5 problem are achieved by a combination of a pure linear function and a log-sigmoidal function:

The Pure Linear transfer function simply takes an input value and multiplies it by a weighting factor W:

purelin(n) = W * n

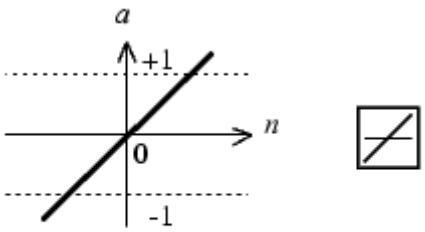

a = purelin(n)

Linear Transfer Function

A Log-Sigmoidal transfer function takes any value in the range from negative infinity to positive infinity and maps it to a value in the range 0-1. This is done by applying the formula:

logsig(n) = 1 / (1 + exp(-n))

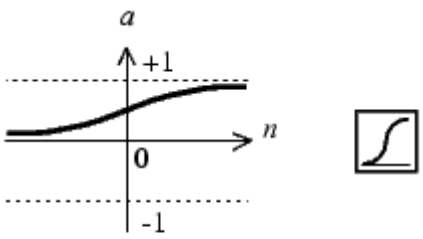

a = logsig(n)

Log-Sigmoid Transfer Function

The neural network set up for processing MM5 data is shown in fig.2.102. This consists of twelve processing channels termed *neurones* which are interconnected at several stages. The network accepts 12 input values, and each neuron will produce a revised output value which should be closer to the true solution for the problem:

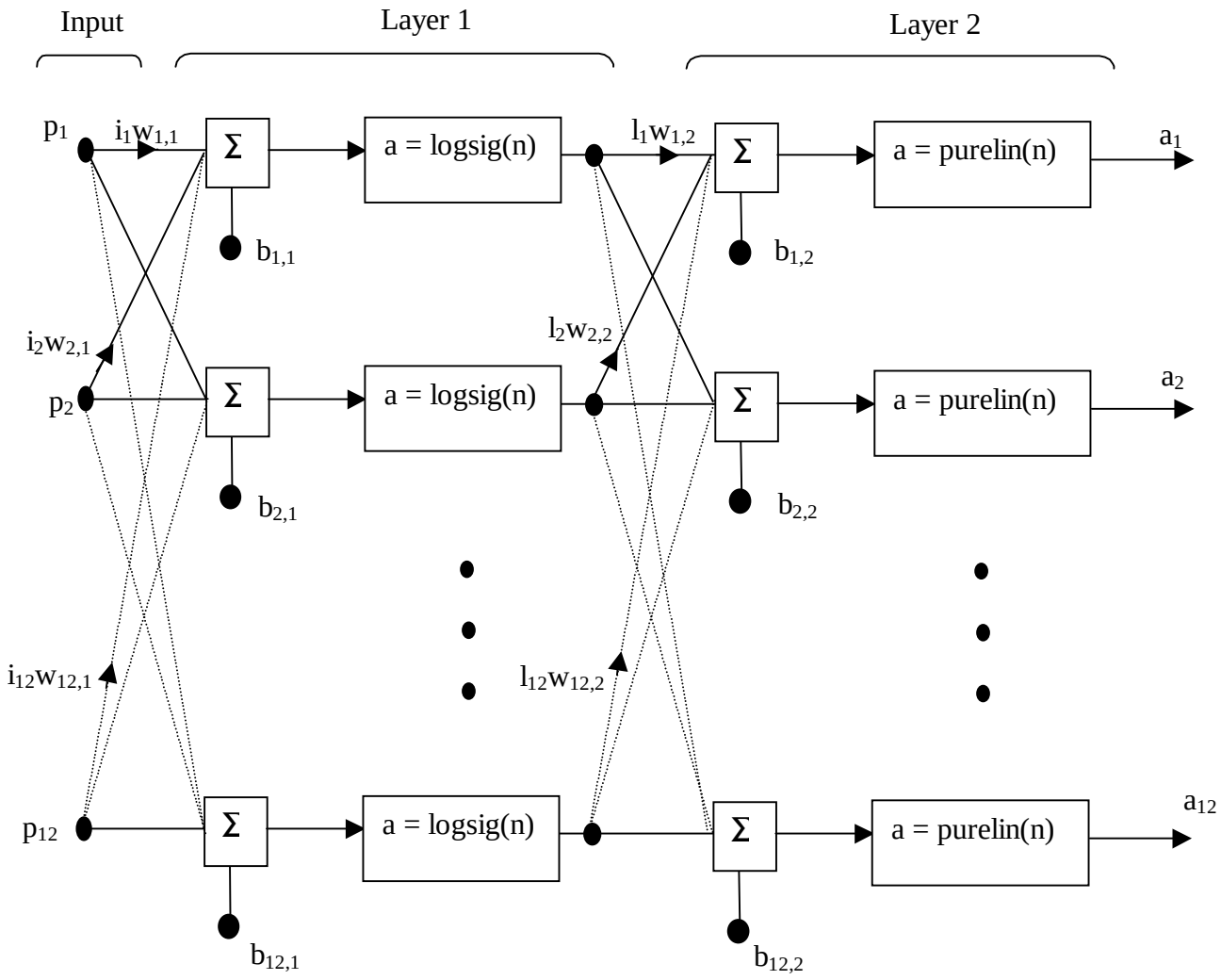

Figure 2.102: Diagrammatic representation of the neural network selected for post-processing of MM5 rainfall simulation data

Inputs to the system are MM5 rainfall forecasts for 12 raingauge sites, and it is hoped the neural network will generate a set of revised forecasts which will be closer to the actual rainfall totals recorded at the 12 sites.

The input values are subject to a sequence of mathematical operations:

- Each of the rainfall forecast values p_1 to p_{12} is multiplied by a weighting value $w_{1,1}$ to $w_{12,1}$ to provide an input to the first layer of the neural network. A multiple of every input value is supplied to each of the 12 neurones.
- Before the first transformation function is applied, a constant $b_{1,1}$ to $b_{12,1}$ is added to the inputs of the 12 neurones.
- The log-sigmoidal transformation is applied to each input n to provide an output a:

$$a = \frac{1}{1 + \exp(-n)}$$

- Each output is again multiplied by a weighting factor, and multiples of this value are transferred to each of the 12 neurones. A further constant $b_{1,2}$ to $b_{12,2}$ is added to the inputs.
- The pure linear transformation is finally applied using weights $w_{1,2}$ to $w_{12,2}$ as multipliers:

$$a = w.n$$

This algorithm provides opportunity to adjust a large number of parameters – multipliers and additive variables – in order to generate outputs which exactly match the true rainfall recordings. We then make an assumption that applying the same parameters to transform subsequent MM5 output values will generate improved predictions.

The purpose of the neural network software package is to provide automated learning for parameter optimisation. Sets of MM5 predictions and the subsequently recorded raingauge totals are supplied to the program in training mode. Progressive adjustment of parameters is carried out until an acceptable fit is achieved. Future MM5 output can then be processed by the neural network to hopefully enhance its accuracy.

Using the Neural Network software package

The first stage in running a neural network is to set up the configuration of neurones and transfer functions required (fig.2.103). The number of neurones is determined by the number of input data values to be processed. The number of layers within a neuron is determined by the complexity of the mathematical relationship which exists between the input estimates and the true values. A two layer neuron structure incorporating a linear and sinusoidal transfer function can exactly represent any non-linear continuous mapping between the predictions and true values.

The neural network structure is displayed diagrammatically by the software, using symbols to represent the chosen transfer functions at each neuron level.

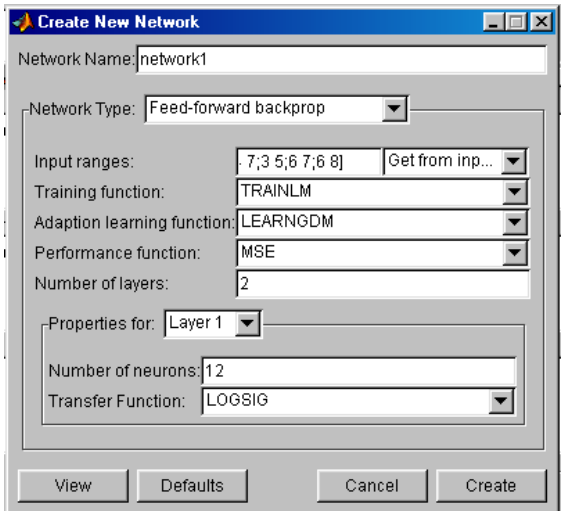

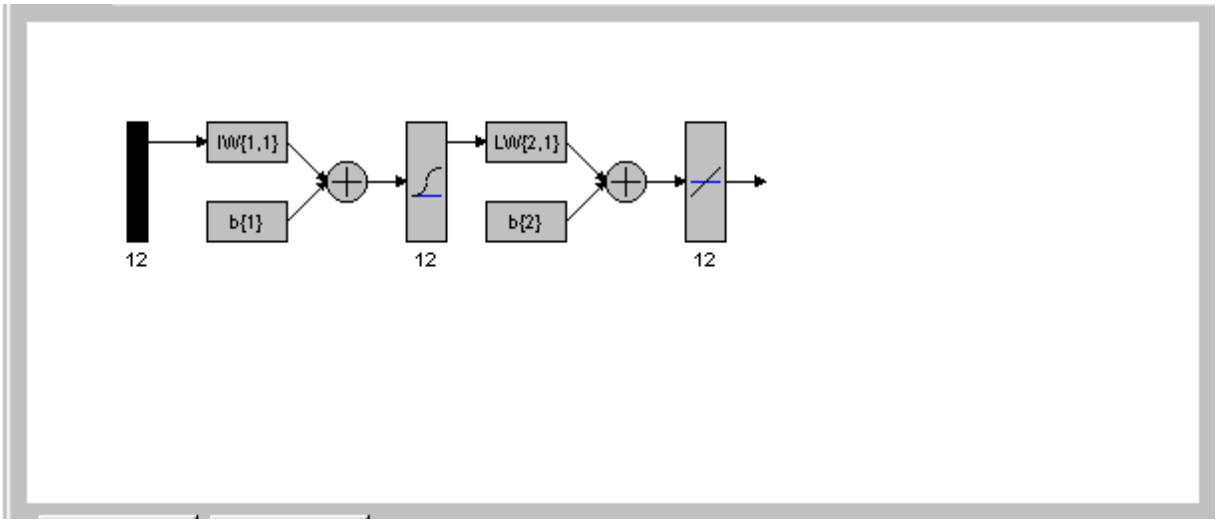

Figure 2.103: Configuration of the neural network. (Left) Specification of the numbers of neurones, number of layers for each neuron, and the transfer functions to be used. (Below) Diagrammatic representation of the neural network.

The next step is to train the neural network to correctly transform sets of MM5 forecast data to give outputs exactly matching the known field data from raingauges. Data sets for a number of time intervals may be input together to form a sequence at each gauge site (fig.2.104). The parameter optimisation procedure is run iteratively until a fit is achieved to the required degree of accuracy (fig.2.105).

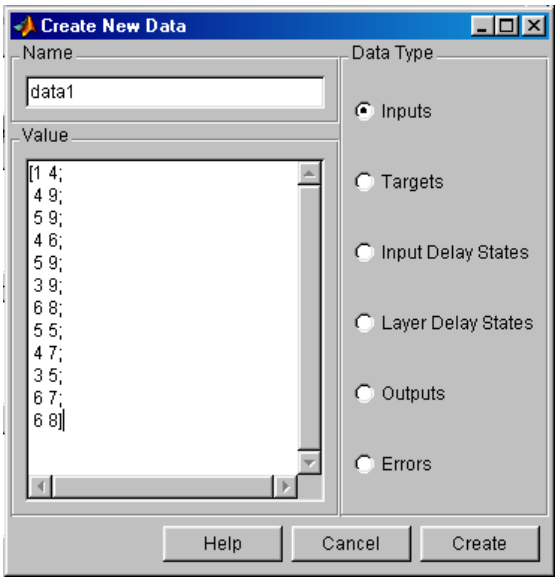

Figure 2.104: Entry of MM5 predicted rainfall values ('Inputs') and actual raingauge readings ('Targets'). This screen shows the input of predicted values for 12 raingauge sites at two time intervals.

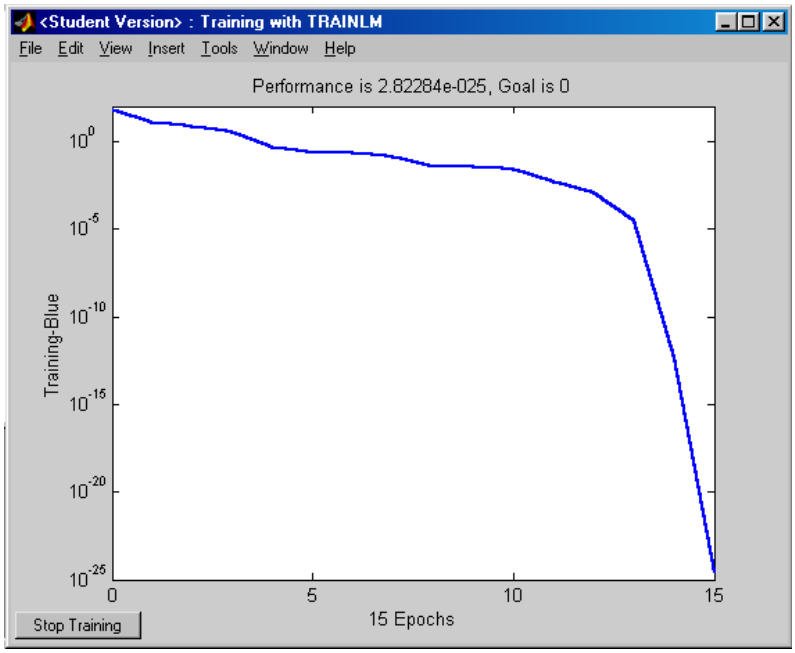

Figure 2.105: Neural Network software running in training mode to determine the optimum parameters for the transform functions. In this case, and exact fit has been found (to a tolerance of less than 10^{-24})

When training is complete, the neural network is run in simulation mode. New MM5 forecast data can be input, and output data generated which will hopefully give a more accurate rainfall forecast than the original estimate (fig.2.106).

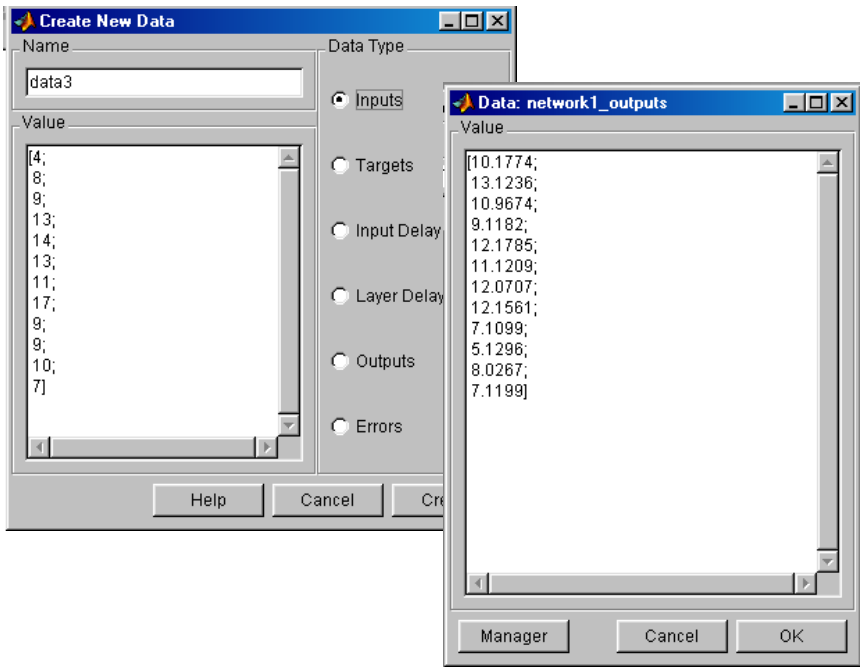

Figure 2.106: After training, sets of input data can be processed by the neural network to possibly provide output data of enhanced accuracy.

Evaluation of results from the Neural Network

Results of successful training and simulation cycles are shown in fig.2.107. Prior to achieving these results, various runs had been recorded where output data sets did not produce an improvement on the original MM5 rainfall predictions:

- A single layer pure linear neuron, and a two layer neuron using a combination of a tan-sinusoidal and pure linear transform gave unsatisfactory results.
- Training with one storm event did not produce improved forecasts when the neural network was applied directly to another storm event. Each storm appears to be mathematically unique, and training needs to take place progressively as an individual storm event develops.
- Training with an inadequate number of time interval data sets may lead to unsatisfactory results. An example is shown in the first block of fig.212 where only two time intervals were used in training with the 8 November 2002 storm

event. Neural network transformation for the third time interval lead to a signed deviation of 36%, which was a slightly poorer forecast than the 34% signed deviation of the original MM5 data.

Given adequate training, small but significant improvements to the forecast data can be consistently achieved. A comparison of accuracy with the original forecasts is given in table 2.2. It is perhaps worth observing that the greatest improvements are achieved in the case where the original MM5 forecast was least accurate. Use of neural network processing may therefore be a means of identifying and improving the least reliable forecasts.

Storm date	Training interval	Simulation interval	MM5 absolute deviation	MM5 signed deviation	Neural Net absolute deviation	Neural Net signed deviation
8 Nov 02	03-12h	12-15h	35.7	34.0	31.8	18.0
8 Nov 02	06-12h	12-15h	35.7	34.0	30.9	21.2
2-4 Feb 04	03h 2 Feb – 09h 3 Feb	09-12h	25.7	6.8	25.4	6.4
2-4 Feb 04	03h 2 Feb – 06h 4 Feb	09-12h	25.7	6.8	25.1	6.2

Table 2.2 Comparison of the accuracy of MM5 initial rainfall forecasts with forecasts after processing by neural network

		Llanbedr		Cwm Bychan		Caerdeon		Erw Wen		Cwm Mynach		Garnllwyd		Tir Penrhos		Trawsfynydd		Bronaber		Aran Hall		Rhobell Fawr		Allt Lwyd		Blaen Lliw		Pared yr Ychain		Dolgellau		Mean absolute difference	Mean signed difference	Total recorded rainfall	Mean absolute difference (mm/h)	% absolute deviation	% signed deviation
08-Nov-02	03-06	4	1	5	4	7	5	7	4			5	5	5	3	6	6	6	5			4	4	3	3	4	6	4	6			1.3	0.7	60			
	06-09	10	4	13	9	11	9	9	6			12	9	11	9	12	8	12	5			7	7	5	5	8	7	7	8			2.8	2.6	117			
	09-12	12	8.2	18	9	17	8.8	18	13			21	13	23	11	18	12	22	11			17	5	13	4	13	8.4	14	7			7.9	7.9	206			
	12-15	10	9	20	14	11	11	16	12			18	12	20	11	11	9	19	9			28	12	18	9	14	7	21	12			6.6	6.6	206			
																																			1.5	37.8	36.1
08-Nov-02	03-06	4	1	5	4	7	5	7	4			5	5	5	3	6	6	6	5			4	4	3	3	4	6	4	6			1.3	0.7	60			
	06-09	10	4	13	9	11	9	9	6			12	9	11	9	12	8	12	5			7	7	5	5	8	7	7	8			2.8	2.6	117			
	09-12	12	4	18	8	17	9	18	13			21	14	23	13	18	11	22	17			17	9	13	9	13	10	14	7			6.8	6.8	206			
	12-15	10	14	20	20	11	18	16	19			18	23	20	25	11	20	19	24			28	18	18	14	14	14	21	15			4.7	-1.2	206			
																																			1.3	31.8	18.0
08-Nov-02	03-06	4	1	5	4	7	5	7	4			5	5	5	3	6	6	6	5			4	4	3	3	4	6	4	6			1.3	0.7	60			
	06-09	10	4	13	9	11	9	9	6			12	9	11	9	12	8	12	5			7	7	5	5	8	7	7	8			2.8	2.6	117			
	09-12	12	4	18	8	17	9	18	13			21	14	23	13	18	11	22	17			17	9	13	9	13	10	14	7			6.8	6.8	206			
	12-15	10	12	20	18	11	17	16	18			18	21	20	23	11	18	19	22			28	17	18	13	14	13	21	14			4.3	0.3	206			
																																			1.3	30.9	21.2
02-Feb-04	03-06	2	7	13	12	13	11	13	11	18	17	12	13			12	11	11	10			11	12	8	10	8	9	12	10			1.7	0.0	133			
03-Feb-04	00-03	4	3	14	8	7	3	14	12	12	10	11	12			13	15	12	17			11	9	12	14	10	19	9	16			3.6	-0.8	129			
	03-06	0	3	12	6	4	3	13	8	12	8	11	8			18	11	17	18			11	8	18	16	17	21	17	19			3.4	1.8	150			
	06-09	6	1	13	4	8	4	14	8	14	6	13	8			17	10	16	14			12	14	16	14	16	16	17	16			4.3	3.9	162			
	09-12	2	1	5	6	3	3.1	9	8	8	7	6	9			11	13	9	11			12	8	13	14	15	13	16	14			1.7	0.2	109			
04-Feb-04	03-06	0	0	6	2	4	1	4	1	7	8	4	7			7	6	3	8			4	4	3	5	2	6	3	5			2.3	-0.5	47			
	09-12	3	3	10	5	6	3	11	6	10	11	11	13			16	12	13	12			24	18	20	18	19	15	16	12			3.1	2.6	159			
	12-15	7	9	12	15	9	10	13	14	12	16	15	20			16	19	15	18			26	22	21	22	16	18	18	16			2.6	-1.6	180			
																																			0.9	25.4	6.4
02-Feb-04	03-06	2	7	13	12	13	11	13	11	18	17	12	13			12	11	11	10			11	12	8	10	8	9	12	10			1.7	0.0	133			
03-Feb-04	00-03	4	3	14	8	7	3	14	12	12	10	11	12			13	15	12	17			11	9	12	14	10	19	9	16			3.6	-0.8	129			
	03-06	0	3	12	6	4	3	13	8	12	8	11	8			18	11	17	18			11	8	18	16	17	21	17	19			3.4	1.8	150			
	06-09	6	1	13	4	8	4	14	8	14	6	13	8			17	10	16	14			12	14	16	14	16	16	17	16			4.3	3.9	162			
	09-12	2	1	5	3	3	2	9	6	8	7	6	10			11	12	9	11			12	9	13	14	15	14	16	12			2.0	0.7	109			
04-Feb-04	03-06	0	0	6	2	4	1	4	1	7	8	4	7			7	6	3	8			4	4	3	5	2	6	3	5			2.3	-0.5	47			
	09-12	3	2.9	10	11	6	4.5	11	12	10	11	11	10			16	15	13	13			24	11	20	15	19	15	16	15			2.5	2.1	159			
	12-15	7	9	12	15	9	10	13	14	12	16	15	20			16	19	15	18			26	22	21	22	16	18	18	16			2.6	-1.6	180			
																																			0.9	25.1	6.2

Figure 2.107. Results of neural network processing of MM5 rainfall forecasts. Training intervals shown in dark blue, simulation interval in light blue.

Structure of frontal rainfall events

An important aspect of evaluating the MM5 model is to assess whether the simulation reasonably represents atmospheric patterns and processes predicted by meteorological theory. As a test of the system, an analysis has been carried out for the sample storm event of 29 December 2002. Output from MM5 is shown as figures 2.108-2.112:

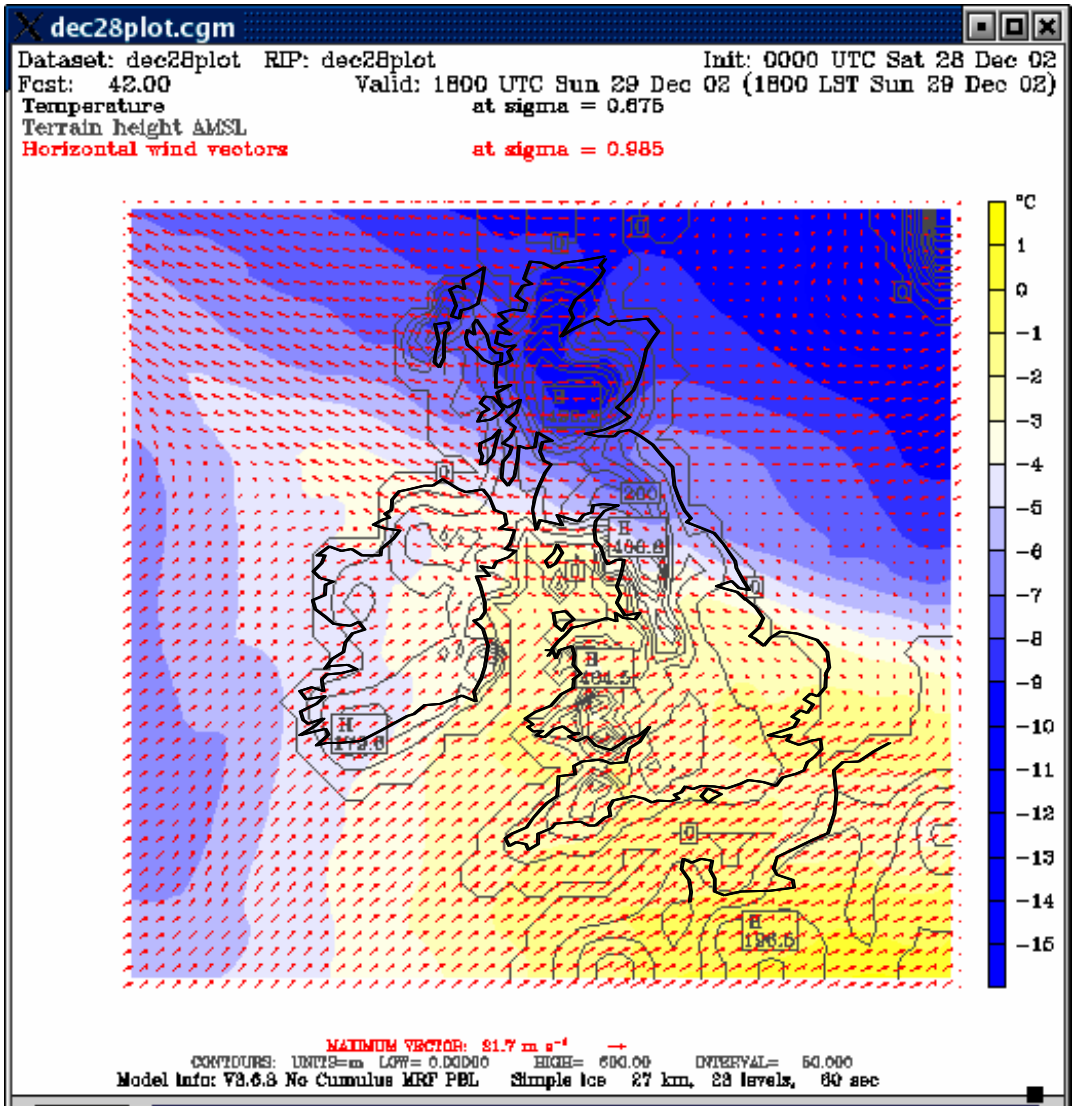

Figure 2.108: MM5 simulation of mid-troposphere temperatures at 18:00h, 29 December 2002. Low level wind vectors are shown as red arrows.

Fig.2.108 shows temperature distribution at mid-troposphere levels. A warm sector extends from Ireland into southern Britain. Low level air flow is towards the north-

east across the warm sector, turning north westwards parallel to the warm front in the direction of the cyclonic low to the south of Greenland.

Fig.2.109 shows vertical air velocities at mid-troposphere levels. Uplift is firstly towards the north-east ahead of the cold front, then north westwards along the line of the warm front. These movements represent an ascending warm sector conveyor.

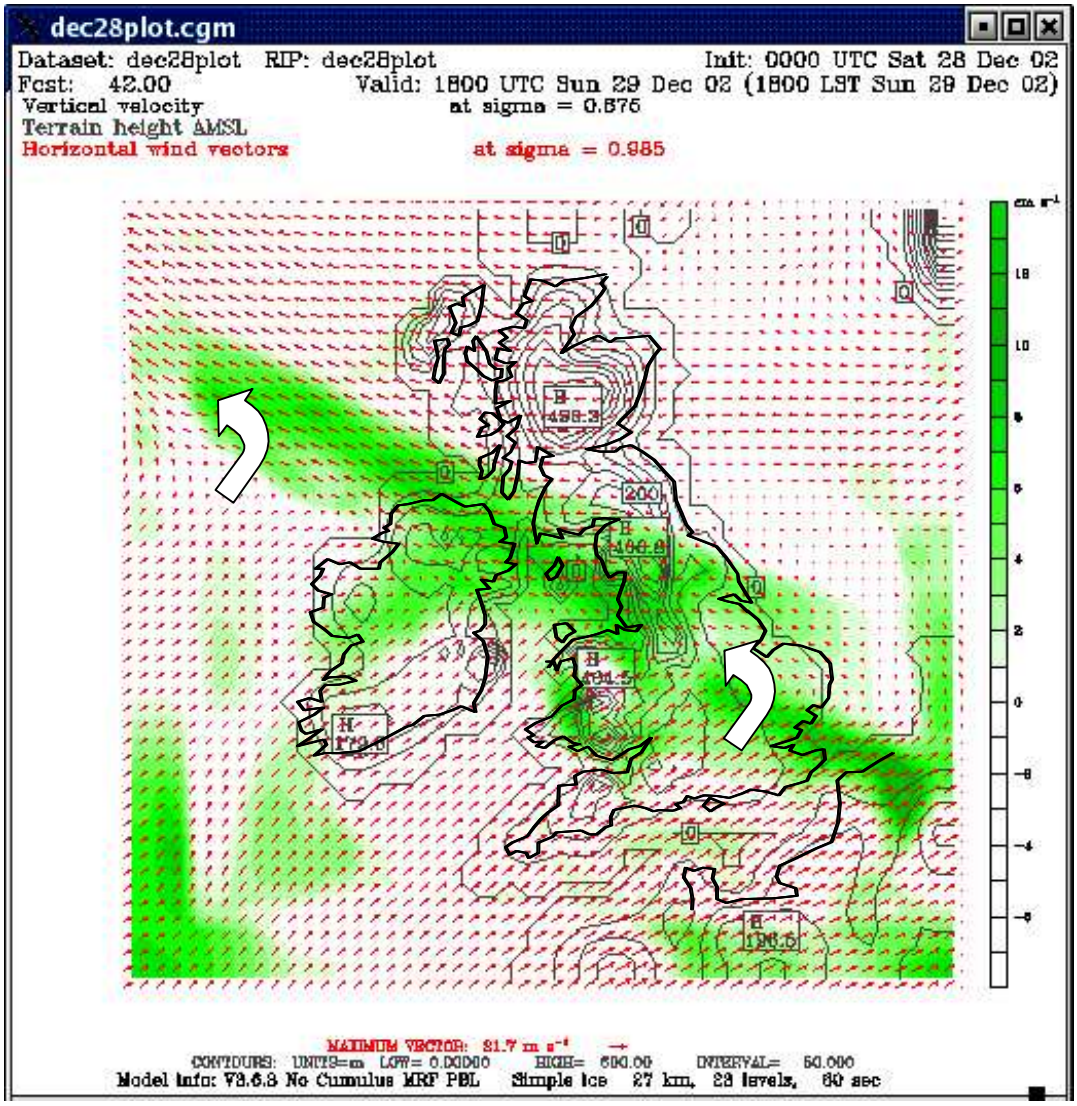

Figure 2.109: MM5 simulation of mid-troposphere vertical component of air flow at 18:00h, 29 December 2002. Low level wind vectors are shown as red arrows.

Fig.2.111 shows total rainfall for the six hour period to 18:00h. Rainfall is concentrated along the warm front conveyor, with subsidiary rain bands oriented north-south across the warm sector. This pattern is consistent with the instability model of Browning et al. (1973), with rainfall enhanced by gravity wave development over the Welsh mountains.

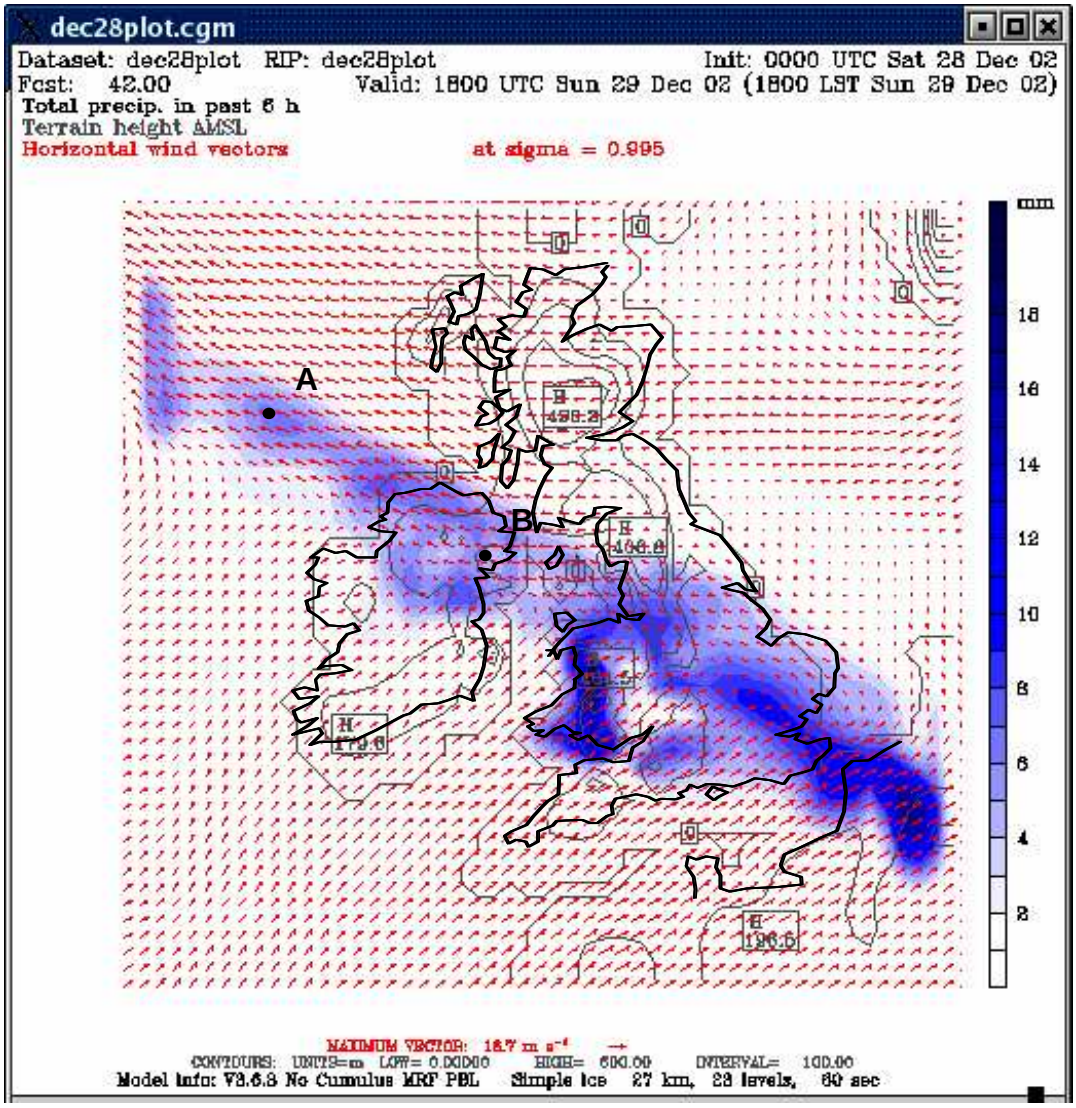

Figure 2.110: MM5 simulation of rainfall for the 6 hour period 12:00h to 18:00h, 29 December 2002. Low level wind vectors are shown as red arrows. A and B are the locations of the tephigrams displayed in fig. 2.112.

Fig.2.111 shows air flow at high troposphere level, with high velocity zones representing a jet stream pattern over eastern Britain and the North Sea. We should note that the upper air flow to the north-east over Wales is approximately perpendicular to the mid-troposphere warm air conveyor ascending to the north-west. This is similar to the situation recorded by Browning and Hill (1985) and represented here as fig.2.21.

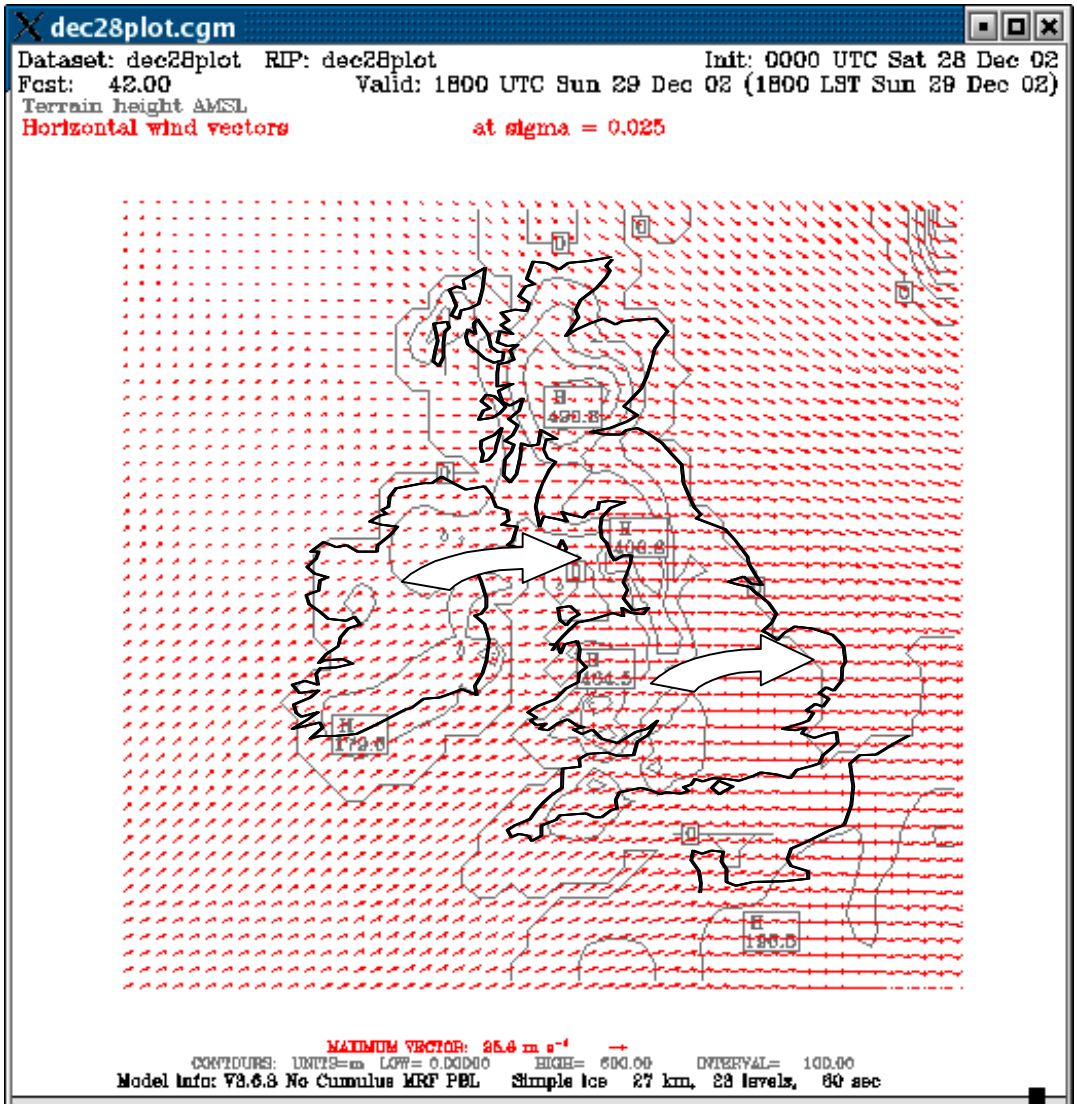

Figure 2.111: MM5 simulation of upper troposphere wind direction at 18:00h, 29 December 2002.

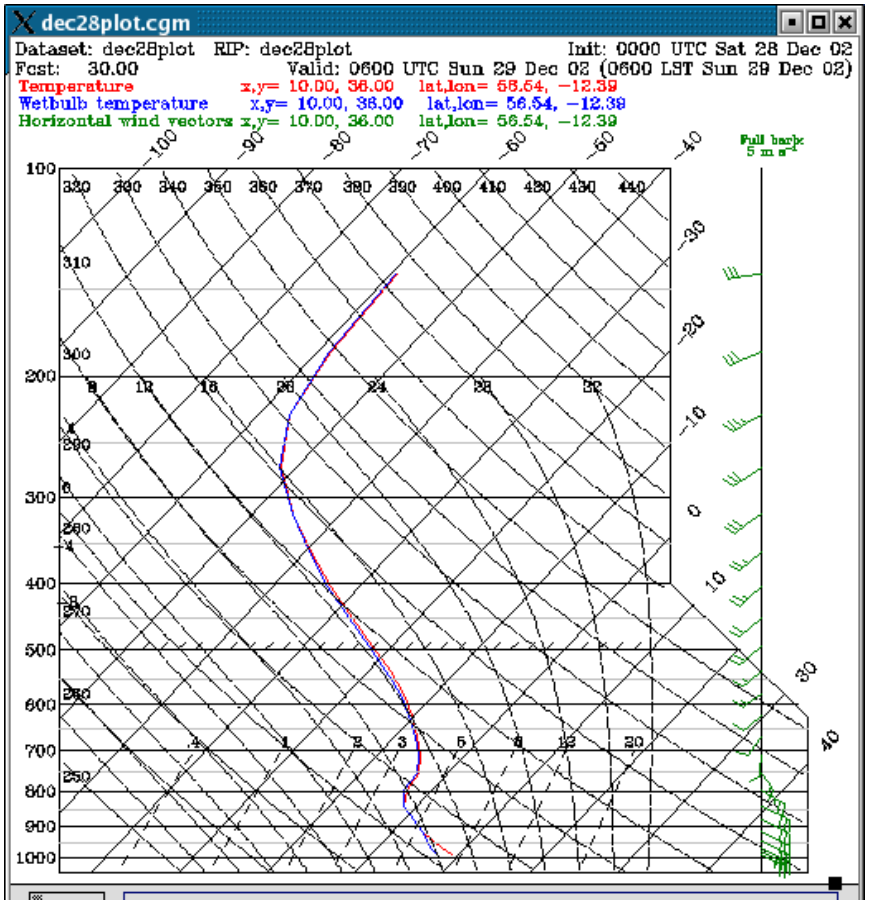

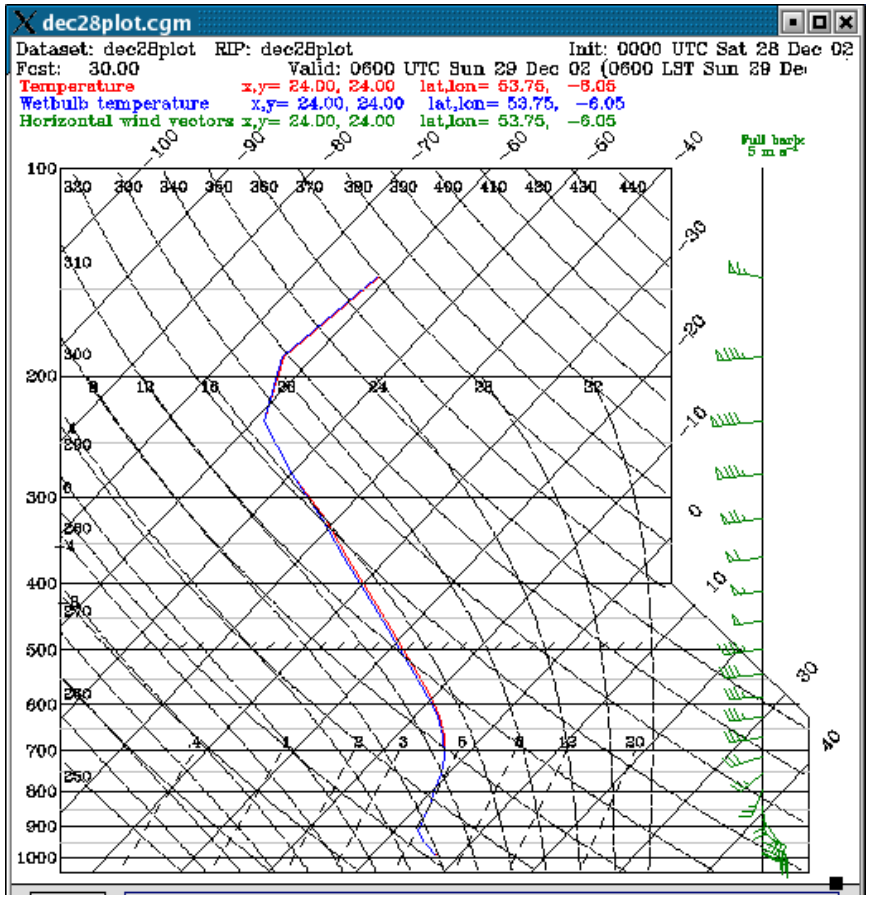

Figure 2.112: Tephigrams generated by the MM5 simulation for location A - off the north west of Ireland, and location B - Belfast, marked on fig. 2.110. 06:00h, 29 December 2002

Example tephigrams generated by MM5 are given in fig.2.112. Dry bulb temperature curves lie to the left of the lapse rate curve in the lower troposphere, indicating instability which can produce uplift within the warm sector conveyor. Maximum instability occurs at 900mb height at location A to the south-east, ascending to 850mb at location A towards the north-west. Temperatures fall rapidly above the conveyor at heights over 700mb.

Horizontal wind vectors are seen to change from a north-west directed airflow within the conveyor, towards the easterly airflow of the upper troposphere jet stream.

Squall line convection

Storms across Wales on 3 July 2001 were the result of intense convective thunderstorm activity along a squall line. The convective nature of the July 2001 event has provided an opportunity to compare the convective parameterisation schemes provided within the MM5 modelling system. The results for two schemes, Anthes-Kuo and Grell are discussed below.

Anthes-Kuo cumulus parameterisation

A rainfall distribution map using Anthes-Kuo parameterisation is given in Fig 2.113. This shows a close correspondence to observed rainfall patterns. The north-south orientation of the squall line is clearly defined, with several thunderstorm cells in observed locations over the mountain region. The only deficiency of the model is that the zone of intense rainfall (>25mm/hour) should extend some 5-10km further northwards along the squall line to account for extensive flood damage in the Arennig area.

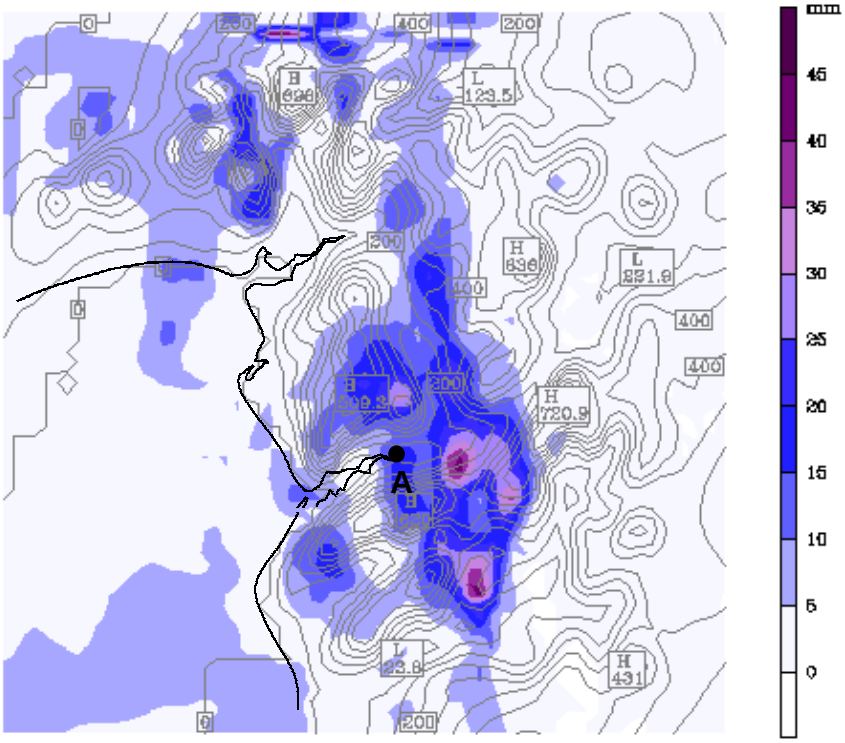

Figure 2.113: One hour rainfall total. 1800-1900, 3 July 2001. Anthes-Kuo model. A marks the location of the tephigram shown in fig. 2.116.

Examination of the MM5 model results shows the intense convective activity associated with the squall line (Figures 2.114-2.115).

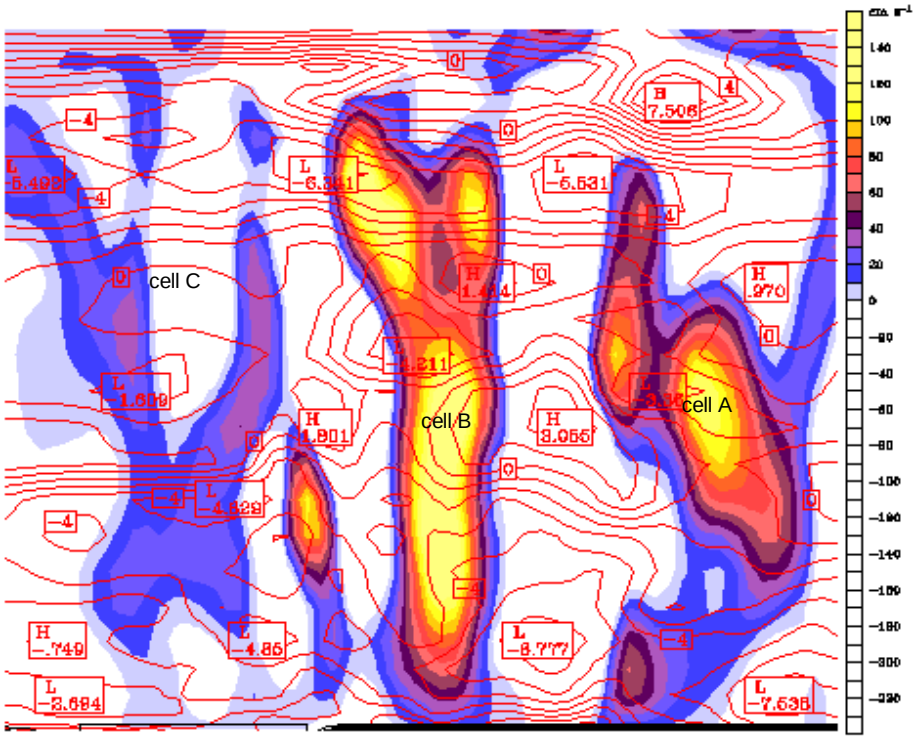

Figure 2.114: Vertical section from Cardigan Bay to the Arenig mountains. Shading indicates vertical air velocity. Contours indicate horizontal velocities. 18:00h, 3 July 2001. Anthes-Kuo model.

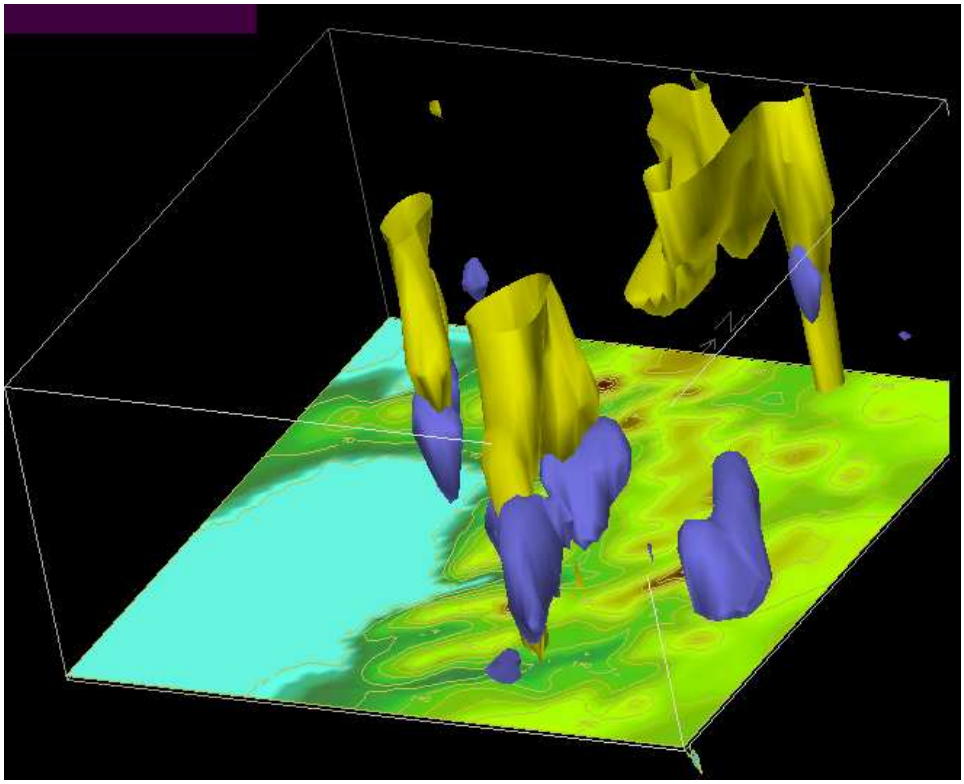

Figure 2.115: Isosurfaces for cloud mixing ratio>0.4 (yellow) and precipitation mixing ratio>0.4(blue). 1800, 3 July 2001. Anthes-Kuo model.

It is seen that the Anthes-Kuo physics scheme produces results in close agreement with the theoretical model of squall line propagation proposed by Fovell and Tan (1998, 2000). The cross section fig.2.114 shows a sequence of convection cell initiation at an advancing cold tongue (cell A), the vertical growth of a second cell (cell B), and evidence of the break-up of an earlier cell during advection towards the rear of the cold pool (cell C). Clear similarities exist with the simulations carried out by Fovell and Tan (cf. fig.2.32).

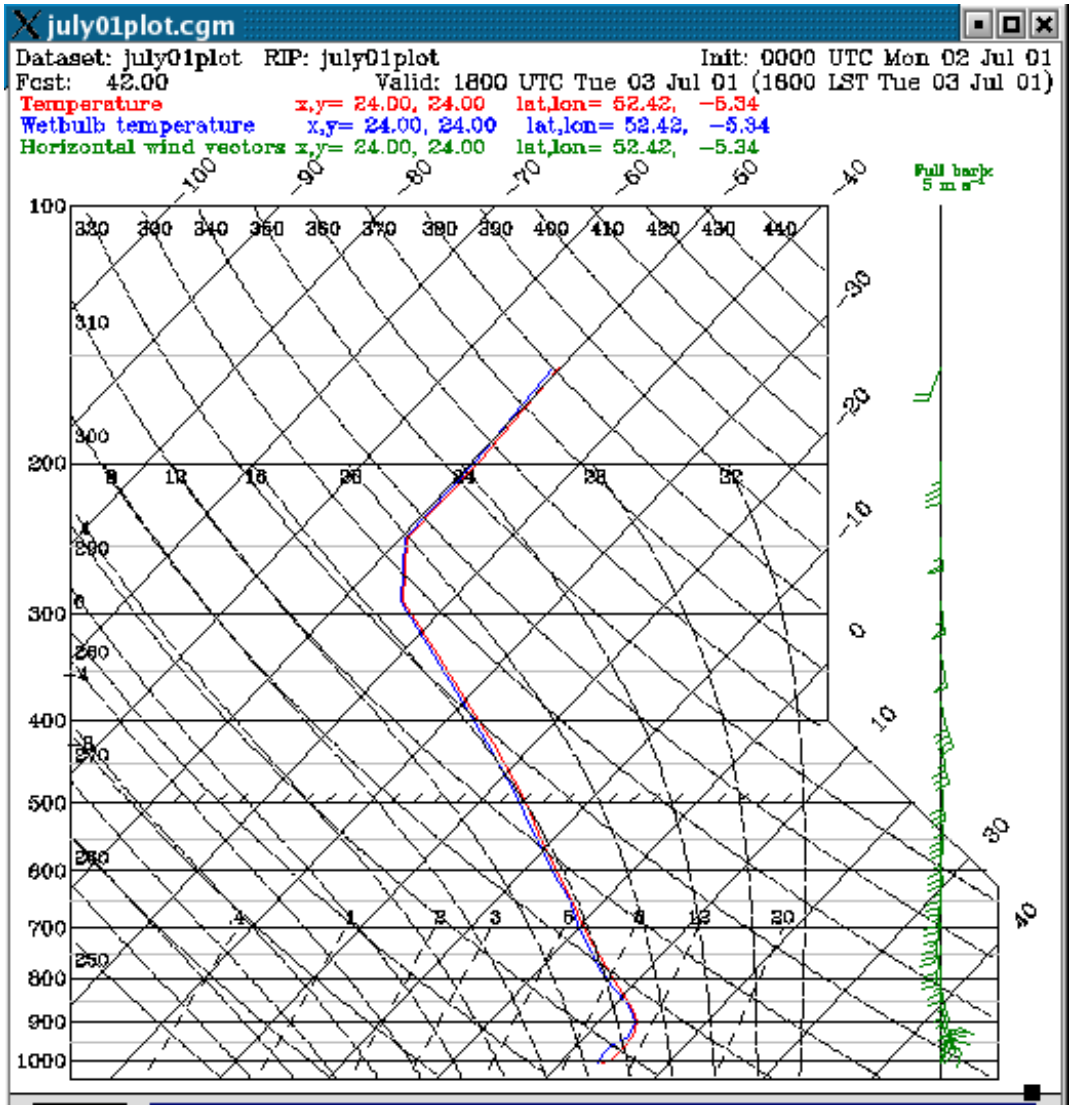

Figure 2.116: Tephigram generated by the MM5 simulation for location A – Dolgellau, shown on fig. 2.113, 18:00h, 3 July 2001

A tephigram is displayed in fig.2.116 for a location towards the rear of the squall line. This shows a fall in virtual temperature towards the ground, confirming the modelling of a pool of cool air below 950mb height. The dry bulb temperature curve lies to the left of the lapse rate curve for altitudes between 800mb and 500mb, indicating a wide vertical band of instability driving convection. Horizontal air flow vectors are towards the north, following the axis of the squall line.

Grell cumulus parameterisation

Results from the MM5 run using Grell cumulus parameterisation (cf. fig.2.89) are very different from those of the Anthes-Kuo model, and bear little resemblance to observed rainfall patterns during the storm event. Rainfall is modelled as occurring mainly over the sea, and is about half of the true intensity (fig.2.117).

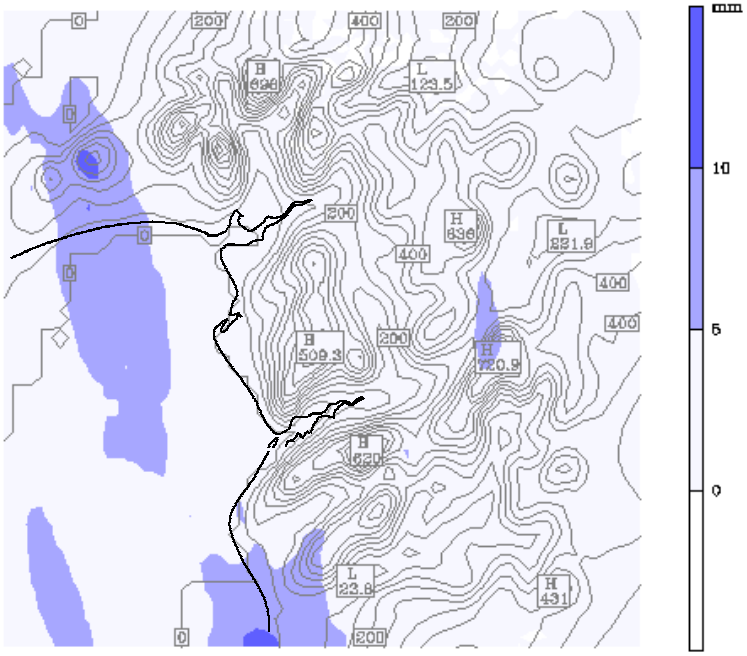

Figure 2.117: One hour rainfall total. 1800-1900, 3 July 2001. Grell model.

Patterns of vertical air motion produced by the Grell model (fig.2.118) indicate a number of small convective cells distributed over a broad belt, in contrast to the few very large cells of the Anthes-Kuo model. Little rainfall is shown as being generated by the convective system.

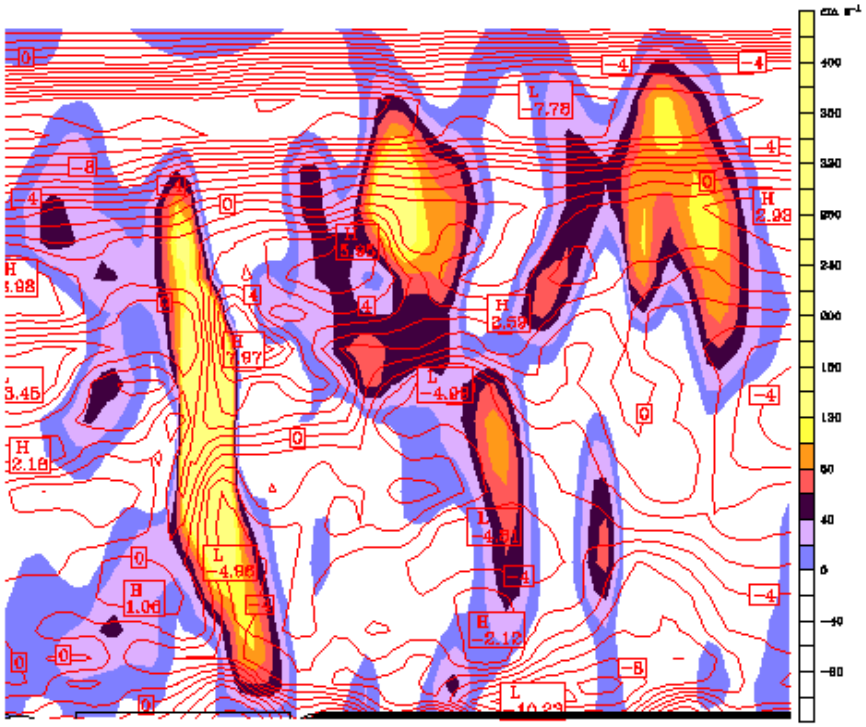

Figure 2.118: Vertical section from Cardigan Bay to the Arenig mountains. Shading indicates vertical air velocity. Contours indicate horizontal velocities. 18:00h, 3 July 2001. Grell model.

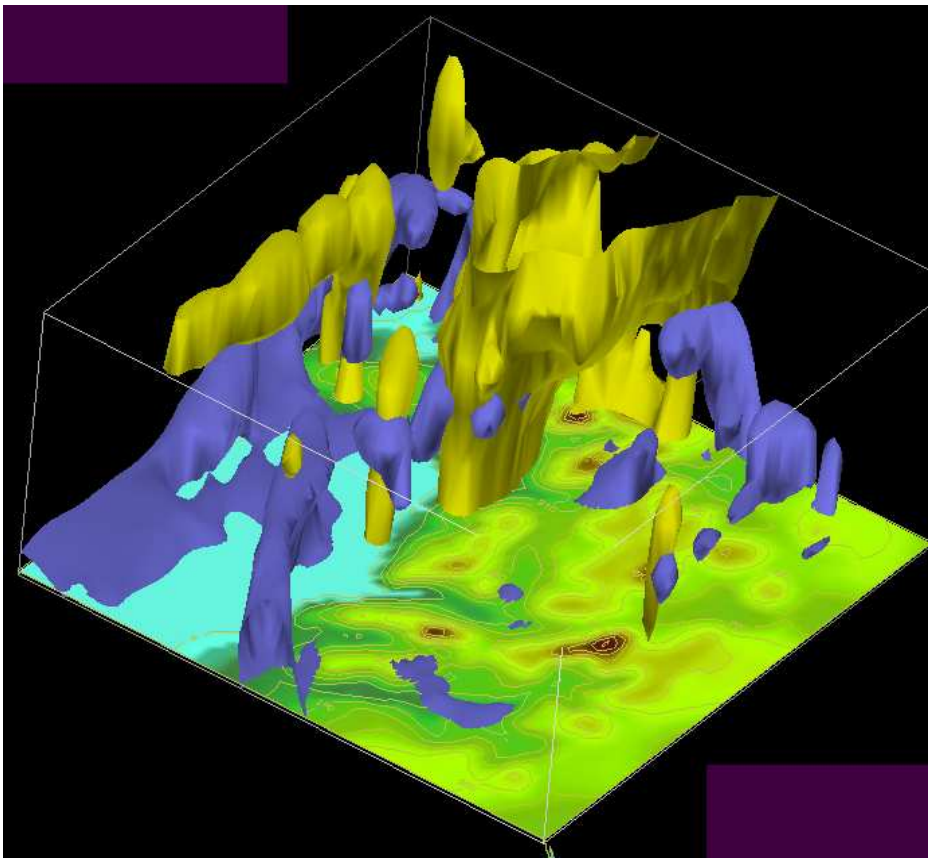

Figure 2.119: Isosurfaces for cloud mixing ratio>0.4 (yellow) and precipitation mixing ratio>0.4(blue). 18:00h, 3 July 2001. Grell model.

Summary

Analysis of frontal rainfall events simulated in the MM5 mesoscale model indicates:

- The general patterns of rainfall are reproduced well, both temporally and spatially. Rainfall distributions obtained from MM5 are in better agreement with field raingauge readings than rainfall radar over the North Wales area.
- Rainfall predictions using MM5 in a 6 hour forecasting mode are likely to be in the order of $\pm 30\%$ accuracy for individual point values, or $\pm 15\%$ accuracy if rainfall averaging across the catchment is allowed.
- Some limited but useful improvement to forecast values can be achieved by neural network processing of initial MM5 output data. Retraining of the neural network needs to be carried out for each individual storm event.
- The MM5 model produces rainfall predictions from realistic simulations of atmospheric conditions within frontal systems, combined with appropriate rainfall enhancement by topographic forcing.

The July 2001 flood event was different in nature, resulting from intense convective thunderstorm activity along a squall line. Simulation of this event with MM5 has produced varied results with different cumulus parameterisations.

- The Anthes-Kuo scheme corresponds well to the sparse rain gauge data available, and gives a rainfall distribution which is largely consistent with field observations of flood damage and maximum river levels. Furthermore, it simulates atmospheric processes consistent with squall line theory.
- The Grell scheme considerably underestimated rainfall volumes. It may be the case that the Grell scheme is more suited to modelling isolated convective storms rather than structured pre-frontal squall line activity.

It may be necessary to carry out multiple runs of the MM5 model with different cumulus parameterisations if thunderstorm activity is expected, then make use of a weighted average of results in the integrated hydrology modelling system. Greater weight should be given to extreme conditions predicted by any of the cumulus schemes, since it seems likely that a severe convective event will be underestimated rather than overestimated by MM5.